"I could not stop looking at the images.
It was like entering a new world"

GERD BINNIG

University of Alberta

Nano-scale Studies of the Assembly, Structure and Properties of Hybrid Organic-Silicon Systems

by

Shoma Sinha

A thesis submitted to the Faculty of Graduate Studies and Research
in partial fulfillment of the requirements for the degree of

Doctor of Philosophy

Department of Chemistry

Fall 2011
Edmonton, Alberta

To my mother, Supti Sinha,
for always encouraging us to achieve our best and
for always being there along the way.

Abstract

Advancements in the field of electronics might be achieved by future molecular scale devices. Hybrid organic-silicon structures have the potential to overcome many challenges facing the use of molecules as devices while maintaining the ability to interface with traditional silicon technology. The objective of this dissertation was to advance our base knowledge of the interactions, behaviour and properties of simple molecular systems and the Si(100):2×1 surface.

Experimental studies conducted with scanning tunneling microscopy (STM) and complemented with theoretical investigations, primarily density functional theory (DFT), were utilized to investigate three principle areas of interest: (1) the transport behaviour of monolayers, patterned regions, or nanostructures, (2) surface diffusion and (3) properties of self-assembled molecular lines.

The tunneling current versus applied bias behaviour of the clean, the monohydride and the styrene passivated Si(100):2×1 surfaces were studied. An energy band model was formed that incorporates surface dipole characteristics and band bending to describe tunneling current transport. The transport behaviour from patterns of clean, styrene covered, and 4-fluorostyrene covered Si(100):2×1 on otherwise monohydride terminated Si(100):2×1 were subsequently studied. Comparison with the observations from the full monolayers provided evidence for conduction through surface states. Studies of the transport behaviour of styrene molecular lines were also performed.

Surface diffusion is an important aspect of self-assembly. A novel experimental method for studying aspects of diffusion that removes STM tip effects was developed and used to study the diffusion anisotropy of styrene and 4-fluorostyrene on H-Si(100):2×1. These studies were complemented with DFT energy calculations and Monte Carlo methods to incorporate dynamic effects.

Various studies were conducted on self-assembled molecular lines. In addition to studying the current-transport of styrene lines mentioned above, the transport of lines terminated on one end by a silver island was explored. The effect of line growth due to surface exposure to 1,4-cyclohexadiene was considered. Finally, a study of ordering phenomena of molecules within molecular lines was conducted. Lines composed of 1-vinylnaphthalene were particularly interesting. They demonstrated the ability to form lines with double the normal periodicity but which can transform into normal lines. Using theoretical calculations, a T-like model was proposed.

Acknowledgements

It is a pleasure to thank the many many people who have made this thesis possible and my experience in graduate studies enjoyable.

First and foremost I offer my sincerest gratitude to my supervisor, Dr Robert Wolkow, who has supported me throughout my dissertation with his patience, guidance and knowledge while encouraging me to explore new and unique aspects of science and nature.

I would like to extend a special thank-you to Dr. Gino DiLabio for his guidance and mentorship in the theoretical aspects of my research as well as my graduate studies as a whole.

All the past and present members of the Molecular Scale Devices Group have also helped me in numerous and essential ways. In particular, thank you to:

Dr. Jason Pitters, for sharing his expertise on UHV, STM and silicon systems;

Dr. Stas Dogel, for also sharing his knowledge of STM and insights into experiments as well as for preparing EBL samples used in my research;

Dr. Adam Dickie, for the work with scanning tunneling spectroscopy;

Mark Salomons, for designing and building the multiprobe STM;

Martin Cloutier, for all the aid and advice on equipment;

And to Josh Mutus, Luca Ramoino, Manuel Smeu, Paul Piva, Radovan Urban, Lucian Livadaru, Iana Dogel, Cristian Vesa, Iain Mackie, Marco Taucer, Baseer Haider, Peter Ryan and Peter Legg: for all their helpful discussions and aid throughout the years.

In addition, I would like to thank the WISEST, UA-WiSE and WISER communities for helping me keep perspective and balance in my life. In particular, I thank the former WISEST Vice-Chair Gail Powley for her valuable mentorship and my past/present WISER Co-chairs Sharon Barker and Samia Sarkar for their insights and dedication to the early career community.

Lastly, but certainly not leastly, I wish to thank my family for their support, guidance and love throughout my life: my parents Nirmal and Supti Sinha; my sisters, Priya and Roona Sinha; and my partner Bhaskar Chanda.

Contents

List of Tables

List of Figures

Chapter 1

Introduction

1.1 Motivation

The modern electronics industry has been grounded in the development of silicon technology. Silicon has been the semiconductor of choice due to its high abundance and thus low cost, its ability to retain its semiconducting properties at high temperature and the facile formation of an even native oxide layer with few interface defects. With silicon at its core, the electronics industry has grown rapidly. This is most often demonstrated with "Moore's Law" which refers to Gordon Moore's observation in 1965 that the number of transistors per cm^2 of silicon doubled every year [1] [1]. Though initially an observation of past progress and a prediction for a single decade into the future, Moore's Law has in many ways acted as a guide for the industry and has been sustained for over four decades. The reduction of component size is a measure related to an increase in speed and density which are related to overall efficiency and progress in the field. The semiconductor industry is now recognized not only as an industry itself but also as a technology enabler and a driving force for economic growth.

The reduction of component size is not without limit. Several challenges exist in the use of conventional techniques for further significant advancements [3]. Photolithographic procedures currently used to fabricate integrated circuits, are limited not only by the diffraction limit but also by the ability to focus the radiation and by the development of appropriate materials for masks and resists. Further development of dielectric materials, such as hafnium(IV) oxide (hafnia) [4], that can be effectively used as insulators at a small length scale is also required. Similarly, small wires or interconnects, must be developed to overcome such challenges as electromi-

[1] This statement that was revised in 1975 to state that overall chip densities would double every two years [2]. In scientific literature, both statements have interchangeably been used as Moore's Law.

gration - the transfer of momentum from electrons to atoms which can cause voids and thus failure of small interconnect components. Many of such challenges are directly linked to the need for heat dissipation and a reduction in power requirements. In addition to the challenges to conventional techniques a fundamental size limit occurs at the atomic scale.

The vision of using single atoms and molecules as devices is not new. The terms 'atomic electronics', 'angstronics' and more popularly 'molecular electronics' have been in use as early as the mid 1950's [5]. The term 'nanoelectronics' is more recent but shares much of the fundamental concepts of the older terms. A more encompassing term is 'molecular scale devices' or simply 'molecular devices' [6] as it more clearly encompasses the possibilities outside of standard electronic schemes - the possibilities for fundamentally new paradigms for information processing, transfer or storage.

The field of molecular devices is still in its infancy; however, it already encompasses a vast array of research initiatives from various sources. Experimentalists and theoreticians from such fields as chemistry, physics, materials science, engineering (electrical, chemical, mechanical) and even biology are working together to overcome the challenges already recognized in the field as well as those not yet recognized.

Several of the challenges from the top-down perspective of the miniaturization of more conventional schemes have already been mentioned. Bottom-up approaches of directly making use of atoms and molecules first requires increasing our understanding and then the control over specific interactions at the molecular level. A thorough understanding is required for the development of reliable products. In addition, the development of fully functional entities faces pure architectural challenges. Many of the architectural challenges facing molecular devices have recently been summarized and ranked according to perceived importance by Beiu [7]. Some of the important considerations identified include the power consumption, heat production, the reliability of components, the redundancy required to compensate for fabrication errors, optimizing communication but reducing connectivity and the optimization of logic and encoding to reduce the number of computations. A consideration not mentioned in this article but which is of significant practical importance, particularly in bottom-up approaches, is the time requirement for the creation of the device. Self-assembled and other parallel fabrication processes are highly desirable over processes requiring, for instance, direct single molecule or atom manipulation.

Despite the challenges, many advancements have been made in the field. Much of the recent progress has been enabled due to advancements in the technology used to study such systems. In particular, the scanning tunneling microscope (STM) [8] and

related probe technology has allowed for direct imaging and manipulation of systems at these size scales. In fact, the STM was instrumental in elucidating the very structure of the surfaces in question. Using modern instrumentation, research into both passive molecular devices (such as tunnel junctions [9,10] and rectifiers [11,12]) as well as active devices (such as sensors [13] and single molecule transistors [14]) have shown promise at the laboratory level.

The production of commercially viable complete molecular scale devices and architectures is likely a long way in the future. Moreover, a direct transition from conventional electronics to such systems is unlikely. A possible first step is the integration of molecular scale devices into traditional semiconductor technology schemes. Compatibility with silicon technology offers the advantage of possible direct integration with modern systems as well as a mature understanding of the base material system. Moreover, the development of future technology that can make use of the vast infrastructure currently in place for the silicon semiconductor industry is desirable from an economic standpoint. Hybrid silicon-organic systems may offer the further advantage of the vast knowledge base of organic chemists [15]. The sheer variety of organic molecules in addition to a base knowledge of methods to tune various molecular properties offers exciting opportunities to enhance the properties of conventional silicon electronics. In addition, simple, low temperature processing techniques such as spin coating and stamping offer the potential for low cost integration.

The goal of increasing our base knowledge for the development of future hybrid silicon-organic molecular scale devices is the prime motivation for the research conducted in this dissertation.

1.2 Overview of Developments in Hybrid Silicon-Organic Systems

Interest in hybrid silicon-organic molecular scale devices has developed from a variety of facets. Only a small subset of the explorations are directly relevant to the studies pursued in this work. For instance, one large area of interest not covered here but which is of great interest for future application development is the area of silicon photonics [16]. Another area pursued with great interest is the study of carbon nanotubes as device components on silicon [17], such as carbon nanotube field effect transistors [18]. Here, we focus on understanding some of the fundamental interactions between simple molecules and the Si(100):2 $\times$ 1 surface.

The Si(100) surface is the common platform for modern silicon electronics due

largely to its ability to easily form a native oxide with few interface defects. The presence of an oxide is most often not required for molecular device studies but the use of the Si(100) surface as a platform persists largely with the hope of increasing compatibility and integration with modern electronics. Other silicon surfaces, such as the Si(111) surface which can form a metallic surface reconstruction, are also gaining interest - particularly as atomic level understanding of their surface structures is increasing. By surface structures I refer primarily to the various surface reconstructions that take place in order to minimize surface energy. Such reconstruction can make surface properties dramatically different from the bulk material properties. For example, while bulk silicon is a semiconductor, the Si(111):7x7 surface reconstruction is expected to be metallic in nature. In the case of Si(100) the 2×1 reconstruction is particularly stable. The STM demonstrated that this surface is composed of rows of silicon dimers [19] with a buckled structure with respect to the surface plane [20]. This structure will be described in greater detail in the following chapter. With this knowledge of the surface structure the possibility for molecular devices became more viable.

One of the key areas of focus in molecular devices is the ability of single molecules to rectify current. Current rectification, an asymmetric current about zero applied voltage, is a key component of electronic devices such as diodes. The study of molecular rectification (MR) is an intensely growing field initially motivated by Aviram and Ratner who considered transport through donor and acceptor moieties linked by a sigma bond bridge (D-σ-A) [21]. Correlation of the donor and acceptor molecular orbitals causes the tunneling current to be favored in the forward direction thus enabling rectification through the molecule. Since this proposal, several studies have demonstrated rectification through Langmuir-Blodgett (LB) monolayers or self-assembled monolayers (SAMs) between metal plate electrodes [22–24] as well as through single molecules with scanning tunneling microscopy/spectroscopy (STM/STS) [25, 26]. However, rectification in these systems has been attributed to not only the asymmetry of the molecular orbitals as originally proposed, but also the placement of the molecules between electrodes as well as structure of the electrode-molecule interfaces [27, 28]. Molecular rectification from SAMs formed on silicon and silicon dioxide have been found to be particularly difficult to control resulting in large variations between samples and between work performed by various laboratories [29]. As such, thiol-gold systems rather than silicon based systems have been pursued with greater fervor in this area.

The variability in observations highlighted the need for a systematic and detailed study of the behaviour of molecules on the silicon surface. Wolkow has reviewed some

of the first truly microscopic pictures of the structure and bonding of several simple organic adsorbates on clean Si(100):2 × 1 [15]. This review particularly highlights the level of detail that is required to understand the situation of even simple surface adsorbates. The reaction of some of these molecules as well as related molecules were further explored by Hamers et al. in a focused study of cycloaddition type reactions on (001) surfaces of silicon, germanium and diamond [30]. In this review, it was observed that several reactions which would normally be symmetry forbidden by Woodward-Hoffmann symmetry rules were instead allowed due to the unsymmetrical buckled nature of the silicon dimer bond. The importance of adsorption dynamics rather than overall thermodynamics was also discussed.

The structures of benzene and styrene on the clean Si(100)):2 × 1 surface will be found to be of particular relevance to the work in this dissertation. Though these molecules are quite simple, their bonding structure to the surface presented quite a challenge to elucidate. For instance, the structure of benzene required careful analysis of STM structural and energetic information, computed structures as well as theoretical and experimental IR and adsorption energies [15] in order to determine which of several candidate structures were the true adsorption structures. Two configurations emerged from the analysis: a single dimer configuration with bonding through carbons 1 and 4 (Fig. 1.1(a)) and a bridged dimer configuration with 'tight' bonding through carbons 1,2,3 and 4 (Fig. 1.1(b)). At low coverage it was observed that the single dimer state converted to the bridged state with an activation barrier of 0.94eV (assuming a pre-exponential of $10^{-13}s^{-1}$) [31].

Styrene reacts with the clean Si(100):2 × 1 surface exclusively through the vinyl group via a [2+2] cycloaddition process that leaves the aromatic phenyl group intact [30, 32]. Surprisingly, calculations predict that a tight bonding configuration which involves breaking the aromaticity of the phenyl group is energetically quite similar to the cycloaddition-like reaction, due to the formation of four silicon-carbon bonds at the surface [30]. It has been proposed that the selectivity of reaction through the vinyl group is largely a result of long range attractive interactions that 'steer' the substituent group towards the surface dimers [30].

The clean silicon surface is highly reactive. For instance, the reaction of styrene with clean Si(100):2 × 1 is extremely facile leading to a sticking coefficient close to unity. In air, the clean surface is easily oxidized and/or otherwise contaminated. In vacuum, the surface can also become dirty with a time constant that varies with the vacuum pressure.

The Si(100) surface is often passivated with a monolayer of hydrogen to form the monohydride 2 × 1 surface. The monohydride surface retains the dimer structure

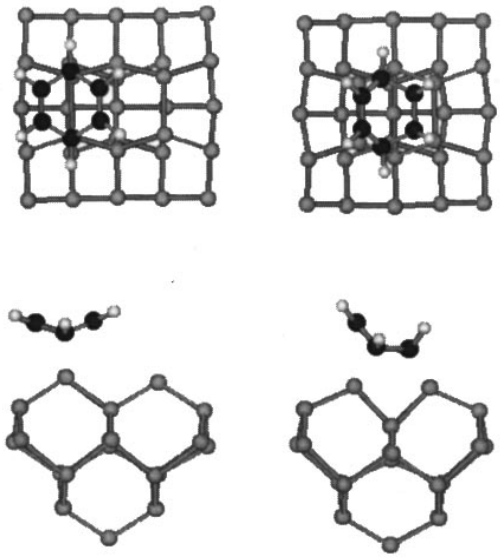

(a) 1,4-Single Dimer (b) Tight Bridge

Figure 1.1: Benzene Adsorption Configurations on Clean Si(100):2 × 1. Adapted with permission from [31], Copyright (1998), American Vacuum Society.

of the clean surface but breaks the π bond interactions between the silicon surface atoms, thus significantly quenching the reactivity of the surface. This surface thus presents a very different reaction profile to adsorbates than the clean surface. Due to the lower reactivity with the passivated surface, there exists a greater chance that adsorbates will not directly chemically react with the surface. In many cases, the adsorbate will first physisorb to the surface through long range interactions but still remain mobile. Such physisorbed entities have the opportunity to diffuse along the surface (Fig. 1.2). Surface diffusion, in general, is dependent upon the shape and chemical constituents of both the adsorbate and the surface. As such, surface structure - such as dimer rows on Si(100):2 × 1 - can impact the manner in which molecules diffuse. While physisorbed to the surface the adsorbate may encounter a site with which it can react. Such sites are often locations of greater energy such as surface defects. For example, a missing hydrogen site - often referred to as a surface dangling bond (DB) - can have a much greater reactivity with adsorbates than the monohydride sites. If it does not encounter a site with which it can react, the adsorbate may eventually desorb from the surface. For molecules in which the physisorption energy is much greater than the barrier to diffusion, the molecule may move laterally on the surface before desorbing or chemically reacting with a surface site.

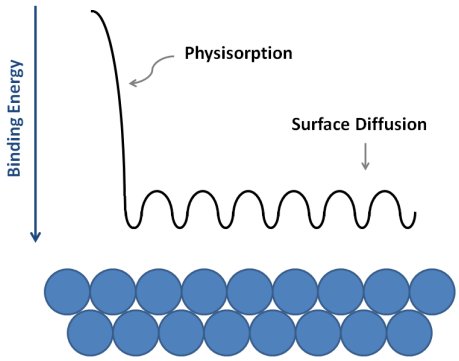

Figure 1.2: Energy Schematic for Diffusion Process

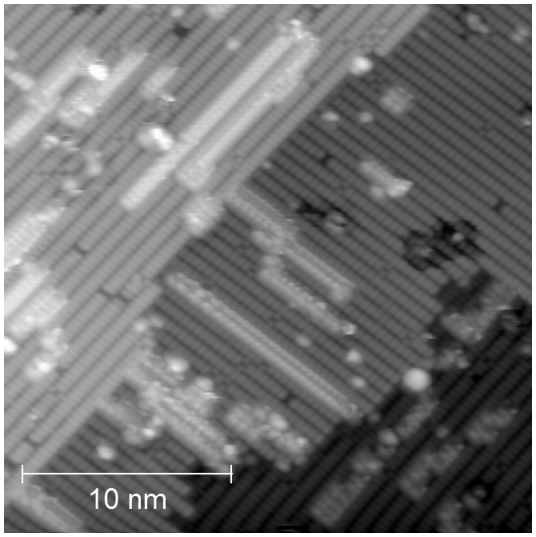

Figure 1.3: STM image of Styrene Molecular Lines. Imaging Set Point: $V_S = -2$V $I_T = 100$pA.

The mobility of molecules on the surface can play a critical role in an adsorbate's ability to self-assemble into ordered structures on the surface. Self-assembly processes are critical in nature and in fact for the very foundation of life. In molecular electronics, manipulating and using such processes could lead to the facile fabrication of molecular scale devices. A promising scheme for the creation of self-directed, linear structures of organic molecules on the hydrogen terminated silicon surface was introduced by Lopinski et al. in 2000 [33]. An example image of a 'molecular line' formed from styrene molecules is presented in Fig. 1.3. The detailed mechanism of molecular line growth process is deferred to later in the text; however, it is noted here that the the self-assembly of molecular lines takes advantage of the ability of

molecules to diffuse on the surface and chemically react with surface DBs. The creation of molecular lines is a source of great interest for several reasons including:

1. the formation of linear, well ordered nanostructures
2. being a self-directed process not requiring individual manipulation of molecules
3. could be formed in parallel at many locations on a surface
4. results in the integration of organic structures on silicon surfaces
5. could be expanded to include a wide range of organic molecules with differing properties and
6. could potentially lead to information transfer along the molecular line through, for example, conduction.

Due to these properties, molecular line structures may provide a viable means of creating molecular scale devices, device components or interconnects.

Since the discovery of line growth, a wide range of studies have been conducted both experimentally and theoretically. A large variety of molecules have been shown to be capable of undergoing line growth with silicon surfaces. Table 1.1 provides a short summary of some of the reactions known to take place and highlights the variety of molecular line growth processes that can occur. In addition to those listed, several heterolines - molecular lines containing more than one molecular species dosed either at the same time or sequentially - have been studied [34–36].

The increasing knowledge gained in the study of molecular lines is one example of a promising start towards future hybrid silicon-organic molecular devices. This start must be met with equal promise in regards to contacting and connecting the systems together. In modern electronic devices metal silicides form a vital component. They are used as local interconnects, Ohmic and Schottky barrier contacts as well as gate electrodes [45]. One of the most common silicides currently used in the semiconductor industry is titanium silicide ($TiSi_2$). A preference for $TiSi_2$ has arisen "because it can be self-aligned, has low resistivity, and is stable at temperatures consistent with device fabrication processes" [46]. However, silicides with appropriate properties have been difficult to develop at small feature sizes.

Scaling of silicide contacts grown on silicon wafers is being studied from both top down and bottom up approaches. From the top-down viewpoint, polyside [2] and

[2]Polyside (polysilicide) processes use patterning techniques such as lithography on polycrystalline silicon to form the silicide.

System	Notes
Styrene on H-Si(100)-2 × 1	Lines along dimer row [33]. Lines "unzip" at 400K [37]
Styrene on H-Si(100)-3 × 1	Lines across dimer row [38]
Methyl Styrene on H-Si(100)-2 × 1	Lines along dimer row [34]
CF_3 and OCH_3 Substituted Styrene on H-Si(100)-2 × 1	Lines along dimer row [35]
2,4-dimethylstyrene on H-Si(100)-2 × 1	Lines along dimer row [37]
cyclopropyl methyl ketone H-Si(100)-2 × 1	Non-linear Lines [39]
vinylferrocenee on H-Si(100)-2 × 1	Lines along dimer row; Molecules in zig-zag pattern due to sterics [40]
linear alkanes on H-Si(100)-2 × 1	Lines along dimer row; 1-octene and larger molecules grow at room temperature [41]; 1-hexene and 1-heptene have been grown at 180K [37]
Allyl mercaptan on H-Si(100)-2 × 1	Lines across dimer row as well as random [42]
1-vinylnaphthalene and 2-vinylnaphthalene on H-Si(100)-2 × 1	Lines along dimer row [36]
1,3-cyclohexadiene on H-Si(100)-2 × 1	Lines along dimer row but molecules separated by one or two dimers [36]
Trimethylene sulfide on H-Si(100)-2 × 1	Lines along dimer row in square pattern on p-type crystal through sulfur atom; Lines along dimer row in square pattern on n-type crystal through carbon atom [36, 43]
Trimethylene sulfide on H-Si(100)-3 × 1	Lines along dimer row for high and medium n-type as well as p-type crystal [36]
1,3-butadiene on H-Si(100)-2 × 1	Lines along dimer row: growth along adjacent rows common [36, 44]
isoporene (2-methyl-1,3-butadiene) on H-Si(100)-2 × 1	Lines along dimer row: both along single dimer row and adjacent row growth observed [36, 44]
2,3-dimethyl-1,3-butadiene on H-Si(100)-2 × 1	Lines along dimer row: Primarily single dimer row growth [36, 44]

Table 1.1: Summary of some known Molecular Line Reactions on Silicon Surfaces

salicide [3] processes suffer from difficulties not only due to the available resolution of patterning techniques but also in attaining the appropriate resistivity in features at small size scales as well as the creation of disconnects in the device as a result of the silicide agglomerating into clusters during annealing cycles [45].

From the bottom-up viewpoint, two directions for the creation of contacts have shown promise. On the clean silicon surface, metal silicide islands [47,48] have been formed by annealing thin films and sub-monolayers of certain metals, including titanium. This process is promising in that it produces well structured crystalline islands of small size; however, it suffers from the inability to control growth location, size and morphology [49]. On the monohydride surface, certain metals have been shown to be able to diffuse readily and preferentially react with individual DBs and patterns of DBs [50]. Studies of silver atoms on H-Si(100):2 $\times$ 1 have demonstrated that on single DBs, silver atoms or small clusters of atoms grow at the DB site depending upon silver exposure. On lines of DBs 1nm wide, the silver atoms form a monolayer and on larger patterns the atoms stick to the outer edge of the pattern and grow as a monolayer in the direction perpendicular to the silicon dimer rows [50]. The ability to grow such metal contacts at precise locations on the surface is promising for contacting molecular structures; however, apart from natural DBs randomly occurring on the surface, the locations of Ag formation must be pre-patterned with the removal of the hydrogen resist by such means as STM tip-assisted hydrogen desorption [51].

1.3 Overview of Dissertation

The objective of this dissertation is to advance our knowledge of the interactions, behaviour and properties of simple organic molecules and the Si(100):2 $\times$ 1 surface. Studies of the rectifying properties of molecules have largely focused on complex molecules such as those adhering to the (D-σ-A) proposal. In this study, we focus on how very simple entities, such as a hydrogen atom or a styrene molecule, can change the tunneling current behaviour of the surface from a monolayer, a patterned region on the scale of 30nm $\times$ 30nm to 100nm $\times$ 100nm, or a self-assembled nanostructure such as a molecular line. We suggest that the resultant electronic transport is not due to the molecular orbitals and band alignment as in traditional molecular rectification concepts. Rather, the chemical interaction controls the suppression or enhancement of tunneling current, and it does so in a polarity asymmetric manner.

[3] Salicide (self-aligned silicide) processes in which the device (gate, source/drain locations etc) is pre-patterned and metal is reacted simultaneously with all exposed silicon regions. Unreacted metal over isolation regions are removed post silicide formation.

In conducting these studies we also look at properties of the molecule necessary for creating and understanding the systems under study such as the ability of the molecules to diffuse on the surface and the ordering of molecules within a line.

Chapter 2 provides background on energy band diagrams and the scanning tunneling microscope. A short description of other techniques, including STM tip preparation techniques is then provided. With this information in hand, the three systems used during this dissertation are described. To highlight the intricacies involved in designing, creating and utilizing such systems a brief description of the challenges faced in optimizing one of the instruments is provided as an appendix. Sample materials and preparation techniques are then described.

In chapter 3 the theory behind methods of obtaining spectroscopy measurements with the STM is discussed and the methods used in this dissertation are presented. The analysis technique is then applied to study the transport mechanisms from the clean Si(100):2 $\times$ 1 surface, the monohydride Si(100):2 $\times$ 1 surface and the styrene passivated surface. The results of this analysis are used to create a proposed energy band model of transport in forward (negative sample bias) and reverse (positive sample bias) sample bias. This model will also be referred to when discussing transport behaviour of structured regions on the surface. Chapter 3 ends with a discussion of observations of the change in current-voltage behaviour of the surfaces as a result of a relatively long range density gradient of passivating styrene molecules.

The first half of chapter 4 focuses on providing a background on Density Functional Theory (DFT). DFT methods are then used to study the dimerization of benzene and naphthalene molecules. We then progress from studying dimers to studying molecules on the monohydride Si(100):2 $\times$ 1 surface. Styrene and various electron donating and electron accepting molecules are studied.

The self-assembly of nanostructures on surfaces is dependent on the molecules ability to diffuse along the surface. In chapter 5 we study styrene and 4-fluorostyrene diffusion on the hydrogen terminated Si(100):2 $\times$ 1 surface. As STM tip effects can often mask intrinsic diffusion effects, a novel method for studying diffusion parameters is first developed. The diffusion of styrene is also studying theoretically using DFT for energy considerations and Monte Carlo methods for dynamic considerations. Together, the experiment and theory demonstrate that styrene diffusion is very slightly anisotropic with diffusion favored along the dimer row direction rather than perpendicular to the dimer rows.

During the study of diffusion on surfaces, methods for creating patterns of clean Si(100):2 $\times$ 1, styrene covered Si(100):2 $\times$ 1 and 4-fluorostyrene covered Si(100):2 $\times$ 1 on otherwise monohydride terminated Si(100):2 $\times$ 1 is presented. In chapter 6 we

study the current transport behaviour from such patterned regions. In such surface patterning, the effect on transport from the surrounding surface is found to be minimal. However, the second half of this chapter indicates that this is not the case for electron beam lithographically defined metal patterns. The patterns studied are much larger in size than the STM lithographically defined patterns but are similar to patterns used and being developed for use in connecting to and studying molecular structures and assemblies.

Chapter 7 focuses on various studies of molecular line nanostructures on the hydride surface. The chapter begins by providing a description of the line growth process. During this process, molecular lines are grown from surface DB sites in a manner that a DB site remains at the end of the line unless terminated by some other process. A discussion of attempts of a detailed study of the current-voltage spectroscopy from styrene molecular lines is provided. The effects on the spectroscopy due to the diffusion of silver atoms to the terminating DBs is also briefly explored.

Following the spectroscopic studies of molecular lines, the reaction of 1,4-cyclohexadiene molecules with the surface was explored. As mentioned in Table 1.1, molecular lines of 1,3-cyclohexadiene have an intriguing structure wherein the molecules making up the line are separated by one or two dimers. By studying the reaction of 1,4-cyclohexadiene we hoped to help elucidate the mechanism of the reaction of 1,3-cyclohexadiene. Moreover, the locations of double bonds in 1,4-cyclohexadiene suggest that its reaction with a surface DB may produce a radical molecule bound to the surface. The use of such a bound radical as the initiator site for the growth of molecular lines is quite interesting. This possibility was studied using styrene molecules as the test system.

Chapter 7 concludes with a preliminary study of possible ordering phenomena of molecules within molecular lines. In general, molecular lines are composed of molecules spaced at the same distance as the underlying silicon dimer rows. However, the molecules within the line can take on different orientations - similar to different crystal phases of a material. Our findings particularly focus on lines of 1-vinylnaphthalene which demonstrate the ability to form a minority line structure which appear in STM as having double the periodicity of normal lines. Many of these minority lines are observed to transform into the normal structure, suggesting that all the lines contain the same number of molecules (per line length) but that those lines that appear with double periodicity are in an energetically less stable configuration.

We conclude in chapter 8 with a brief summary of the work conducted and some suggestions for future directions that researchers in the area may consider.

Chapter 2

Background, Materials and Methods

2.1 Chapter Introduction

This chapter will focus on providing a strong background on the materials, methods and essential concepts used throughout this dissertation. We will begin with a short introduction to energy bands with a focus on metal-insulator-semiconductor systems. This will be followed with a description of the scanning tunneling microscope (STM) including both an overview of tunneling theory as well as some practical considerations in STM experimentation. The STM systems used in this thesis will then be introduced. While the STM was the primary tool for investigation, several other techniques were employed to prepare tungsten tips and for manipulating tips on the sample. These techniques will be briefly outlined. Finally, the materials and sample preparation techniques will be described.

2.2 Energy Bands

In chemistry, molecular orbital (MO) theory is commonly used to describe the electronic structure of molecules. Discrete bonding and antibonding MOs are formed by the interaction of atomic orbitals. As the number of atoms increasing from a small molecule, to small cluster, to an extended solid MOs become closer and closer in energy such that they eventually form energy bands rather than discrete levels. The conduction band (CB) is the lowest unoccupied energy band while the valence band (VB) is the highest occupied energy band. In metals there is no energy gap (E_g= 0 eV) between the CB and the VB where as in insulators the gap is large (E_g is several electronvolts). In semiconductors the energy gap is on the order of 1 eV thus permitting finite thermal excitation of electrons from the VB to the CB.

Moreover, the conductivity can be tuned by the controlled introduction of dopant atoms into the solid. For group IV semiconductors such as silicon, group III elements (ex. boron) introduce a 'missing electron' to create p-type materials which have 'holes' as majority carriers. The Fermi level, in essence the dividing line between filled and empty states, for p-type semiconductors is thus closer to the valence band with respect to the intrinsic Fermi level, which is the mid-gap energy or the Fermi level of the undoped semiconductor. Group V elements (ex. phosphorus, arsenic) introduce an 'extra electron' to create n-type materials with electrons as majority carriers. The Fermi level for n-type semiconductors is thus closer to the conduction band with respect to the intrinsic Fermi level. The interplay between metals, insulators and semiconductors of various doping levels forms the basis of modern semiconductor devices.

Metal-Insulator-Semiconductor (MIS) structures, including the common metal-oxide-semiconductor (MOS) structures, are some of the most useful structures in device technology. The energy band diagram of an ideal MIS diode for an n-type semiconductor with no applied bias is shown in Fig. 2.1. Such band diagrams show the potential energy of an electron (y-axis) over the cross-section of the MIS junction. In the ideal case, the difference between the metal work function and the semiconductor work function is zero, such that the bands are flat at zero bias [52]. In real systems, the work functions are generally not exactly equivalent and the potential difference causes slight band bending in the semiconductor at zero bias leading to a Schottky-type barrier. [1]

The useful behaviour of an MIS junction arises when a potential is applied across the structure. For consistency with the future discussions of scanning tunneling microscopy, all potentials will be stated in terms of a bias applied to the semiconductor (also later referred to as the sample bias), V_S[2]. Under an applied bias, MIS structures are classified under three regimes depicted in Fig. 2.2. When $V_S < 0$, the CB for n-type bends downwards and majority carriers (electrons) accumulate near the semiconductor surface. Similarly, when $V_S > 0$, the VB for p-type bends upwards and majority carriers (holes) accumulate near the semiconductor surface. This regime is often referred to as 'forward biased'. When the bands bend towards the opposite direction in what is referred to as 'reverse biased', the majority carriers are depleted from the surface region. If a large enough reverse bias is applied, the intrinsic Fermi level may cross over the Fermi level at the surface. In such instances,

[1] Other non-ideal behaviour arises from charges in the oxide and interface states.

[2] It should be noted that in most devices, the voltage applied to the metal (the gate) is used as a reference. As such, the voltage polarity must be considered when comparing STM systems to traditional junction structures.

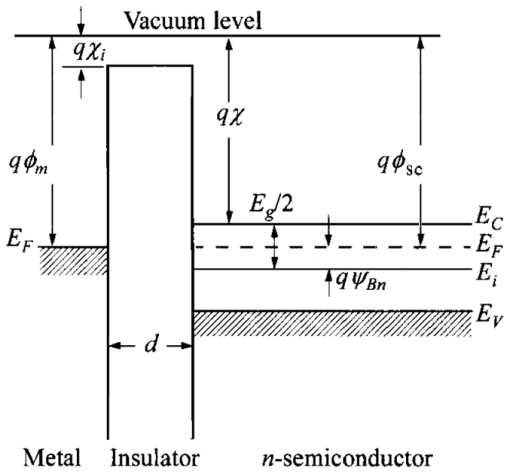

Figure 2.1: Energy Band Diagram of an Ideal MIS Diode Structure. E_F: Fermi Level; E_i: Intrinsic Fermi level of semiconductor; E_C: Conduction Band energy minimum; E_V: Valence Band energy maximum; E_g Semiconductor band gap; χ_i: insulator electron affinity; χ: semiconductor electron affinity; ϕ_m: metal work function; ϕ_{SC}: semiconductor work function; Ψ_{Bn}: potential difference between the intrinsic Fermi level and the Fermi level of the doped semiconductor. Adapted from [52], Fig. 7.2, p364.

the number of minority carriers is greater than the number of majority carriers at the surface. This is referred to as inversion.

In conventional semiconductor electronics, ideal MIS junctions minimize electron transport through the insulator layer. As such, the insulator layer is generally quite thick. This is one of the restrictions in the minituarization of semiconductor devices. If the barrier is too thin and the barrier height is not sufficiently great, carriers may tunnel through the barrier which can significantly alter the behaviour of the device. However, researchers have also found that they can take advantage of this tunneling process and MIS tunnel junctions are a source of great interest. MIS tunnel diodes have been used in microwave devices, memory devices as well as energy conversion (solar cells) [52]. The tunneling process is also the foundation for scanning tunneling microscopy (STM) where a vacuum gap is the insulator, and will be discussed in detail in conjunction with STM in the following section.

2.3 Scanning Tunneling Microscopy Overview

Atomic level imaging of surfaces is the hallmark of the scanning tunneling microscope (STM) and related scanning probe techniques such as atomic force microscopy (AFM). With the potential for sub-nanometer image resolution, the STM can be

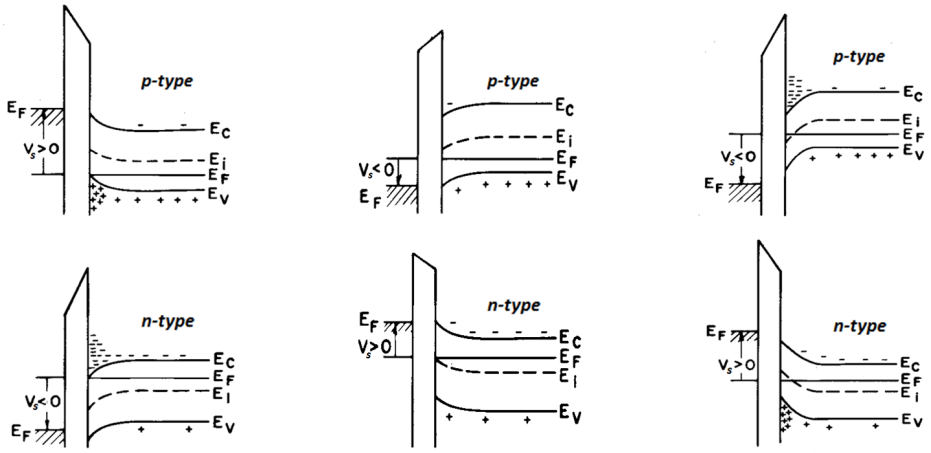

(a) Accumulation (b) Depletion (c) Inversion

Figure 2.2: Energy Band Diagrams of Biased MIS Structures for p-type and n-type semiconductors. V_S refers to a potential bias applied to the semiconductor. '+' is generally used to represent hole carriers while '−' is used to represent electron carriers. Adapted from [52], Fig. 7.3, p365.

routinely used to image surface structure precisely and even manipulate molecules and atoms on the surface. The advent of STM thus opened the doors to a vast new frontier in microscopy and nanotechnology.

Gerd Binnig and Heinrich Rohrer (IBM Zürich) developed the STM in 1981 and were awarded the Nobel prize in physics only five years later [8, 53]. The Nobel prize committee accredited Russell Young the inventor of the predecessor of the STM, the Topographiner (a field emission based scanning probe instrument) [54], with the insight that the electron tunneling effect could provide the means for high resolution imaging. Specifically, since the tunneling probability is exponentially dependent upon distance, the tunneling current between two materials provides a high resolution probe to the distance between the materials. In STM, a tunneling barrier is created by bringing a sharp metallic tip, within a few angstroms (∼5Å) of the surface of interest. An STM micrograph is created by using a feedback loop to maintain a constant current while measuring the height (or less often, maintaining a constant height while measuring current) while the tip is scanned in a raster pattern across the surface. Some of the theory behind electron tunneling in STM and physical aspects of acquiring an STM image will be explored in this section.

2.3.1 Tunneling Theory

Electron tunneling is a quantum mechanical phenomenon in which the wave nature of a particle allows it to tunnel through a potential energy barrier that it would not be able to overcome classically. The tunneling current is generally described through one of two basic theories: the solutions to the planar junction using the Wenzels-Kramer-Brillouin (WKB) approximation and Bardeen's Transfer Hamiltonian Formalism. Several extensions have been made to both these approaches but the basic theories themselves can provide substantial understanding of STM.

The Wenzels-Kramer-Brillouin (WKB) approximation is the simpler of the two tunneling models. The approximation itself is used to find solutions to the time-independent Schrödinger equation applied directly to a planar tunnel junction. The set-up of the planar tunnel junction can be compared with ease to that of metal-insulator-metal (MIM) and metal-insulator-semiconductor (MIS) junctions. Generally this method of describing tunneling in STM does not require an explicit description of electronic states, however, the densities of states in the tip (ρ_T), and sample,(ρ_S) are taken as functions of position as well as energies. In the WKB approximation, the tunneling current can be expressed by the integral over the densities of state and a transmission function which depends on electron energy, applied bias and gap distance [55]:

$$I = \int_0^{eV} \rho_S(r, E)\rho_T(r, E - eV)T(E, eV, r)dE \tag{2.1}$$

where,

$$T = exp\left(-\frac{2z\sqrt{2m}}{\hbar}\sqrt{\frac{\psi_s + \psi_t}{2} + \frac{eV}{2} - E}\right) \tag{2.2}$$

In 2.2, z is the gap distance and ψ_s and ψ_t are the work functions of the sample and tip respectively.

The WKB approximation has been found to be very useful in describing STM; however, one must be aware that it is only valid for slowly varying potentials. For molecules on surfaces, this situation does not always apply.

Bardeen's theory of tunneling [56] is a first order time dependent perturbation approach to tunneling that was applied to STM by Tersoff and Hamann in 1983 [57]. In this outlook, the wavefunctions of the tip and sample are first considered as separate systems described by the Schrödinger equations and stationary states summarized in Fig. 2.3. The two sets of wavefunctions are assumed to be approximately orthogonal such that when the systems are brought close together there exists a probability that the electrons in one system will tunnel to the other with time. This

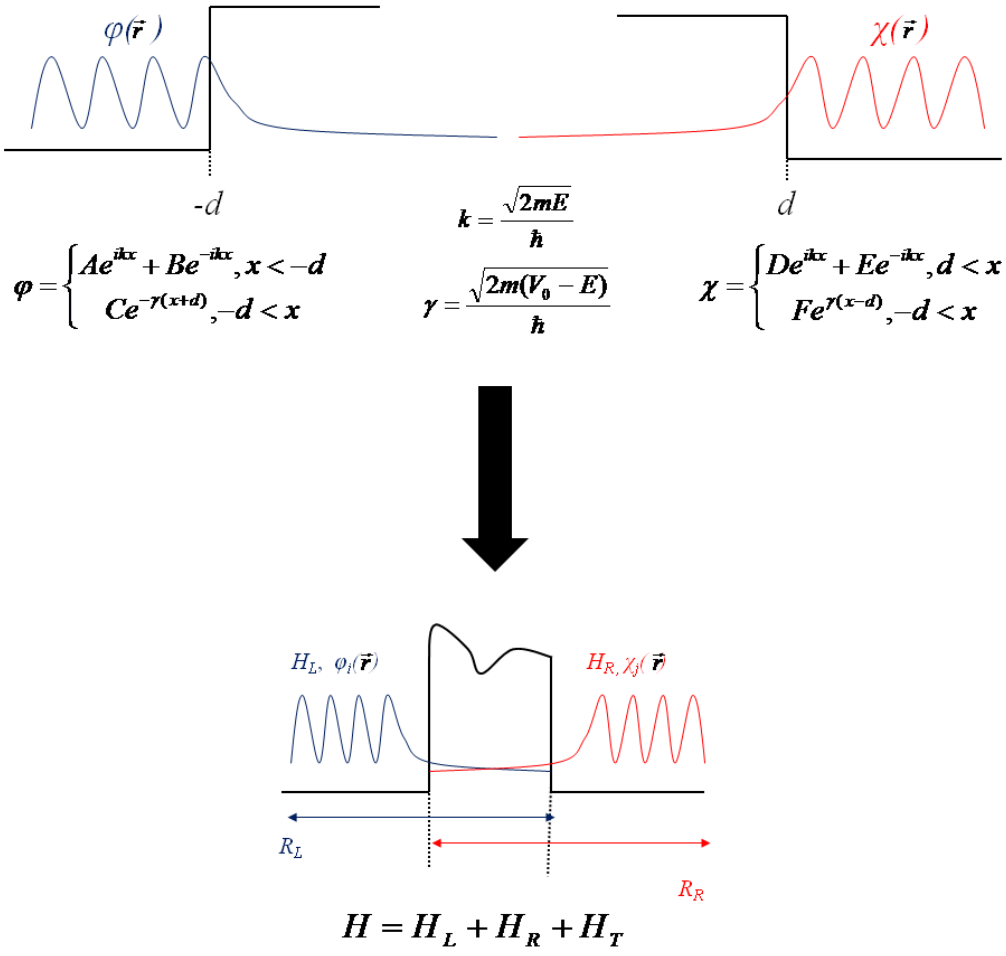

Figure 2.3: Bardeen's Transfer Hamiltonian Theory: Initial states of the tip and sample are considered separately as shown. When they are brought together they begin to interact through a transfer Hamiltonian.

probability is related to an unknown transfer Hamiltonian, H_T. Bardeen assumed that, when a tunneling event occurs, the transfer Hamiltonian would act to empty a state in one system and fill a state in the other. This would occur with a certain probability determined from a tunneling matrix M. The elastic tunneling current from a sample state of energy ϵ (with respect to the Fermi level) to an available state in the tip at the same energy is then:

$$I_{s\to t} = -2e\frac{2\pi}{\hbar}|M_{\mu\nu}| \underbrace{(\rho_S(\epsilon)\cdot f(\epsilon))}_{\text{Number Filled States in Sample}} \underbrace{\rho_T(\epsilon+eV)\cdot[1-f(\epsilon+eV)]}_{\text{Number Empty States in Tip}} \quad (2.3)$$

where the number of participating electron states, is determined by the densities of states of the sample (ρ_S) and tip (ρ_T) and the Fermi distributions of each. $M_{\mu\nu}$ is the matrix element describing the transfer probability suggested by Bardeen and is given by:

$$M_{\mu\nu} =< \psi_\mu|H_T|\chi_\nu >= \frac{\hbar^2}{2m}\int(\psi_\mu\Delta\chi_\nu^* - \chi_\nu^*\Delta\psi_\mu)\cdot d\mathbf{S} \quad (2.4)$$

A total tunneling current is found by integrating over all energies and summing over the currents in either direction (tip to sample, sample to tip). Furthermore, by assuming a low temperature (hence a step wise Fermi distribution) and a low bias voltage the total tunneling current reduces to:

$$I = \frac{4\pi e}{\hbar}\int_{-1/2eV}^{1/2eV}\rho_S(E_F+\frac{1}{2}eV+\epsilon)\rho_T(E_F-\frac{1}{2}eV+\epsilon)|M(\epsilon)|^2 d\epsilon \quad (2.5)$$

The matrix elements are often assumed to be relatively constant but in reality the energy dependence of the matrix elements can in fact have a significant effect, particularly at higher applied biases. Tersoff and Hamann [57] applied s-wave tip orbitals to the above equations and more complex tip states have since been applied [58]. The resulting expressions for the tunneling current can be quite complicated.

Together, the WKB approximation and Bardeen's Formalism have been useful in understanding the foundation as well as results from STM. In many cases, the two have been found to provide qualitatively similar results.

2.3.2 Obtaining an Image

The most common and safest method of obtaining an STM image is through constant-current imaging. Once within tunneling distance from the sample at a specified sample voltage, the tip is raster scanned across the surface while a feedback loop maintains a constant tunneling current. The height of the STM tip required to maintain the current is recorded as a function of surface position. Though often described as a "topographic image" the STM image is not strictly a depiction of

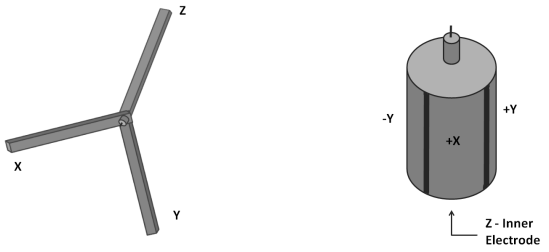

(a) Tripod Scanner (b) Tube Scanner

Figure 2.4: Common Piezoelectric scanners used in STM.

the surface real space topography. As the tunneling theory indicates, the tunneling current depends upon the tunneling distance as well as the local densities of states of both tip and sample. One must therefore be careful of one's interpretation of STM micrographs.

The ability to raster scan the surface while maintaining a tunneling gap between the sample and tip is imperative to the operation of an STM. The fine control of the STM tip position is accomplished through the use of piezo scanners. A piezoelectric material is one in which an applied voltage induces a change in physical dimension (or vice versa). Piezo scanners make use of this effect to achieve extremely small changes in position. Two common types of scanners are the tripod (Fig 2.4(a) and tube scanners (Fig 2.4(b)). The former is an intuitive and simple method of obtaining three dimensional movement through the use of three independent piezoelectric elements. Such scanners exhibit low sensitivity to piezo creep but are rather bulky in overall size. The latter, the tube scanner, is a rather ingenious design consisted of a tube with a single inner electrode and four outer electrodes - each occupying a quarter of the circumference. The inner electrode drives the STM z-signal - which is effectively the "height". Application of bipolar voltages to opposite outer electrodes (i.e. electrodes not beside each other), can induce a bending motion in the tip in order to control x or y motion. The tube scanner is more compact in design and exhibits a relatively high resonance frequency rendering the instrument more noise immune. However, cross-talk between channels must be taken into account and the design is sensitive to piezo creep. Cross-talk is the effect by which a voltage applied to one channel (such as the x-axis) causes a change in another channel (such as the z-axis). Piezo creep is related to the response time to a voltage change applied to the piezo.

Some of the most challenging considerations that are required for the successful

operation of an STM are mechanical and electrical noise as well as the cleanliness of the sample and tip. As mentioned above, the scanning tip must be maintained at distances of only a few angstrom from the surface. Building vibration and/or acoustic noise can easily destroy the ability to perform measurements. Commonly used vibration isolation systems often make use of an internal spring suspension system with eddy current damping [58]. Microscope units themselves may be mounted on active vibration cancellation systems [59]. In addition to vibrational noise, electrical noise can also significantly effect the resolution of STM images. Electrical noise largely originates from ground loops and incorrectly configured leads. As such, electrically isolating STM electronics and reducing the distance from the measurement point to the current amplifier can significantly reduce noise. High resolution STM also requires the ability to create and maintain atomically clean tip and sample surfaces. One of the primary factors in determining how long a surface can be maintained clean is the number of gas molecules impinging on the surface from the gas phase. Thus, to ensure that the background pressure does not significantly effect the sample under study, the use of ultra-high vacuum (UHV), 10^{-12} Torr to 10^{-9} Torr, environments are often required. The instruments and techniques used to achieve and measure UHV pressures have been described in detail elsewhere [60,61]. Section 2.5 details the general background pressures achieved in the instruments used throughout this work. A more detailed examination of noise and pressure considerations will be discussed through the context of optimizing the Multiprobe STM System in the appendix.

2.4 Other Techniques

2.4.1 Tip Preparation

In 1988, Demuth concluded that tip treatment was one half of an STM experiment [62] and even at this time it was not an expression of a new sentiment. Tip quality and preparation methods were considered since before the realization of a functional STM [53]. Simply put, the production of high quality STM studies is directly dependent upon the STM tip. Ideal tips have a small aspect ratio in order to reduce mechanical vibration. The tip apex must terminate in a single atom in order to achieve atomic resolution. However, the tip configuration should also be stable enough to create realiable and reproducible images. In addition, the tip must be clean in order to ensure a stable tunnel junction with a relatively flat density of states near the Fermi level.

For the studies presented in this dissertation, preparation of an STM tip involved

an electrochemical etching process followed by a combination of various UHV cleaning procedures. 0.25 mm diameter polycrystalline tungsten wire was cut and etched in 2M NaOH solution. Due to concentration gradients of etching products and reactants, the etching rate is enhanced at the bottom of the meniscus between the tip and solution. The weight of the wire below the neck eventually causes the wire to break and the circuit is quickly shut off in order to leave behind a sharp tip. Etched tips were lightly washed with deionized water, dried with pressurized air or nitrogen gas and visually inspected using an optical microscope. Those tips which appeared "sharp" were prepared in a manner appropriate to the UHV-STM system in which they were used. For the Omicron systems (STM1 and VT-STM) this required mounting in specially designed tip holders and for the Multiprobe system the tip was cut to 13.5-14.0 mm in length before loading into the tip slots in the system's load lock arm.

Once in UHV, several cleaning procedures were used to remove oxide, contaminants and otherwise clean the tip as well as to determine its potential for use in the STM. Tip cleaning techniques used included simple annealing, electron bombardment (EB), field emission (FE) [or field emission microscopy (FEM)] and/or Field-Ion Microscopy (FIM).

Simple annealing to a temperature of roughly 1200 K is often used to remove contaminants from both the shaft and the apex of the tip. This was particularly useful in the Multiprobe STM, where annealing by passing a current through the tip was facilitated by the system design.

In EB, a filament is heated so that it emits electrons. The emitted electrons strike the tip, which is biased positively with respect to the filament. The process can help remove adsorbates on the tip or reshape the tip itself. EB is quite fast however it can be harsh and somewhat unpredictable. In FE, a high negative voltage is applied to the tip. With a sharp tip, the field at the apex is high enough to cause the field emission of electrons. The resistive heating effect can lead to tip cleaning. FE is more gentle than EB but often requires more time (many hours in comparison to several seconds) to obtain a stable tip. However, as the FE current increases directly with a decrease in tip radius, monitoring the current drawn from the tip and the required voltages can also be a good diagnostic tool to help determine if the tip is sharp. A combination of EB and FE cycles can often yield quite satisfactory results with relatively fast turnover.

Field emitted electrons can also be imaged by replacing the filament with a fluorescence screen to form a field emission microscope (FEM). The screen captures a map of the electrons which have traveled along the field lines after being emitted from

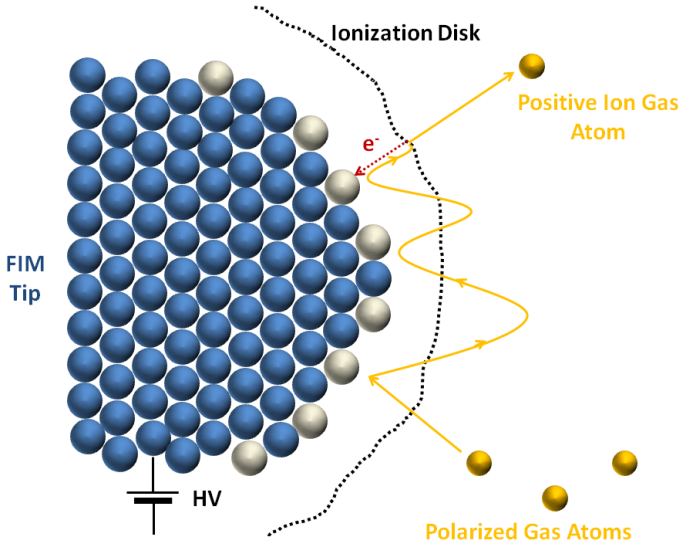

Figure 2.5: Image Formation in Field Ion Microscopy. Yellow: Imaging gas; Blue: tip atoms; Grey: tip apex atoms corresponding to positions of greatest field and thus greater imaging probability.

the tip. The emission of electrons strongly varies with the local work function, which in turn varies with the structure of the crystal plane. As such, FEM images indicate changes in the crystal planes. FEM has relatively poor resolution in comparison to field-ion microscopy, described below, but is a very quick technique and, unlike FIM, does not require an imaging gas which allows for better preservation of vacuum pressure. FEM was therefore sometimes used in the Multiprobe STM to quickly observe tips - particularly those used in the probes.

Field-Ion Microscopy is more involved then EB or FE. FIM was the first microscopy technique capable of imaging single atoms [63]. After its conception in 1951, it was used extensively for studying diffusion processes on sharp conductive surfaces or the end of tips. More recently, the use of FIM as both an imaging and cleaning tool for scanning probe tips has proven to be of great value - even allowing for the meticulous creation of single atom tips [64].

The FIM imaging process, summarized in Fig. 2.5, can only be conducted on sharp tips ($\leq$ 30nm radius) since the presence of a high local field at the tip apex is necessary. A high field is obtained by applying a large positive potential, in the range of 3-20 kV depending upon tip sharpness, to the tip. Often, the tip is also cooled to liquid nitrogen temperatures to increase resolution, however this was found to be unnecessary for general tip observation performed on a daily basis. An imaging gas, generally helium in the systems used, is introduced into the FIM vacuum chamber.

The electric field at a tip, causes a polarization of the imaging atoms and accelerates their trajectory towards the tip. At the tip, the gas molecule can lose some of its kinetic energy to the surface lattice through a thermal accommodation process. While the atom is within a critical distance - known as the ionization disk - of the high electric field of the tip apex, it can undergo field ionization. That is, the high field narrows and lowers the barrier seen by valence electrons in the atom thus allowing the atom to undergo auto-ionization by electron tunneling, a process first proposed by Oppenheimer in the late 1920's [65]. The positive ions produced are immediately projected outwards from the tip following the electric field lines. Collision with a microchannel plate allows for the conversion of the ion signal to an electron signal as well as signal amplification. Each atom on the tip maps to a unique location on the imaging screen thus allowing for visualization of the atomic structure of the tip apex. As the ionization probability of the imaging gas is highly sensitive to the local field, the probability changes substantially based upon local curvature changes caused by surface atoms. Thus, more signal is generated and atomic resolution can be obtained for protruding atoms and atomic step edges. Increasing the potential of the tip even slightly above the FIM imaging conditions increases the probability of field evaporation or the removal of surface bound atoms - including both contaminants and substrate (tungsten, in our case) atoms. Careful use of field evaporation allows one to clean and sharpen the tip, however, too much field evaporation can actually smooth the tip surface and decrease tip sharpness. Of the three systems used during this work, FIM was available and regularly utilized on the Multiprobe STM.

Figure 2.6 (a-c) provides some examples of FIM images of typical electrochemically etched tungsten tips that were annealed in UHV for approximately 10s. Figure 2.6(a) demonstrates a standard etched tip. The atom at the center of the concentric rings is the most protruded from the surface and is believed to be the imaging atom in STM. Figure 2.6(b) provides an example of a tip that was gradually withdrawn from the solution during the etching process. This enabled creation of high aspect ratio tips necessary to avoid collision of probe tips in the Multiprobe system. Figure 2.6(c) is an example of a particularly sharp tip and 2.6(d) is the corresponding FEM image. This provides an example of the resolution difference between FIM and FEM. With a standard tip, FEM does not truly provide an indication of tip shape; however, the voltage magnitude required to observe the signal is useful in gaining some insight into the relative sharpness of the tip.

For high quality STM studies, tip cleaning is not a one-time occurrence. It is imperative to use a clean sharp tip and maintaining such a tip is required to obtain

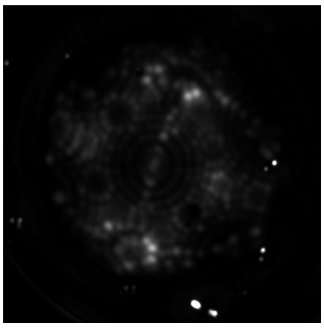

(a) FIM Image of a standard tungsten tip

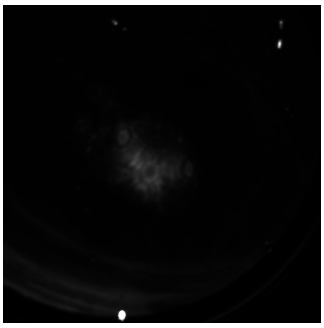

(b) FIM Image of a tip that was withdrawn from solution during the etch

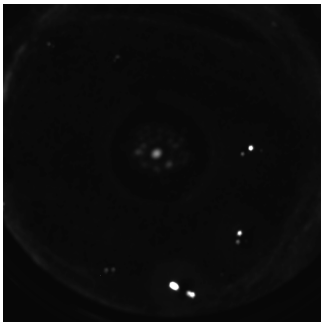

(c) FIM Image of a sharp tungsten tip

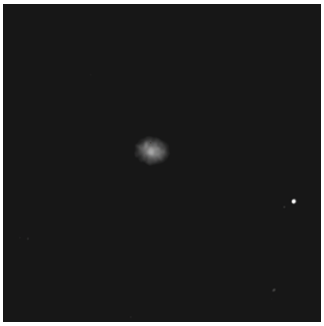

(d) FEM Image of a sharp tungsten tip

Figure 2.6: Example FIM and FEM Images of Etched and Annealed Tungsten Tips. The bright white dots on the images correspond to defects on the microchannel plate and should not be confused with tip structure - which largely appears gray in colour.

quality images and/or spectroscopic information about the sample throughout the analysis. This is particularly true after dosing molecules in the vacuum chamber. Contaminants and multiple sharp protrusions on the tip apex decrease the quality of STM images and can drastically alter the tip behaviour. For instance, it was found that tip contaminants can change the behaviour of STM induced desorption. Moreover, spectroscopic information is highly dependent upon the density of states of both the sample and tip. Contaminants on the tip can significantly alter the local density of states of the tip thus making the spectroscopy of the sample unreliable. It is often necessary to clean the tip in a gentle manner or in a manner that will allow one to retain the position of the tip on the STM sample being studied. In situ cleaning is accomplished through the application of voltage pulses, imaging at slightly higher voltages and currents and even FE to the sample surface.

2.4.2 Scanning Electron Microscopy

The use of scanning electron microscopy is crucial to studies performed on the Multiprobe STM. The Multiprobe STM is equipped with a JEOL TM-Z040161 model ultrahigh vacuum field-emission scanning electron microscope (SEM) mounted at a 45 degree angle to the sample. At the time of purchase, this SEM was one of the only UHV compatible, vacuum chamber mountable columns commercially available. The SEM on the system could be run under two modes: (1) Secondary Electron Imaging (SEI) and (2) Electron Beam Induced Current (EBIC) imaging.

SEI is one of the most standard detection modes in scanning electron microscopy. In brief, a secondary electron (SE) is a specimen electron that has obtained energy by inelastic collisions with beam electrons. The SE leaves the sample with a very small kinetic energy. The low energy of the SE ensures that only electrons near the surface can exit the sample and be detected. Furthermore, any changes in topography in the sample can change the yield of SEs. In our system, SEs are detected using an Everhart-Thornley detector [66] which primarily consists of a scintillator inside a Faraday Cage. A small positive voltage is applied to the Faraday cage to attract the SEs. A large positive voltage is applied to the scintillator to accelerate the incoming electrons prior to their conversion to photons. The signal is then amplified by a photomultiplier and converted to a voltage signal used to create the SEI. SEI thus provides information about morphology and surface topography. For our studies, SEI was used as the primary tool for the fine alignment of the three probes with respect to the other probes and structures on the surface. A typical example of a SE image of three tips in the multiprobe is provided in Fig. 2.7(a) and a higher magnification view of the main STM tip close to an EBL defined contact consisting

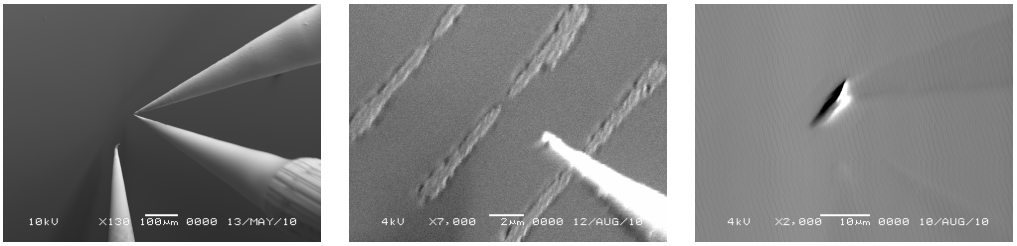

(a) (b) (c)

Figure 2.7: Example SEM Images (a) Typical SE image of the three tips in the Multiprobe (b) SE image of main tip near EBL Defined contacts (c) EBIC image of one tip touching down on the right hand side of a contact.

of two titanium silicide contacts separated by a small gap is presented in Fig. 2.7(b).

EBIC imaging is a much less common mode of imaging than SEI [36, 67]. In EBIC, the primary electron beam induces a current in the sample which can be collected with a current amplifier. The current collector is the only grounding point on the sample. Thus, as the primary beam is scanned across the sample, only regions that have a current path to the collector will produce a signal on the image. An EBIC image is formed through the display of this current. For our studies, the current collector was generally one of the probes of the multiprobe system, and a low noise current to voltage amplifier (FEMTO DLPCA-200, set at a gain of 10^6 V/A) was used to collect the signal. In this manner, the connectivity of structures on the sample as well as the connectivity of the sample itself to the probe can be tested. An example of an EBIC image of one STM tip in contact with an EBL defined contact is provided in Fig. 2.7(c).

2.5 UHV-STM Systems Utilized

Three different UHV-STM systems - referred to as the "STM-1", the "VT-STM" and the "Multiprobe" - were used throughout my doctoral research. Like most instruments, each of these systems has its own advantages and disadvantages. The first two systems consisted of commercial STM units purchased from Omicron NanoTechnology GmbH combined with specially designed vacuum systems while the later is a completely custom designed homebuilt system. All three systems consisted of at least three connected vacuum chambers with transfer capabilities between the chambers:

1. The load lock allowed for convenient introduction of samples and tips into the

system while maintaining the UHV pressure of the main chambers.

2. The preparation chamber provided a region dedicated to the in-vacuum preparation of both samples and tips.

3. The main STM chamber housed the STM unit.

In addition to the main UHV chambers, each system contained 'dosing' lines connected to the chambers for the introduction of molecules into the chamber via variable leak valves. In all systems the main chambers were pumped with ion and titanium sublimation pumps (TSPs). The load locks and dosing lines were generally pumped with turbo-molecular pumps backed by a roughing pump. Pressures in the main chambers were monitored with ion gauges while those in the load lock and dosing lines were generally monitored with convectron gauges. On all three systems, the vacuum quality and molecular doses could also be monitored using a quadrupole mass spectrometer.

2.5.1 STM-1 System Overview

The Omicron 'STM-1' [68] system is highly regarded for its simplicity and high resolution. The first iteration of the STM-1 system was commercially available within a year after the Nobel Prize was awarded to Binning and Rohrer. It was the first commercial system to introduce eddy current vibration isolation. The system has had a great impact in the STM community and is often considered as an industry standard. Table 2.1 provides a summary of some of the STM-1 system's capabilities and areas of this dissertation in which it was utilized.

2.5.2 VT-STM System Overview

The Omicron variable temperature STM or "VT-STM" [69], has the advantage of performing experiments at temperatures in the range of 25 K to 1500 K through the combination of heating and cooling procedures. In the system's design, the sample temperature varies while the microscope stage and STM tip holder remain at ambient temperatures. Heating is achieved either by direct heating by passing a current through the sample or indirect resistive heating through the incorporation of a heating element on the sample plate. All heating performed in this dissertation was through direct heating. Reduced temperature STM is achieved either with a liquid nitrogen or liquid helium continuous flow cryostat. Liquid helium was used for studies in this work. While the VT-STM allows for variable temperature, it has an increased sample holder complexity and generally less crisp image quality

with respect to the STM-1. Table 2.1 provides a summary of some of the VT-STM system's capabilities and areas of this dissertation in which it was utilized.

2.5.3 Multiprobe System Overview

The 'Multiprobe' system, was designed and built by Mark Salomons, P. Eng., an engineer in our group, along with Dr. Janik Zikovsky - a former graduate student. This is a novel system with three fully functional STM scanners and an integrated SEM for probe positioning. A detailed account of the unique features and capabilities of this instrument has been reported by Dr. Zikovsky in his doctoral dissertation [36]. The central STM scanner is mounted perpendicular to the sample, has the best resolution and is often referred to as the main STM tip. The two remaining STM scanners are mounted at an angle of 45 ° to the sample and are often referred to as the STM probes. As mentioned in 2.4.2, the sample and tip positions in the Multiprobe are monitored with a UHV compatible commercial SEM column. The SEM can also be used to study the sample surface and tip quality. This system has the great advantage of being able to perform multiple probe measurements as well as greater sample throughput. However, again with increased functionality comes increased complexity. Some of the challenges that were faced in optimizing the system's performance are described in the following section.

Table 2.1 provides a brief summary of some of the primary differences between these systems as well as their use throughout this thesis. One feature not mentioned in the table is the sample throughput. The throughput relates to the time required between having a sample in air and being able to image it in the STM. Both Omicron systems require loading the sample into a special holder. The STM1 holder is quite simple in design while the VT-STM holder is rather complex. The load lock for the Omicron holders were able to accommodate one sample or one tip at a time. In the Multiprobe, there was no sample holder and four tips and four samples could be loaded simultaneously. In all systems, the load lock chamber was pumped with a turbo pump for at least half an hour before opening it to the main chambers; however, an hour or longer would generally be better for all. Both the Omicron sample holders required degassing overnight at 600 °C before a sample can be prepared. In the Multiprobe system design, samples generally only required a 600 °C degas for 5-10 minutes depending upon how well the load lock was pumped before transferring the sample. However, it was found that the best surface quality was seen if the pliers, the system for holding the samples and tips, were degassed occasionally using an old sample at 600 °C for several hours or overnight. After sample preparation, the samples require cooling in order to avoid thermal drift in

Table 2.1: Comparison of UHV-STM System Features. Base Working Pressure is the general pressure achieved during every day use of the instrument (i.e. with standard exposure to molecules used in this work). Lower pressures could be achieved for example, after a system bake.

System	Omicron STM-1	Omicron VT-STM	Multiprobe
Scanner Type	Tripod scanner	Tube scanner	Tripod scanner on main STM, Tube scanners on probes
Resolution	Best	Good	Good on main STM, somewhat lower quality on probes
Noise	Very Good	Good	Ok
Base Working Pressure (STM chamber)	9×10^{-11} Torr	8×10^{-11} Torr	See sec (A.1.1)
Operation Temperature	Room Temperature	50K - 1100K	Room Temperature
Drift at Stable Temperature	Extremely Low	Greatest of the three	Low
UHV Tip Preparation	EB, FE (now has FIM and FEM)	EB, FE	EB, FE, FIM, FEM, direct heating
Multiprobe	No	No	Yes
Other Facilities	RGA, optical camera, pyrometer, H_2 cracking filament, Ag evaporation source	RGA, optical camera, pyrometer, H_2 cracking filament	SEM (SED, EBIC), RGA, optical cameras, pyrometer, H_2 cracking filament, Tectra e-beam evaporator
Software	Scala (Omicron) Software control	Scala (Omicron) Software control	Nanonis Software used for main STM, Homebuilt STM.net software [36] interface used for probes
Summary	Ease of use combined with high resolution!	Variable Temperature!	Multiprobe Techniques!
Thesis Areas	spectroscopy measurements, diffusion studies	Ordering in Lines, 1,4-cyclohexadiene studies	Multiprobe system optimization, I_T/V_S near titanium silicide contacts

Si(100)				
	n-type (As)		p-type (P)	
Doping Level	Resistivity ($\Omega \cdot cm$)	Dopant Density (cm^{-3})	Resistivity ($\Omega \cdot cm$)	Dopant Density (cm^{-3})
High	0.003 - 0.004	1.6×10^{19} - 2.3×10^{19}	0.001 - 0.003	2.0×10^{19} - 8.0×10^{19}
Medium	0.08 - 0.1	8.0×10^{16} - 1.1×10^{17}	0.01 - 0.03	5.0×10^{17} - 4.0×10^{18}
Low	1 - 5	9.0×10^{14} - 5.0×10^{15}	1 - 5	9.0×10^{14} - 5.0×10^{15}

Table 2.2: Properties of Silicon Wafers Used

the images. The STM1 required a minimum of 20 min to cool while the VT-STM required at least an hour. Again, the elimination of the holder in the Multiprobe allowed samples to cool faster and they could be used directly after preparation. In summary, in terms of throughput, the Muliprobe offered the best results followed by the STM1 and finally the VT-STM.

2.6 Sample Materials and Preparation

2.6.1 Silicon Samples

Silicon technology dominates the semiconductor industry. Despite being an indirect band gap material, silicon has been esteemed for its ability to interface well with dielectrics, maintain its semiconducting properties at high temperatures and its high availability with relatively low cost. Bulk silicon is formed in the diamond crystal structure such that each atom has a tetrahedral bonding configuration. The two most commonly used surfaces are the Si(100) and Si(111) surfaces. In this dissertation, research focused on the Si(100) surface.

Silicon wafers were purchased from Virginia Semiconductor at various doping levels summarized in Table 2.2. All wafers were grown using the Czochralski process [70]. The resistivities given are for the bulk (units of $\Omega \cdot cm$) but the sheet resistance at the surface (units of Ω/square or $\Omega/\square$), can vary greatly depending on, for example, surface reconstruction, surface defects and preparation technique.

In order to minimize surface energy, the bonding configuration at the surface reconstructs in order to maximize the number of surface atoms with a fully bonded configuration. Even after reconstruction, the surfaces are generally quite reactive and hydrogen-passivation is often employed to modify surface behaviour. The primary surfaces of interest in this work are the clean Si(100):2×1 surface and its

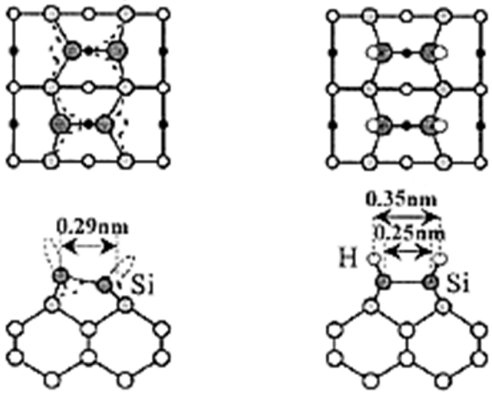

(a) Clean Si(100):2 × 1 (b) H-Si(100):2 × 1

Figure 2.8: Top and Side View Schematic Models adapted from [71]

hydrogen passivated counterpart.

In modern electronics, the Si(100) surface is the most commonly used surface. In order to reduce surface energy, the clean Si(100) surface reconstructs to form a surface layer that has double the periodicity as the bulk in one direction and the same periodicity in the other. This 2 × 1 surface structure, schematically depicted in Fig. 2.8(a), has become a surface of some import. The Si(100):2 × 1 surface is composed of rows of π-bonded Si dimers separated by 'gulley' regions. In many ways, the Si(100):2×1 surface mimics an alkene organic reagent as the weak π-bonds of the surface dimers are highly reactive. The dimers themselves are characterized by a bistable 'buckled' structure, in which one Si atom protrudes slightly and the other dips slightly into the surface [20]. This Jahn-Teller like distortion is dynamic at room temperature unless stabilized by a nearby defect. The distortion is also associated with a zwitterionic character in the dimer: the protruded atom, being more sp3-like, carries a slight negative charge while its low lying partner, being more sp2-like, carries a slight positive charge.

The Si(100):2 × 1 surface is formed in UHV by simply flashing the sample to 1470 K. This flash is often repeated several times in order to fully remove the native oxide as well as help remove carbon contaminants from the surface.

The clean silicon surface is often passivated with a monolayer of hydrogen. The H-Si(100):2 × 1 surface, Fig. 2.8(b), is very similar to the Si(100):2 × 1 surface, however the addition of hydrogen to each surface Si atom removes the π states and the buckling structure. This surface was prepared from the Si(100):2 × 1 surface by first backfilling the preparation chamber with hydrogen molecules (10^{-6} Torr)

which are then cracked to atomic hydrogen with a tungsten filament held at 2100 K. The sample is flashed to 1470 K and then lowered to a temperature to 570 K and held for two-four minutes depending upon the system and the particular alignment with respect to the cracking filament.

Hydrogen termination of the surface does not lead to complete hydrogen coverage. Some silicon surface sites remain uncapped by hydrogen. These sites are often referred to as 'Dangling Bonds' (DBs). In STM, the DB sites appear brighter or taller than the surrounding terminated regions due to greater LDOS at the DB at the energies probed by STM. DB sites may also be associated with negative (two electron occupation), neutral (one electron occupation) or positive (zero electron occupation) charge states. Neutral DBs can be thought of as surface radicals. The charge state of a DB is affected by many conditions including: the doping level of the crystal, possible band bending near the DB, sample bias as well as the proximity to other DBs and defects.

The surface of a silicon wafer is not atomically flat. Using the STM, flat silicon terraces separated by step edges are seen along the surface. On Si(100):2×1, the terraces above and below a single step edge have dimer rows oriented in perpendicular directions to each other.

Sample handling and processing plays a crucial role in surface quality. Contaminants, such as nickel and carbon, can be easily transferred to the sample from, for instance, contact with dirty/stainless steel instruments. Both nickel and carbon can have a severe effect on the surface and electronic properties. Nickel can cause dimer defects, agglomeration of vacancy channels and macroscopic surface roughening with increasing contamination [72]. Carbon tends to cause the formation of large peaked islands topped by carbide and surrounded by silicon with a high step density [73]. Samples were thus handled and prepared with caution both while outside and inside vacuum.

2.6.2 Surface Molecules

Throughout the course of this work, I will often refer to the 'dosing of a molecule' into the vacuum chamber. In such instances, the chemicals used were introduced into the chamber in the vapor phase through a variable leak valve. All solid and liquid chemicals used as surface adsorbates were purchased from Sigma-Aldrich in purities of 99+%. Prior to introducing the molecules into the chamber they are treated to help ensure their purity upon entering the chamber.

For room temperature gases, such as hydrogen and helium, the gas line is run through a liquid nitrogen cold trap. This helps freeze out any impurities, primarily

water, that may otherwise have been introduced into the chamber along with the gas of interest.

Liquids at room temperature are degassed using several Freeze-Pump-Thaw (FPT) cycles [74]. FTP cycling makes use of Henry's law which states that the amount of dissolved gas in a liquid is proportional to the partial pressure of the gas above the liquid. In a FPT cycle, the molecule is first flash frozen by immersion into liquid nitrogen. While the liquid is frozen, the gas above it is pumped out using a turbomolecular pump for 2-3 minutes. The liquid is then isolated from the vacuum pump and allowed to thaw - thereby releasing any dissolved gases. This process is repeated until no visible bubbles emerge while thawing.

Only one room temperature solid was used during this work - (2,2,6,6-Tetramethylpiperidin-1-yl)oxyl or TEMPO for short. It was treated by simply pumping the gas above the solid for several minutes with a turbomolecular pump.

Once clean, the gaseous molecules were introduced into the vacuum chamber through a variable leak valve. In all cases, the vacuum lines connecting the molecular source to the leak valve on the chamber were cleaned by pumping overnight and/or purging with the gas of interest. This was particularly important when a gas line and leak valves were switched from one molecule to another.

The gas exposure or 'dose' of a molecule is typically measured in Langmuirs (L) [75] where 1L is equivalent to exposure to a pressure of 10^{-6} Torr of the gas for 1 second - the approximate dose to create a single monolayer of a molecule with a sticking probability of unity. In cases where the vapor pressure of the molecule was low, such as vinylanthracene in chapter 7, it was heated with a warm water or oil bath. In some cases, the dosing line was also heated to ensure that the molecule remained in the vapor phase. The pressures and doses reported in this work were taken with an ion gauge placed in the vacuum chamber. Ion gauges are typically calibrated for nitrogen gas and the sensitivity can vary for other molecules; however, in this thesis the gauge readings have not been corrected for different molecules.

Chapter 3

STM Spectroscopy: Surfaces

3.1 Chapter Introduction

Modern electronics relies on the ability to understand and manipulate electrical current in devices. As mentioned in the introduction, the ability to gain such control at the molecular scale is one of the great challenges of nano-electronics. To achieve this goal we must first gain a better understanding of how a single molecule or even a single monolayer of molecules can alter the transport properties from a surface. The STM offers scientists the ability to probe such effects - particularly through methods related to scanning tunneling spectroscopy (STS).

In this chapter, we will begin by introducing the theory behind STS. We will then proceed to study the behaviour of the tunneling current from the clean n^+−Si(100):2× 1 surface followed by an exploration of the effect of passivating this surface with a monolayer of hydrogen and a monolayer of styrene. It will be shown that these simple molecules can tune the current rectification ratio. The mechanism leading to such current-voltage behaviour will be discussed in terms of a simple qualitative energy band model. The results of the clean and passivated surfaces form the subject of a recent article [76]. Similar measurement techniques will then be used to study how an STM tip can shadow a region of the surface from vapor phase molecules (specifically styrene) in the vacuum chamber.

3.2 STS Theory

Interestingly enough, the original concept of STM arose not out of the goal of achieving an atomic resolution microscope but instead "to perform spectroscopy locally on an area less than 100 Å in diameter" [53]. Scanning tunneling spectroscopy (STS) surpassed this goal by enabling the study of the local density of states down to regions more than 10× smaller than the original goal. STS generally refers to

an analysis of the tunneling current versus sample bias voltage (I_T/V_S) behaviour. More generally, STS can also include an analysis of current versus tip-sample separation (I_T/Z) and/or tip-sample separation versus sample bias (Z/V_S) behaviour. I_T/V_S and I_T/Z analysis were performed for this body of work and are described in more detail below.

3.2.1 Tunneling Current versus Sample Bias (I_T/V_S)

In STS, spectroscopic information can be determined due to the connection between the tunneling current and the density of states of the tip and sample - ρ_S and ρ_T respectively. From the Bardeen tunneling theory discussed in 2.3, the tunneling current with an applied bias V, is given by equation 2.5:

$$I = \frac{4\pi e}{\hbar}\int_{-1/2eV}^{1/2eV} \rho_S(E_F + \frac{1}{2}eV + \epsilon)\rho_T(E_F - \frac{1}{2}eV + \epsilon)|M(\epsilon)|^2 d\epsilon \qquad (2.5)$$

If the matrix elements are assumed to be relatively constant, the derivative of I with respect to voltage - the conductance - can be directly related to the densities of states of the tip and sample. Moreover, the main contribution can be assumed to originate from a small energy interval near $\epsilon = \mathrm{eV}/2$. For a positive sample bias $V_S > 0$, the electrons tunnel from occupied states in the tip into empty states of the sample:

$$\frac{dI}{dU}_{U=V} \approx \rho_S(E_F + eV)\rho_T(E_F) \qquad (3.1)$$

For a negative sample bias, $V_S < 0$, the electrons tunnel from occupied states in the sample to unoccupied states in the tip:

$$\frac{dI}{dU}_{U=V} \approx \rho_S(E_F)\rho_T(E_F + e \mid V \mid) \qquad (3.2)$$

In the WKB approximation, by differentiating equation 2.1 the conductance [55] is found to be :

$$\frac{dI}{dU}_{U=V} = \rho_S(r, E_F)\rho_T(r, 0)T(eV, eV, r) + \int_0^{eV} \rho_s(r, E)\rho(r, E - eV)\frac{dT(E, eV, r)}{dV}dE \qquad (3.3)$$

The transmission probability is assumed to increase smoothly and monotonically with the applied bias. As such, the first term in 3.3 is considered the dominant term. In order to normalize the effect of the transmission probability in the first term, Feenstra et al. proposed dividing the conductance by an averaged ratio of I_T/V_S [77, 78] such that:

$$\frac{\frac{dI}{dU}_{U=V}}{\frac{I}{V}} = \frac{\rho_S(r, E_F)\rho_T(r, 0) + \int_0^{eV} \frac{\rho_s(r,E)\rho(r,E-eV)}{T(eV,eV,r)}\frac{dT(E,eV,r)}{dV}dE}{\frac{1}{eV}\int_0^{eV} \rho_S(r, E)\rho_T(r, E - eV)\frac{T(E,eV,r)}{T(eV,eV,r)}dE} \qquad (3.4)$$

The second term in the numerator of the left hand side, is believed to be related to the influence of the electric field and is assumed to be small, while the denominator normalizes the density of states. This normalized conductance is a dimensionless quantity and also offers the advantage of highlighting band edges.

Using both the Bardeen formalism and the WKB approximation, an ideal tip would have a constant DOS so that the observed conductance can be directly proportional to the sample DOS. In reality, this is not the case. However, to reach towards this ideal, a tip with a flat band structure near the Fermi level of the bulk solid, such as a metal (in this case, tungsten), is chosen. Furthermore, even with a tip approaching a constant DOS, one must be conscious of the effect of the state of the real tip on the conductance spectra. For instance, if a molecule is dosed into a chamber it may coat the tip altering its DOS and thus the observed spectra.

Spatial variation (mapping) and often the comparison of the I_T/V_S behaviour of different samples in STM deserves a special remark. The exponential dependence of the tunneling current with tip-sample separation can cause spatial mapping of the conductance to be convoluted with topographic information. Moreover, the conductance diverges as V approaches zero, preventing investigation of the densities of states near the Fermi level.

For the experiments performed in this thesis, the qualitative aspects of the tunneling current and voltage data were the primary concern. Direct current-voltage measurements were acquired in these experiments. Numerical derivatives of this data were found to be somewhat noisy and did not provide great insight on the exact sample DOS. Lock-in techniques used to directly measure the conductance were later set-up on the instrument, however this technique was not used for the results presented here.

3.2.2 Tunneling Current versus Tip-Sample Separation (I/z)

Since the advent of STM techniques, the height of the barrier that an electron sees when tunneling between the sample and tip has been of great interest to both experimentalists and theoreticians. The ideal vacuum barrier (Φ) is related to the work-functions of the tip (ϕ_T) and sample (ϕ_S) as well as the sample bias by $\Phi = \frac{\phi_T+\phi_S}{2} - \frac{qV_S}{2}$. However, the true work functions of tips and surfaces are themselves complex and are related to such aspects as the sample voltage as well as tip shape and placement. Using a simple model of a one-dimensional potential barrier and assuming an s-like wave function for the tip, an expression for an apparent barrier

height, Φ_A [79], has been found to be:

$$\Phi_A = \left(-\frac{1}{A} \frac{\mathrm{d}lnI_T}{\mathrm{d}z} \right)^2 \tag{3.5}$$

Where, $A = 1.025 eV^{-1/2} \mathring{A}^{-1}$.

Measurements of the natural log of the tunneling current versus the tip-sample separation can thus be used to measure the apparent barrier height of the sample material. The apparent barrier height is related to the microscopic work function of the sample and can be used to map materials on the sample surface or used to compare and understand the properties of different materials and structures.

Although, this one dimensional model has been of great use in a comparative analysis of similar systems, one must be careful in its use to real three dimensional systems. Moreover, it is widely recognized that STM apparent barrier heights of unpinned semiconductor surfaces "yield unusually low values" [80]. This barrier lowering is a complex phenomenon. The voltage difference applied to semiconductor systems, appears as a combination of the electric field near the sample surface and band bending within the sample [80]. The relative contribution of both effects depends partly on the tip-sample separation such that a larger separation results in a decreased potential at the unpinned surfaces and thus low apparent barriers.

Analysis of $\frac{dlnI}{dz}$ versus z, provides an indication of changes in the barrier height and can be used as an indication of direct contact between surface and tip. This graph is expected to be relatively flat for tunneling current measurements with a sharp drop indicating contact with the surface. It has been found that for passivated surfaces this drop can be more gradual [81]. In such cases, the inflection point is often taken as the point of contact.

3.3 STS Settings

The spectroscopy measurements performed in this work combines I_T/V_S and I_T/Z analysis. During measurement, every attempt was made to avoid obvious surface defects, such as clean silicon surface atoms on the H-terminated surface. The spectroscopy measurements were taken using a custom designed and optimized script in the Omicron Scala software. Typical imaging conditions of V = -2.0 V and I = 100 pA were used as a reference set point and then the STM feedback loop was turned off. The tip was then moved 3 Å away from the sample. From this distance, 9 I_T/V_S spectra were recorded in 1 Å increments towards the sample. Thus, spectra were recorded from distances (z values) of -3 Å to +5 Å from the set-point. All spectra represent tunneling spectra in the sense that true contact between tip and sample

was not reached. Any spectra for which contact was obvious, in the form of surface damage were excluded from the results. $\frac{dlnI}{dz}$ versus z analysis was also performed to ensure that a drop indicative of surface contact was not apparent.

For each individual I_T/V_S spectrum, the largest voltage range used for measurements was -2.5 V to +2.5 V in increments of 0.02 V. Presented I_T/V_S curves were taken only from low voltage to high voltage in order to reduce the total time taken for each measurement. During optimization of the macro, multiple sample spectra in both directions were taken to ensure limited hysteresis (indicative of a stable tip position) for measurement of similar time requirements. The voltage range for the spectra was reduced as the sample distance decreased in order to keep the current through the tip at a reasonable level as well as reduce chances of damaging the tip or sample during measurement. Spontaneous tip structural changes and surface damage is often apparent through spikes in the I_T/V_S curve as well as visible changes in the before and after images. All measurements where such anomalies were observed were removed from the analysis. I_T/V_S measurements in this chapter were averaged over 50 to 150 spectra with the lower averaging for the reproduction of the results for the clean silicon system.

It was also found that the lighting conditions in the UHV chamber had a significant impact on observed spectra. A standard laboratory tungsten halogen lamp (USHIO Lamp, EKZ bulb) with a wide spectral distribution is often directed into the UHV chamber at a distance of approximately 25 cm from the sample, in order to aid in STM tip placement and approach. Fig. 3.1 demonstrates how the lighting condition in the chamber using this lamp can affect the I_T/V_S spectra.

The spectra for 'Lamp off' refers to the general lighting in the room with no extra lighting directed into the chamber. At 'Low lighting' and 'Medium light', the lamp was set to low and medium intensity respectively. In either case, very little thermal drift was apparent in the STM images - indicating that sample heating was minimal. At the high setting on the lamp, drift was apparent in the STM images and in order to compare constant temperature measurements, the I_T/V_S behaviour at this condition is not included in Fig. 3.1.

It should also be noted that in order to compare I_T/V_S for the same z-position, the setpoint of $V_S = -2$V and $I_T = 100$pA for the illuminated spectroscopy measurements, was established prior to turning the light on - that is the feedback loop was turned off before the light was turned on and this was followed by a short delay to allow any transient effects to take place before the measurements were taken. As such, only the light off-condition spectroscopy intersects the setpoint on the graph. Measurements for the 'lamp off' case were taken both directly after turning off the

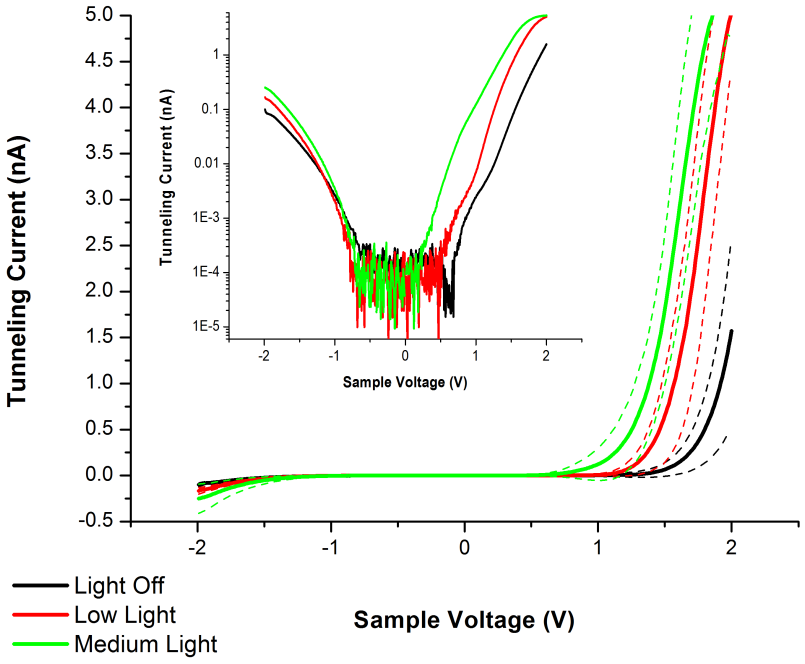

Figure 3.1: Effects of UHV chamber lighting on Current-Voltage measurements of medium n-type H-Si(100):2 × 1. The dashed lines indicate one standard deviations away from the average. The Black lines are results for while the lamp was off, Red for the lamp on low and Green for the lamp on medium. The inset shows the same data on a semi-logarithmic scale to highlight the differences between the settings. For clarity, the standard deviation is not shown on the inset.

feedback loop as well as waiting the estimated period of time required to turn off the lamp and the established short delay without any appreciable difference. As the lamp could be controlled from a distance, the total wait period was relatively short, however, it still demonstrates an advantage of the high stability of the STM1 system.

The main figure presents the average results for 30 I_T/V_S curves taken at the setpoint (no change in z) in a linear graph while the inset demonstrates the absolute value of the same results in a semi-logarithmic graph. The dashed lines in the main graph represent one standard deviation. It can be noted that the standard deviation can be quite high at the larger biases. For instance, at 2V in the light off condition, the standard deviation was found to be almost 1nA. This was found to be consistent for different settings and indeed for different surface passivations. In addition, it should be noted that detail in the I_T/V_S curves is more apparent in the logarithmic form. It is for this reason that the measurements in the remainder of the chapter will primarily be shown on a logarithmic scale.

The observed increase in tunneling current with increasing sample illumination can be understood by considering the effects of generating electron-hole pairs. Under constant applied voltage, the generation of electron-hole pairs causes a decrease in the surface potential and thus a lowering of the band bending and an increase in capacitance. In n-type silicon, in forward bias ($V_S < 0$) the lowering effect is in the same direction as the voltage effect on band bending. As such, the current onset is slightly earlier but in general there is little effect. In reverse bias ($V_S < 0$) the lowering effect opposes the voltage effect and a significant increase in current is observed.

In order to alleviate lighting effects on spectroscopy in the remainder of this chapter, the light was turned off for all measurements.

3.4 Tunneling Current Behaviour of Clean and Chemically Modified Si(100):2×1 Surfaces

3.4.1 Clean Degenerately n-type Si(100):2×1 surface

Before we can understand the effects of chemical modification of the silicon surface, we must first have a firm understanding of the behaviour of the underlying surface. This was explored in depth by Dr. Adam Dickie, a former post-doctoral fellow in our group [81] using an Omicron VT-STM system. I was able to reproduce these results on the STM1 [Fig. 3.2(a,b)]. Reproduction of the earlier observations not only with a different tip and silicon wafer but also with an entirely different system

and operator, indicate that the experimental findings are highly reproducible. The standard deviations of the average were quite large, very similar to those shown in the exploration of light effect in figure 3.1, but were also similar to the deviations found in the earlier work by Dr. Dicki.e. The observations and discussion of the clean high n-type Si(100):2 $\times$ 1 surface are summarized below for easy comparison with the modified surfaces discussed later.

As mentioned in section 2.6.1, the clean silicon (100) surface with the 2 $\times$ 1 reconstruction is composed of rows of buckled dimers. This buckling produces an asymmetric charge distribution resulting in a small intrinsic surface dipole pointing out from the surface (i.e. slightly elevated Si atoms are slightly negative) [82]. The dimerization process involves silicon-silicon σ and π bonding resulting in the creation of several different surface states. The π^* surface states enforce band pinning and provide a surface-parallel conduction channel [83]. The bands are pinned at approximately 0.2 eV and 0.4 eV below the valence and conduction band edges. This surface conduction channel increases in importance with decreasing tip-sample separation and low biases and is visible with the appearance of an ohmic shoulder region in the I_T/V_S spectra (arrow in Fig. 3.2(b)) and uncharacteristically low current onset voltages (Fig 3.3).

For the degenerately doped n-type surface, the Fermi level is located slightly above the conduction band and π^* state edges. Recent results in our group now suggest that the sample preparation technique of flashing to 1200 °C, may, in the case of As highly doped samples, result in slightly less than the expectant dopant density at the surface [84]. Nonetheless, we expect that the Fermi level is still quite close to or slightly above the band edge. The high surface state density explains the large currents observed in both the reverse ($Vs > 0$) and forward ($Vs < 0$) bias directions. Partial filling of the π^* state allows for majority carrier transport in both bias directions: electrons are able to tunnel out from occupied π^* states and into unoccupied π^* states. The change in current versus z in both bias directions is highly exponential indicative of the expected majority carrier tunneling behaviour. The transport characteristics are thus very similar in both bias directions leading to essentially zero rectification behaviour, hence the forward to reverse current rectification ratio, $RR_{F/R}$, is essentially constant at one (Fig 3.4). Using equation 3.5, the apparent barrier height at -1.5 V was found to be approximately 2.2 eV. This was, as expected, slightly less than the apparent barrier found for a lower doped n-Si(100)-2 $\times$ 1 surface [85]. An energy band model of the electron transport summarizing these effects is provided in Fig. 3.5.

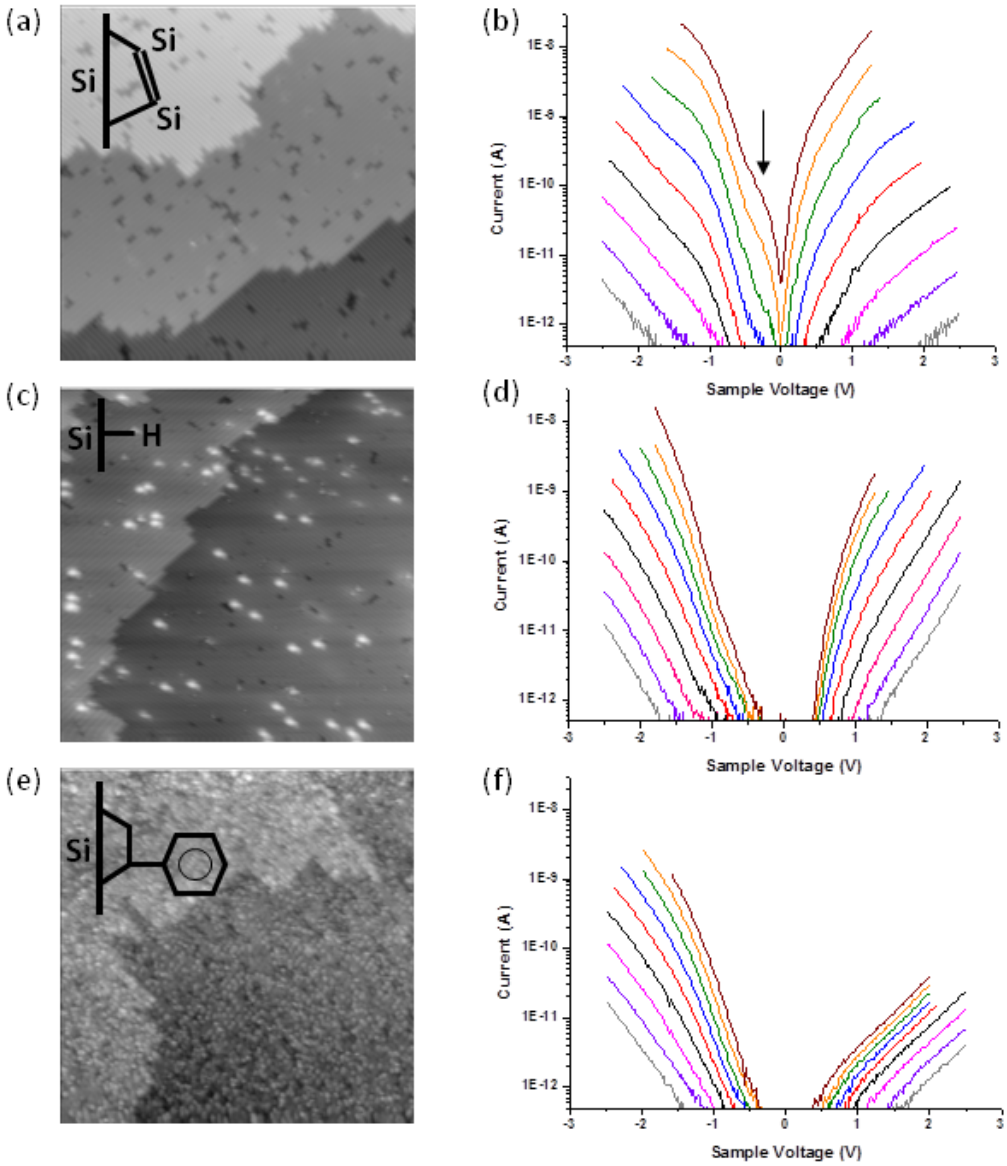

Figure 3.2: STM Micrographs and Spectroscopy of Surfaces: (a,c,e) 50 nm × 50 nm STM images taken at V_S = -2.0 V and I_T = 100 pA. (b,d,f) Averaged semi-logarithmic IV spectra for z = -3 Å(bottom curve) to +5 Å(top curve) towards the sample from the set-point. (a, b) Clean n^+-Si(100):2 × 1 surface. The arrow in (b) highlights the Ohmic shoulder region caused by surface-parallel conduction; (c, d) the hydrogen terminated surface; and (e, f) the styrene terminated surface. Adapted from [76], Copyright (2009) with permission from Elsevier.

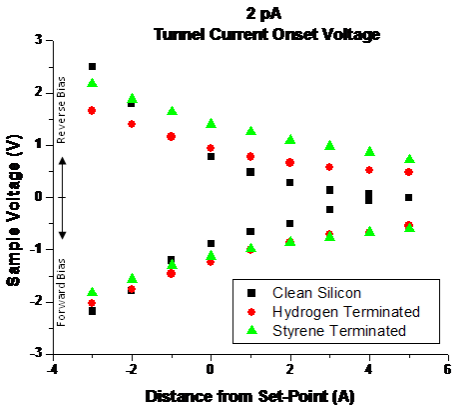

Figure 3.3: Onset voltages required for 2 pA tunneling current versus z. Reprinted from [76], Copyright (2009) with permission from Elsevier.

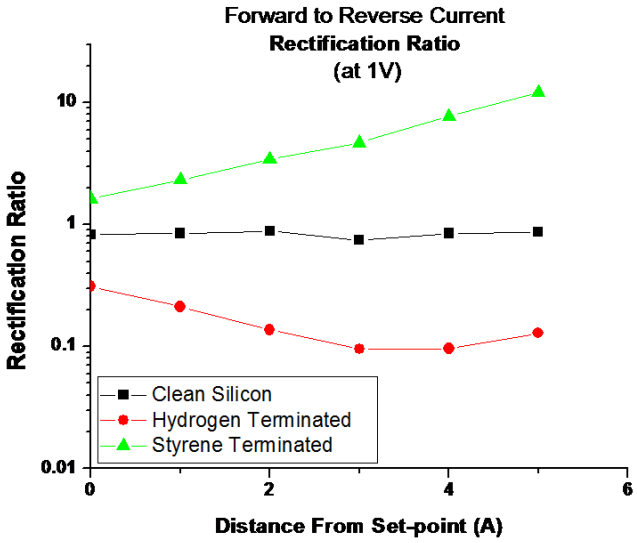

Figure 3.4: Forward to reverse current rectification ratios ($RR_{F/R}$) taken at $\pm$1V versus z. $RR_{F/R}$ for $z < 0$ are not shown as the currents in this region are very small (largely lie below the 1 pA current onset) and relatively noisy. Reprinted from [76], Copyright (2009) with permission from Elsevier.

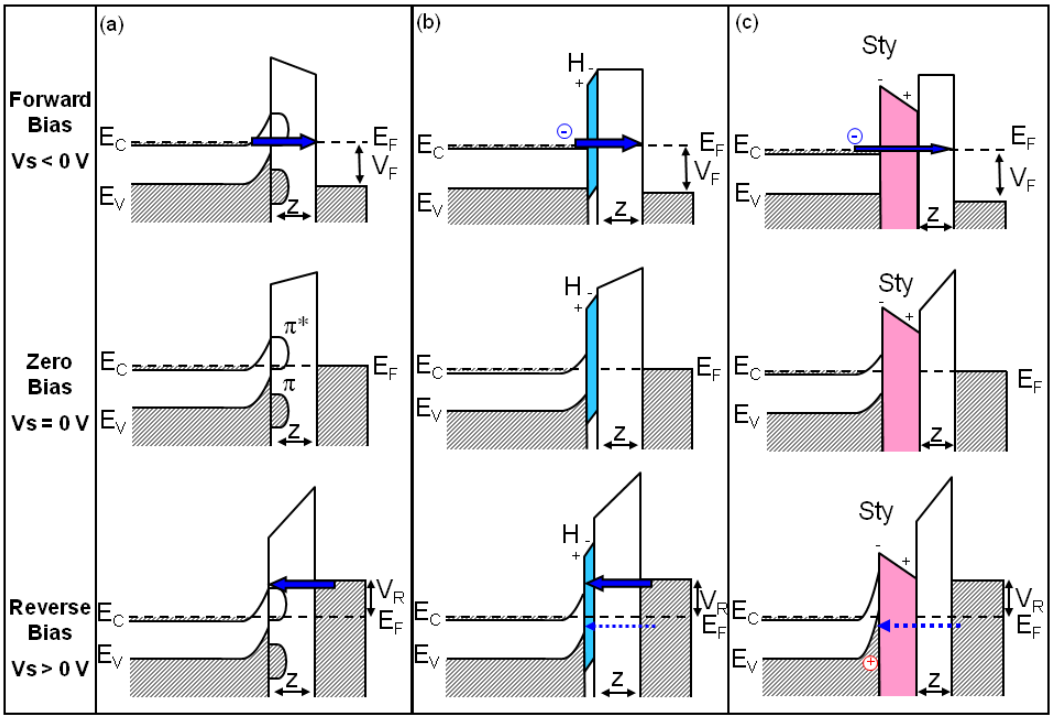

Figure 3.5: Energy band diagrams in forward bias (top), zero bias (middle) and reverse bias (bottom). (a) The clean n^+-Si(100):2×1 surface has pinned bands due to theπ^* surface states. Tunneling current is dominated by majority carrier transport in both polarities. (b) The hydrogen terminated surface has unpinned bands and a barrier due to the HSi bond polarity. Majority carrier current is dominant in both biases, however, the depletion region in reverse bias allows for a minority carrier component. (c) The styrene terminated surface has unpinned bands and a barrier due to the combination of CSi bond polarity, molecular dipole, the size and polarizability of the molecule. Majority carrier current is still dominant in forward bias however, due to increased tip induced band bending, the reverse bias current is minority carrier dominated.Reproduced from [76]

3.4.2 Preparation and Observations of Passivated Si(100):2×1 surfaces

In this study, two passivations of the clean surface were studied: (1) passivation with a monolayer of hydrogen and (2) passivation with styrene. The results shown in figure 3.2, demonstrate averaged results for a single tip and prepared sample. However, qualitatively similar results were found for different tips and samples for each system.

Passivating the n^+- Si(100):2×1 surface with a monolayer of hydrogen - also known as the silicon hydride surface and the hydrogen terminated surface - was prepared according to the H-termination procedure described in section 2.6.1. An STM micrograph of the surface and the averaged spectroscopy results are shown in Fig. 3.2(c,d) . For clarity, the standard deviations have not been shown in the figure. The deviations are quite large but are of similar magnitude to those found on the clean surface. The observations indicate large currents in both forward and reverse biases. In addition, the change in current with z is largely exponential in both bias directions. However, the I_T/V_S spectra are by no means symmetrical. In reverse (positive) bias, the tunneling current is consistently greater than those in forward (negative) bias. This is particularly observable by looking at the forward to reverse current rectification ratios displayed in Fig. 3.4 where it can be seen that the rectification at 1 V is lower than the clean surface and decreasing with increasing distance from the sample.

Passivation of the clean surface with styrene was accomplished by retracting the tip from the surface and exposing the clean surface to short (2-3s) doses of 1×10^{-9} Torr pressures of styrene vapour until close to monolayer coverage was observed with STM. As Fig. 3.2(e) indicates the coverage was not a perfect monolayer. However, it was found that further small doses resulted in messy surfaces where the underlying silicon step edges were not clearly visible[1]. Since STM has been used to monitor surface coverage, a natural question that might arise is: Why not make use of STM to monitor a continuous low exposure of styrene until monolayer coverage is observed on the surface? In fact, this method was used as the first attempt at creating styrene passivated surfaces. However, it was found that the presence of the tip in tunneling distance to the surface strongly affected the results. This will be discussed in detail in section 3.5. Styrene interacts with the clean silicon surface in a process analogous to a [2+2] cycloaddition reaction [32,86]. The STS data from the styrene terminated surface is presented in the final section of Fig. 3.2. As can be seen, the currents

[1]Incidentally, the I_T/V_S behaviour of these slightly overexposed surfaces was not very different from the spectra shown here. However, even further exposure created tip instabilities.

in forward bias are again quite large and change approximately exponentially with z. However, in reverse bias, the currents are observed to be quite low and with a sub-exponential change with z. This difference in current magnitude is observable as a $RR_{F/R}$ greater than 1 and increasing with tip-sample distance (Fig 3.4).

3.4.3 Discussion of Passivated Si(100):2×1 Surfaces

Hydrogen Passivated Si(100):2×1 Surface

To understand the changes in the spectroscopic signal in going from the clean silicon(100)-2×1 surface to the Si(100):2×1 hydride surface, it is important to first consider the chemical changes of the surface layer. This surface preserves the underlying 2×1 reconstruction but removes π and π^* surface states and introduces a Si-H sigma bond state. Removal of the π and π^* surface states removes pinning thus allowing the bands to bend in response to the applied voltage. This has a significant impact on the barrier to electron motion in both bias directions. Furthermore, removing the π^* surface state also eliminates the π^* surface conduction channel thus removing the ohmic shoulder seen at small z and low bias on the clean surface and resulting in higher onset voltages in forward bias (Fig. 3.3).

As mentioned above, the buckled dimers on the clean surface are associated with a small intrinsic surface dipole. On the passivated surface, this bucking is not present, however the Si-H bond has a dipole of similar direction but lower magnitude than the buckled dimers on clean Si. The barrier to electron transport associated with this surface dipole is thus reduced. The dipole also serves to reduce tip-induced band-bending with respect to a "fictitious" unpinned, non-polar surface. However, there is still some band bending. Both the smaller surface dipole present as well as the reduced apparent barrier mechanism discussed in section 3.2.2, would cause a reduction of the apparent barrier height in comparison to the clean n^+-Si(100)-2×1 surface. Indeed, the apparent barrier height at -1.5V was found to be approximately 1.3 eV in comparison to 2.2 eV on the clean surface.

We suggest that the upward band bending of the valence band allows for the addition of minority carrier transport in reverse bias. This would account for an increase in the observed current in reverse bias over forward bias leading to the rectification ratio, $RR_{F/R}$, of 1:10 at z=5Å. An energy band model of the electron transport summarizing these effects is provided in Fig. 3.5.

Styrene Passivated Si(100):2×1 Surface

Passivating the n^+- Si(100):2×1 surface with a layer of styrene is similar but more complicated than the case of hydrogen. π and π^* surface states are once again

removed allowing the dimers to unbuckle, the bands to bend in response to the applied voltage and removing the π^* surface conduction states resulting in higher onset voltages (Fig. 3.3). Using equation 3.5, the apparent barrier height at -1.5 V was found to be only 0.8 eV. This is less than both the pinned, clean n^+-Si(100)-2×1 surface and the hydride surface. The observed reduction is once again caused by a combination of the tip-induced band bending effect discussed in section 3.2.2 as well as changes in surface dipole.

When styrene covalently bonds to clean silicon, two Si-C bonds are introduced per molecule [86] and each bond has a dipole of similar polarity to the buckled dimers on clean Si. In addition to the created Si-C bonds, the styrene molecule itself has a molecular dipole of opposite polarity and greater magnitude than the sum of the Si-C bonds. The resulting overall dipole is thus of the opposite polarity to that seen on the clean and H-terminated surfaces. In addition, the styrene molecule is a relatively large and polarizable molecule. While the size of the molecule lowers the tunneling currents in both directions the effect of the polarizability is minimal with respect to the magnitudes of the molecular and bond dipoles. The resulting opposite polarity charge at the surface enhances band bending in reverse bias which we propose hinders majority carrier transport in reverse bias but encourages minority carrier transport. In essence, the extra band bending produces a new barrier to majority carriers. At the same time the high concentration of holes at the interface and the ability of electrons to tunnel directly into empty states in the valence band enhances minority carrier transport. In the I_T/V_S spectra, evidence for minority carrier transport is apparent in the very small changes - sub-exponential changes - in current with z. It is unlikely that this less than exponential change can be accounted for solely by the change in tip induced band bending with z. Such sub-exponential changes can be better explained by semiconductor limited minority carrier dominated current which has been described theoretically by Green et al. [87] and shown experimentally by Shewchen et al. [88] for metal-insulator-semiconductor diodes. Such minority carrier governed transport suggests that inversion has occurred at the surface. The resulting current is however much smaller in magnitude with respect to the majority carrier current seen in forward bias. This would account for an increase in the observed current in forward bias over reverse bias leading to the rectification ratio of $RR_{F/R}$ of 10:1 at z=5 Å. An energy band model of the electron transport summarizing these effects is provided in figure 3.5.

A short time after the publication of our group's results [76, 81], Yaffe et al. [89] also came to the conclusion that minority carriers dominated transport across n-Si-alkyl monolayer/Hg junctions. The authors showed that alkyl chain lengths varying

from 1-2 carbons up to 18 carbons produced very little difference in current at reverse and low forward bias. Moreover, they demonstrated that the experimentally measured built-in potential for their system was larger than the minimal potential required for deep inversion [89]. At deep inversion, charge transport is minority carrier dominated. Such findings provide further credit to the proposal of minority carrier transport in our passivated systems and the use of chemical means to tune tunneling current behaviour.

3.4.4 Model Implications

The presented results demonstrate the ability to controllably tune silicon surface properties. The clean Si(100):2×1 surface has a dipole moment directed away from the surface but has pinned and a $RR_{F/R}$ of 1:1 for all tip-sample separations. The hydrogen terminated surface has a dipole moment directed away from the surface and a $RR_{F/R}$ of 1:10 at z=5 Å. The styrene terminated surface has a dipole moment directed towards the surface and a $RR_{F/R}$ of 10:1 at z=5 Å. While the magnitude of the observed rectification is low in comparison to true diode like behaviour, the capability of using simple molecules to tune and even reverse current rectification may be beneficial to the design of future devices. However, it must be recognized that such adsorbates are often unstable at biases greater than -2 V.

The proposed model can also provide the ability to have a greater understanding of the structure of entities bonded to the surface. For instance, benzene is known to have two stable, covalently bonded structures on the clean Si(100):2×1 surface [90, 91]. The first structure bonds across two silicon dimers through carbons 1, 2, 3 and 4. After considering the orientations of each bond, the net dipole of this structure is directed away from the surface similar to the case of hydrogen. However, the second structure bonds only to a single silicon dimer through carbons 1 and 4 and has a net dipole moment directed towards the surface as in the case of styrene. The I_T/V_S spectra for a benzene monolayer has been studied by Dickie et al. [81] and demonstrated behaviour similar to the styrene passivated surface. This suggests that for the densely packed layer, the benzene structure bonded to a single dimer is the dominant structure. Moreover, benzene lies nearly flat on the surface and is a slightly smaller molecule than styrene. As such, the thinner barrier of benzene allows more current to flow than the thicker barrier of styrene. However, the increase in current has a greater effect on the majority dominated current resulting in a $RR_{F/R}$ of 30:1 at the same tip-sample separation and a ratio of 200:1 at contact [81].

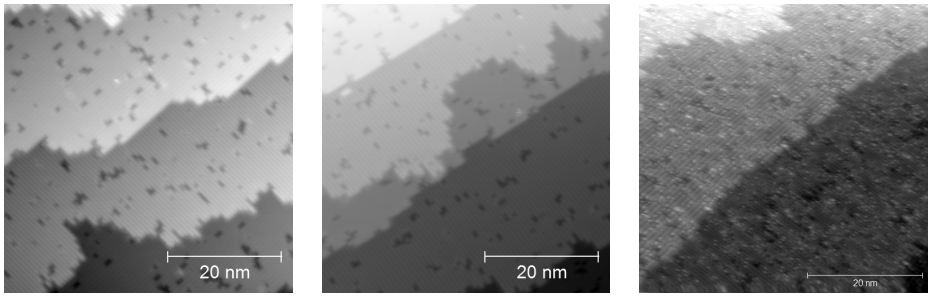

(a) Imaging Location During Styrene Dose

(b) 985 nm Away from Imaging Location

(c) 1347 nm Away from Imaging Location

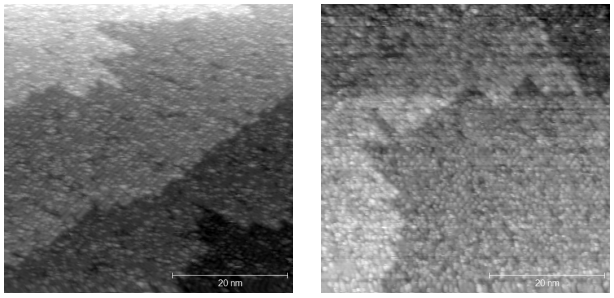

(d) 1867nm Away from Imaging Location

(e) Macro Step Away from Imaging Location

Figure 3.6: Tip Shadowing effects Observed when Dosing Styrene on Clean Si(100):2 × 1 with tip in Tunneling proximity. As the distance from the location of the tip during the dose increases, the styrene coverage increases.

3.5 Tip Shadowing Effects on Styrene Coverage

In the earliest attempts at creating monolayer coverage of styrene on Si, the sample was exposed to a low styrene pressure of 1×10^{-9} Torr while being imaged with the STM tip. Despite the known high reactivity of styrene on clean silicon(100):2 × 1 [32], very little - essentially zero - styrene was seen under the tip even after 30 min (a dose of 1.8 L). However, after styrene exposure was stopped, lateral movement of the tip away from the original imaging location displayed increasing styrene densities. For example, Fig. 3.6(a) as the location of the tip during the dose and there appears to be no styrene on the surface. Comparison of the spectroscopy at this location 3.7(a)with that of the clean surface in section 3.4.1, is indicative of very similar behaviour to the clean silicon surface. However, an ohmic shoulder region in the IV is difficult to discern, which suggests that the surface state conduction is disrupted. Even at a distance of 985 nm there is still no observable styrene in the micrograph 3.6(b) and the spectroscopy (not shown) is similar to that already discussed. However at a distance of (d) 1347 nm there is some indication in the

STM image of reacted styrene on the surface. We can also see changes in the I_T/V_S behaviour: the current in forward bias ($V_S < 0V$) has dropped slightly and that in reverse bias has dropped even more ($V_2 > 0V$) 3.7(b). These changes were observed despite the fact that all measurements were taken at locations on the surface that did not appear to have any styrene. At (e) 1867 nm we see even further characteristics of a styrene monolayer and yet full monolayer coverage was still not observed and measurements were still being taken on clean locations on the sample. The spectroscopy at this location (Fig. 3.7(c)) is quite similar to the distance of 1347 nm away; however, the change in the tunneling current with z is observed to be less than in the former case. In our model, this can be interpreted as an increasing barrier for majority carrier current and a greater influence of minority carriers. The unusual curvature in the reverse bias spectra at close z distances to the surface, may also be a consequence of the interplay between minority and majority carrier currents with varying voltage for these sub-monolayer passivated surfaces. However, the origin of the curvature is not truly understood. Unfortunately, the piezo limit of the STM1 system was only 2μm and a coarse step of the piezo mover was required before the spectroscopic signal saturated. At this location, the measurements could not be taken over areas of clean silicon as such areas were not discernible from styrene covered regions[2]. Comparison of this saturated signal (Fig. 3.7(d)) and the signal of the evenly covered surface created with the tip retracted (Fig. 3.2) demonstrates that the I_T/V_S characteristics are very similar. As expected, the forward to reverse rectification ratio is also similar (Fig. 3.7(e)).

It was found that different tips could have quite different length scales for the shadowing effect. For the tip shown, styrene was first observed at slightly over 1 μm from the imaging region. For some tips this distance was only 400 nm while for others still it was closer to 1.5 μm. This shows a large difference depending upon the shape of the tip. Tip retraction by the length of the piezo (1 μm) was also found to sometimes cause a reduction of molecules in the vicinity of the tip. However, retraction by the length of the piezo as well as a course step in z, always produced even coverage across the sample.

The effect of tip proximity, though initially unexpected, is quite simple. The presence of an object close to the surface, in this case the STM tip, reduces the ability of molecules in the vapor phase of coming in contact with the surface directly under the object. In addition, the clean Si(100):2×1 surface is highly energetic and reactive towards styrene molecules. This means that extremely little to no surface

[2]Unfortunately, the actual distance corresponding to a coarse step in the STM1 system was not calibrated.

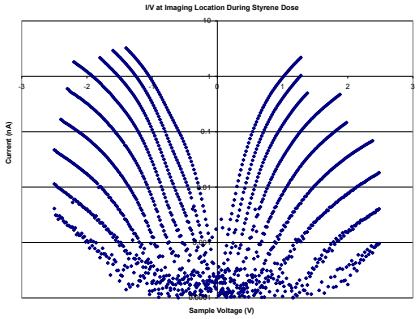

(a) Imaging Location

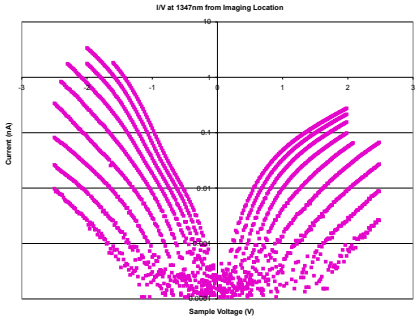

(b) 1347 nm Away from Imaging Location

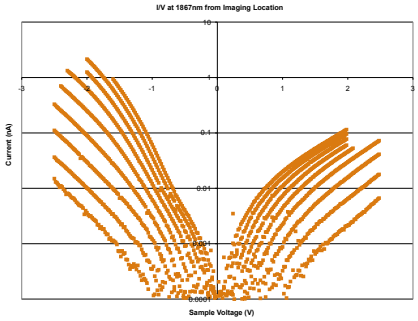

(c) 1867nm Away from Imaging Location

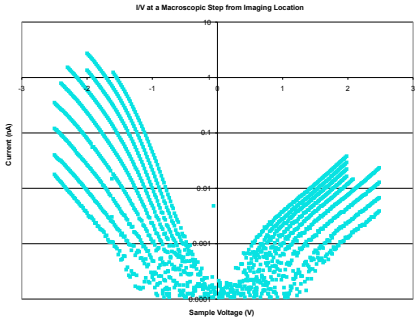

(d) Macro Step from Imaging Location

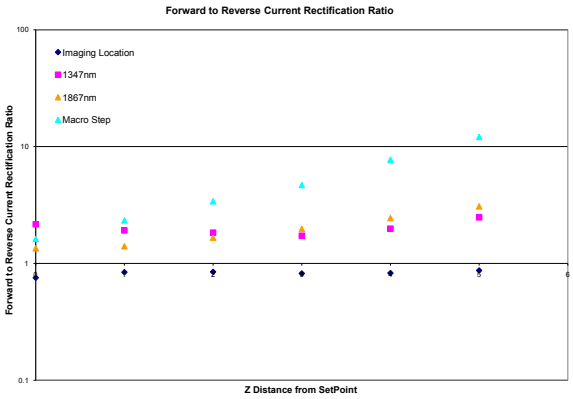

(e) Forward To Reverse Rectification Ratios

Figure 3.7: Semi-logarithmic I_T/V_S spectra for z = -3 Å(bottom curves in each set) to +5 Å(top curves in each set) towards the sample from the set-point of V_S = -2.0 V and I_T = 100 pA. A change from clean Si(100):2 × 1 behaviour to styrene passivated surface behaviour is observed with increasing distance from the location of tip during the styrene dose. The forward to reverse rectification ratios changes accordingly.

diffusion of the molecule on clean silicon in a "physisorbed" state will occur. In fact, the 'sticking probability' of styrene to the surface can be taken to be unity.

The I_T/V_S behaviour of the locally sub-monolayer styrene surface is in of itself quite interesting. Each spectrum in figure 3.7 is a single unaveraged set of data curves taken over a point of the surface in which there was no obvious surface defect including absorbed styrene (except perhaps the macro-step, for which styrene positions were more difficult to identify). One may have expected to see spectroscopy similar to the clean surface until the macro-step. Instead, we still see a gradual change from the clean I_T/V_S behaviour to the I_T/V_S behaviour of a styrene passivated layer. This indicates that the local environment has a strong impact on the I_T/V_S behaviour. It also suggests how I_T/V_S spectra may be effectively used as a means to identify the extent of surface coverage which can sometimes be difficult to quantify from STM images alone.

3.6 Chapter Summary

In this chapter we first introduced the theory behind STS methods and then discussed the methods and settings used throughout this dissertation. I_T/V_S spectra at varied tip-sample separations were taken for the clean Si(100):2×1 surface and compared with previous studies of the same surface. The clean surface was also passivated with either a monolayer of hydrogen or styrene. It was found that the current was greater in the reverse bias for the monohydride surface while it favored the forward bias in the case of the styrene passivated surface. Based on the I_T/V_S results an energy band model was formulated. The model was also used to discuss previous results found for a benzene terminated surface. The last section of this chapter studies tip shadowing effects on styrene adsorption using STM imaging and I_T/V_S measurements. In the region directly under the tip essentially no styrene molecules were able to adsorb to the surface and the I_T/V_S spectra appeared similar to the clean surface minus effects that have been attributed to surface conduction through π^* states. As the tip moved away from the center the density of styrene adsorbates increased and the I_T/V_S spectra took on hybrid characteristics until appearing similar to the fully styrene passivated surface at large distances.

Chapter 4

Density Functional Theory

4.1 Chapter Introduction

In order to gain a more thorough understanding of molecular systems, experimental studies are often complemented by theoretical treatment. Many such theoretical studies rely on the use of Density Functional Theory (DFT) approaches [92]. DFT's primary advantage is a balance between computational cost and result accuracy. In this chapter, a short overview of DFT will be conducted followed by an explanation of the need for and implementation of Dispersion Correcting Potentials (DCP). DCP-DFT will be used to study the interactions of the benzene and naphthalene dimers. This will be followed by a short survey of the interaction of some molecules with the H-Si(100):2×1 surface.

4.2 Schrödinger Equation

Theoretical treatments of chemical systems, invariably necessitate revisiting fundamental quantum mechanics - particularly, the Schrödinger Equation (SE). In the non-relativistic, time-independent framework the SE is given by:

$$\hat{H}\Psi(\vec{x},\vec{R}) = E\Psi(\vec{x},\vec{R}) \tag{4.1}$$

where: $\hat{H}$ is the Hamiltonian operator corresponding to the total energy E of the system, and $\Psi(\vec{x},\vec{R}) = \Psi(\vec{r}_1,\vec{r}_2,\cdots;\vec{s}_1,\vec{s}_2,\cdots;\vec{R}_1,\vec{R}_2,\cdots)$ is the many particle wavefunction with $\vec{R}_i$ the spatial coordinates for nucleus i and $\vec{r}_i$, $\vec{s}_i$ are the spatial and spin coordinates for electron i.

With the Born-Oppenheimer approximation, the nuclei can be treated as being stationary with respect to the lighter electrons and the SE can be separated into nuclear and electronic parts. The electronic SE is then:

$$\hat{H}_e\Psi(\vec{x}) = E_e(\vec{R})\Psi(\vec{x}) \tag{4.2}$$

The electronic Hamiltonian includes the electronic kinetic energy ($\hat{T}$), the interaction with an external potential ($\hat{V}_{ext}$), and electron-electron interaction energy ($\hat{U}_{ee}$). For the N_e electron system in an environment of N_n nuclei it is given by:

$$\hat{H}_e = \hat{T} + \hat{V}_{ext} + \hat{U}_{ee} \tag{4.3}$$

$$= -\frac{\hbar^2}{2m_e}\sum_i^{N_e}\Delta_i^2 - \sum_i^{N_e}\sum_k^{N_n}\frac{Z_k e^2}{4\pi\epsilon_0|\vec{r}_i - \vec{R}_k|} + \sum_i^{N_e}\sum_{i<j}^{N_e}\frac{e^2}{4\pi\epsilon_0|\vec{r}_i - \vec{r}_j|} \tag{4.4}$$

The many-body problem, equation 4.2 with 4.4 is also subject to restrictions. Firstly, the wavefunction must be normalizable. Secondly, the motion of an electron is not independent of other electrons; rather, it is correlated to other electrons in the system. In particular, the Pauli Exclusion principle must apply. Direct and exact solutions of the Schrödinger Equation are impossible the moment that the system has more than one electron. Moreover, approximations to Ψ become increasingly difficult as the number of electrons increases causing an exponential increase in the dimensionality of the solution. This infeasibility in determining the direct solution of the SE is the primary motivation for the development of density functional theory.

4.3 Density Functional Theory

4.3.1 Foundation for DFT

The basic premise for density functional theory is that "electron-density as a basic variable is sufficient to describe the properties of a material system in its ground state" [93]. In other words, rather than requiring the construction of a many dimensional complex wavefunction, only a three dimensional electron density is required. This premise was suggested by Fermi as early as 1927 [94]. However, it was not until the mid 1960's, that Hohenberg and Kohn established two theorems that form the true basis for DFT [95–97].

The first of these theorems indicates that the ground state electron density uniquely determines the external potential to within an additive constant. Thus, given the ground state density, the full Hamiltonian operator can be constructed and any ground state property can be determined. This theorem can be proven by contradiction [95].

The second theorem is actually a variational principle. It establishes that the functional for the ground state energy is minimized by the true ground state electron density $\rho_0(\vec{r})$. Hence for trial electron densities, $\rho_t(\vec{r})$ such that $\int \rho_t(\vec{r})\mathrm{d}\vec{r} = N$, $E[\rho_t(\vec{r})]_{\min} = E[\rho_0(\vec{r})]_{\min}$. The Hohenberg-Kohn variational principle arises directly from their first theorem and the well established variational principle of the

Schrödinger Equation.

The unique outcome of these theorems is the establishment that there exists a universal functional, $E[\rho(\vec{r})]$, which could be used to determine the exact ground state energy for any system - if we knew its form.

4.3.2 The Energy Functional

Similar to the Hamiltonian operator, the energy functional contains three terms corresponding to the kinetic energy, the external potential and electron-electron interaction, where we simplify $\rho(\vec{r})$ as ρ:

$$E[\rho] = T[\rho] + V_{ext}[\rho] + U_{ee}[\rho] \tag{4.5}$$

The external potential term can be given by considering the classical electrostatic energy of a charge distribution in an external potential $v_{ext}(\vec{r})$ [1]: $V_{ext}[\rho] = \int v_{ext}[\vec{r}]\mathrm{d}^3\vec{r}$. However, both the kinetic and the electron-electron interaction terms are unknown. Finding good approximate functionals which could then be used to minimize the energy is the subject of much research in density functional theory.

Kohn and Sham introduced the use of a fictitious system of N non-interacting electrons that has the same electron density as the system of interest. In this fictitious system, rigorous solutions to independent single-electron orbitals (Ψ_i) can be expressed using the wave equation in an effective external potential. This leads to a set of equations, known as the Kohn-Sham equations, that must be solved self-consistently with the total electron density. The kinetic energy, T_s, can then be determined (in atomic units, for simplicity) from:

$$T_s = -\frac{1}{2}\sum_i |\Delta\Psi_i|^2 \tag{4.6}$$

In addition, a significant component of the electron-electron interaction can be determined from the Coulombic Interaction, $J[\rho]$:

$$J[\rho] = \frac{1}{2}\iint \frac{\rho(\vec{r}_1)\rho(\vec{r}_2)}{\vec{r}_{12}}\mathrm{d}^3\vec{r}_1\mathrm{d}^3\vec{r}_2 \tag{4.7}$$

Then, to bring the fictitious system in line with the true system, a new functional representing the error in both the kinetic and electron-electron interaction energies is introduced: the exchange-correlation energy functional $E_{xc}[\rho]$. The total energy functional is then:

$$E[\rho] = T_s[\rho] + J[\rho] + V_{ext}[\rho] + E_{xc}[\rho] \tag{4.8}$$

[1] Note: the external potential is now given by lower case 'v' which is a function of particle positions where as capital 'V' is the resulting energy contribution which is a functional of the electron density

As the true form of the exchange-correlation energy functional is unknown, the practical use of DFT rests on solving the Kohn-Sham equations and determining appropriate approximations for $E_{xc}[\rho]$.

4.3.3 Approximations for E_{xc}

The first generation of approximate DFT, was implemented upon the theory of the homogeneous electron gas. In this scheme, known as the Local Density Approximation (LDA), E_{xc} can be approximated as a simple function of the local charge density:

$$E_{xc}^{LDA}[\rho] = \int \epsilon_{xc}(\rho(\vec{r}))\rho(\vec{r})\mathrm{d}^3\vec{r} \tag{4.9}$$

where, $\epsilon_{xc}(\rho(\vec{r}))$ is the exchange-correlation energy per particle of a uniform electron gas:

$$\epsilon_{xc}(\rho(\vec{r})) = \epsilon_x(\rho(\vec{r})) + \epsilon_c(\rho(\vec{r})) \tag{4.10}$$

$\epsilon_x(\rho(\vec{r}))$ is determined from the Dirac/Slater Exchange energy of the gas [97] and $\epsilon_c(\rho(\vec{r}))$ has been estimated in several different manners including interpolations of Monte Carlo Data [97]. The LDA approximation can also be thought of as the zeroth order approximation of the density matrix expansion. It has yielded remarkable success in describing many properties, however, much of this success has relied upon a fortuitous cancellation of errors in the exchange energy density and the correlation energy density.

Improvements in DFT then came in the form of adding non-local effects to the LDA. Significant advancement came with the Generalized Gradient Approximation (GGA) which particularly provides improvement on the calculated binding energy of molecules with respect to LDA. The GGA is similar to LDA but includes first order terms of the density matrix expansion, such that E_{xc} takes the form:

$$E_{xc}^{GGA}[\rho] = \int f^{GGA}[\rho(\vec{r}), \Delta\rho(\vec{r})]\mathrm{d}^3\vec{r} \tag{4.11}$$

The functional form of the GGA thus depends upon the density and its gradient while at the same time retaining much of the analytical properties of the LDA exchange-correlation. The actual form of the integrand, f, can be quite complex.

Another sophisticated approach to approximating the exchange-correlation functional is the use of hybrid functionals. Hybrid functionals generally consist of a linear combination of exact exchange from Hartree-Fock theory (which tend to overbind) and exchange correlation from other DFT functionals - such as LDA and GGA implementaitons (which tend to underbind). The weight of each component is generally determined by fitting the solution to experimental or high level computational data.

4.3.4 Basis Sets and Effective Core Potentials

In addition to the choice of functional, DFT solutions also depend upon the choice of basis functions used to represent the electronic wavefunctions. Often, basis functions that resemble atomic orbitals are used to construct wavefunctions for the system through a linear combination of atomic orbitals (LCAO).

A convenient form for basis functions is that of a gaussian function. Exploiting the mathematical properties of gaussian functions, significantly reduces the time required to integrate two-electron integrals. As a single gaussian function does not adequately represent an atomic orbital, linear combinations of 'gaussian primitives' are used to represent each atomic orbital. In addition, valence electrons are often composed of more than one basis function (each of which is itself a linear combination of primitives).

A major concern in computational chemistry is the efficiency of the calculation process. The number of electrons in a DFT system greatly impact the number of Kohn-Sham equations that must be solved and thus the overall computation time. It is well known in the chemical community, that it is most often the valence electrons that contribute the most towards chemical bonding and properties. In order to take advantage of this property, effective core potentials (ECPs) (or pseudopotentials), are often used to represent the core electrons. In this simplification, only valence electrons participate in the calculation however they feel an external potential due to the surrounding nuclei and core electrons. ECPs can often take the form [98]:

$$U = U_L(r) + \sum_{l=0}^{L-1} \sum_{m=-1}^{l} (U_l(r) - U_L(r))|l,m><l,m| \tag{4.12}$$

where l and m are the usual descriptors of angular momentum such that '$|l,m><l,m|$' is a projection operator onto a given $|l,m>$ state and U_l is used to replace the core-valence Coulomb and exchange terms as well as reduce the nuclear charge. The U_l are consistent with:

$$[-\frac{1}{2}\Delta^2 - \frac{Z_\nu}{r} + U_l + W_l]\chi_l = \epsilon_l \chi_l \tag{4.13}$$

for pseudo-orbitals χ_l, corresponding energy ϵ_l, effective nuclear charge Z_ν and Coulomb and exchange interactions with valence electrons W_l. ECP's are most often taken in an expansion of Gaussian-like forms:

$$U_l(r) = \sum_{i=r}^{M} c_{li} r^{n_{li}} exp(-\zeta_{li} r^2) \tag{4.14}$$

where, r is the distance from the nucleus, M is the number of terms in the expansion and c_i , n_i and ζ_i are the coefficient, power and exponent respectively of i-th term.

The use of such ECPs can dramatically reduce computational cost and be quite accurate in many cases. However, in certain situations - particularly the cases of high polarizability and high pressures - ECPs are found to be poor representations of the real system.

4.4 Dispersion Interactions in DFT

The development of practical Density Functional Theory has enabled chemists as well as scientists from various fields to study a wide range of systems. The ever increasing number of studies being conducted with DFT as well as the relatively good correlations that can be found between DFT and high level calculations or experimental results attest to is valuable impact on the scientific community [97]. However, there are many challenges still facing the application of DFT. One of the major challenges in common DFT methods is the ability - or rather the inability - to model non covalent interactions. For this dissertation, the ability to model dispersion interactions is particularly relevant. An excellent review of this topic has recently been presented by Johnson et al. [99]. As such, only a concise introduction is provided here.

Dispersion interactions (also known as London forces), are weak intermolecular or, in the case of single atoms, interatomic interactions between instantaneous dipole moments within electronic distributions that do not contain permanent dipoles [100]. Though individually small in magnitude, dispersion interactions can play a major role in such processes as phase change, protein folding and self-assembly. The dispersion energy takes the form of a series expansion [99]:

$$E_{disp} = -\frac{C_6}{R^6} - \frac{C_8}{R^8} - \frac{C_{10}}{R^{10}} \cdots \tag{4.15}$$

here R is the separation distance and the Cs are dispersion coefficients which can be quite difficult to determine both experimentally and theoretically.

Dispersion interactions are difficult to model with most theoretical methods including some correlated wavefunction techniques such as MP2 [99]. Standard DFT methods are known to have extreme difficulty modeling dispersion and will most often predict repulsive interactions between dispersion bound complexes. Moreover dispersion-like binding behaviour of some functionals has been shown to serendipitously originate from errors in the exchange functional or basis set incompleteness. Recently, advancements have been made in incorporating dispersion into DFT. These include:

Dispersion-correcting DFT (DFT-D) which explicitly calculates an attractive $-C_6/R^6$ term between atomic pairs. This method has shown much

success but requires empirical dispersion parameters and is often time consuming.

Exchange-hole dipole Model (XDM) which incorporates C_6, C_8 and C_{10} dispersion terms obtained from properties of the local electron density. This method has also shown much success but can not be used in calculations such as geometry optimizations, vibrational frequencies, spectroscopic parameters and solvation.

Another method for accounting for dispersion which has garnered much success and will be used in this thesis, is the use of Dispersion Correction Potentials (DCPs). This is an empirical method that uses local, atom-centered effective core-like potentials to modify the valence electron environment. This techniques requires parameterized DCPs for different elements using specific basis sets and functionals, but once parameterized can be used with ease in standard quantum chemical programs without any code modification. DCPs can be used with small basis sets and may even help minimize basis set incompleteness issues. Moreover, the treatment does not add any calculation time and can be used in conjunction with the full array of calculations available in standard program packages.

As mentioned above, DCPs make use of atom-centered effective core-like potentials to correct for long range behaviour in DFT. From section 4.3.4 we know that these potentials can take the form given in equation 4.14. DCP's have been constructed from this general form using two (M=2) simple Gaussian functions (n_{li}=0). The first function, with exponent ζ_1 "is used to produce a weakly attractive potential at midrange inter-monomer distances" [101] while the second function, which is repulsive and tighter with $\zeta_2 > \zeta_1$, "is used to prevent overbinding at shorter distances" [101]. DCP functions for carbon and silicon have been optimized by minimizing the mean absolute deviation between calculated binding energies of a benchmark sets of systems consisting of dispersion bound carbon containing dimers [102] and dispersion bound silicon containing dimers [101] treated with high level wave function theory.

4.5 Hydrocarbon Dimerization

Dispersion interactions are critical for the intermolecular interactions that lead to the dimerization of molecules. The benzene dimer has been studied by a large variety of methods. Larger poly-cyclic aromatic hydrocarbons (PAHs) have also gained interest particularly as the interest in graphene and few layer graphite has increased. In relation to this dissertation, interest in such species will be shown

to stem from studies of molecules in molecular lines discussed in chapter 7. The study of the benzene dimer in the parallel dimer configuration is first discussed to demonstrate the efficacy of the DCP-DFT method followed by a discussion of the naphthalene dimer.

The parallel benzene dimer configuration consists of two benzene molecules lying parallel to each other but spaced apart vertically and transversely. In this short study only one transverse direction was studied and is shown in Fig. 4.1. Calculations of the potential energy surface of the parallel benzene dimer using the optimized DCPs for carbon atoms was performed. The binding energy was calculated as a function of the distance between the dimers [h (Å)] and the distance between the center of each ring [d(Å)]. Fig. 4.1, presents the results of the calculation along with results of similar calculations performed by Pavone et al. [103] for DFT-D and standard DFT without any dispersion correction (albeit with a different functional). It can be seen that both dispersion correction schemes produce quite similar results with weakly attractive binding at the height of approximately 3.5 Å that is not observed in standard DFT.

The PES of the benzene dimer was studied here to allow for a comparison with another form of dispersion correction with DFT. However, this portion of the PES does not include the true global energy minima of the system. For benzene, a tilted T-shape arrangement of the molecules has recently been predicted to be the energy minima, with slipped parallel and standard T-Shape dimer configurations only slightly higher in energy [104].

Naphthalene consists of two fused benzene-like rings. The reduced symmetry in the molecule, as compared to benzene, causes the PES of the two molecule system to be even more complex. Several different potential minima structures have been studied [104–108]. Common configurations studied in the literature include slipped parallel (Fig. 4.2(b)), graphite-like (also called parallel displaced) (Fig. 4.2(c)), crossed (Fig. 4.2(d)), and T-Shape (Fig. 4.2(e)). For each of these structures a cross section of the PES using single point energy calculations of monomers separated by the specified distance was calculated and are shown in Fig. 4.2(a). The overall results are similar to previous calculations in the literature [104, 108]. The slipped parallel, graphite type and crossed dimers had similar binding curves with the graphite-type emerging as the lowest energy. The graphite-type also had the strongest curvature near the optimum dimer distance, such that small changes in the distance result in a greater change in the BE as compared to the less curved PES curves such as the crossed dimer structure. The T-Shaped structure had a significantly different curve. The results for T-Shape are plotted with respect to

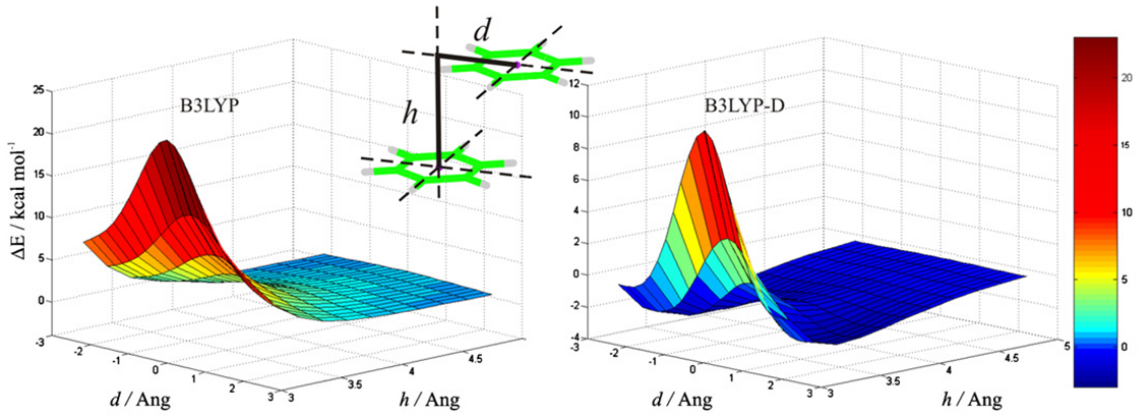

(a) Standard DFT and DFT-D

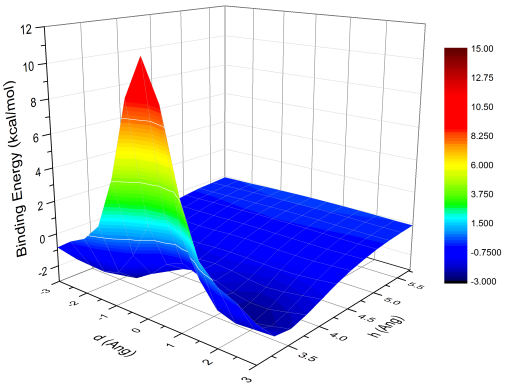

(b) DCP-DFT

Figure 4.1: Potential Energy Surface of the parallel benzene dimer. (a) Standard DFT results and DFT-D results for the B3LYP functional reproduced with permission from [103], Copyright (2008), Elsevier. (b) DCP-DFT results for the B971 functional and 6-31+G(d,p) basis set. Note that while attempt was made to simulate the colormap used by Pavone et.al., the colorscheme is not exactly the same. However, in the energy region of interest in the dispersion corrected calculations, the colormap is very similar.

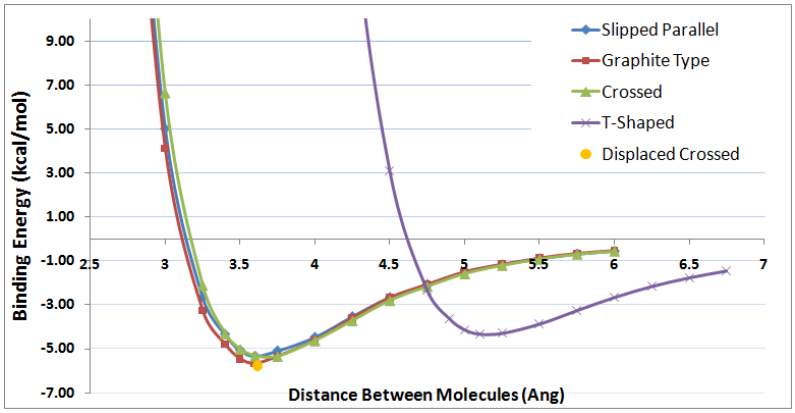

(a) Binding Energy Profiles

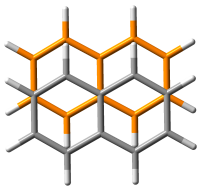

(b) Slipped Parallel (C_{2h})

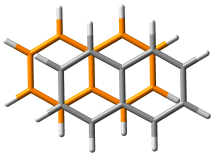

(c) Graphite Type (C_i)

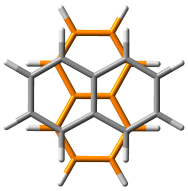

(d) Crossed (D_{2d})

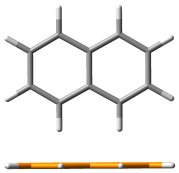

(e) T-Shape (C_{2v})

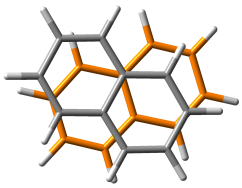

(f) Displaced Crossed

Figure 4.2: Naphthalene Dimer Binding Energies and Conformations (a) DCP-DFT calculation results for Naphthalene Dimer potential energy surface cross sections using the B971 functional and 6-31+G(d,p) basis set. The binding energy for the displaced crossed configuration results from a full optimization calculation. The distance between the molecules is given in terms of the distance between the planes for the first three conformations, the distance between the center of mass for the T-Shape conformation and, the average distance between the atoms in the molecule for the optimized displaced crossed conformation. (b)-(f) Conformations of the Naphthalene dimer studied with reference names and symmetry groups indicated. Shown in top view except the T-Shape configuration which is more easily understood from the side view. In each case, carbon atoms in one molecule are colored grey while those in the second molecule are colored orange for clarity.

Table 4.1: Naphthalene Binding Energies (kcal/mol) and optimum intermolecular distances (Å). For '*' the geometry was optimized for a lateral shift and may is not identical to the others. MP2/CBS: MøllerPlesset partitioning of the Hamiltonian with complete basis set (CBS) estimates; SAPT(DFT):symmetry-adapted perturbation theory based on the density functional description of the monomers; MP2/CCSD(T): MøllerPlesset with a coupled cluster method involving single, double and non-iterative triple excitations.

	Slipped Parallel		Graphite Type		Crossed		T-shape	
Method	R	BE	R	BE	R	BE	R	BE
MP2/CBS [107]	3.5	9.69	3.5	10.28	3.6	9.66	5.0	6.56
SAPT(DFT) [104]	3.6	5.12	3.6	5.19	3.6	5.08	5.1	4.36
MP2/CCSD(T) [107]*	3.5	5.32	3.5	5.73	3.6	5.28	5.0	4.34
DCP-DFT	3.6	5.33	3.6	5.67	3.75	5.34	5.1	4.32

the distance between the center of mass of the molecules. The calculations indicate that this structure is significantly less bound than the other configurations studied. This is unlike the benzene dimer, where the T-shape is found to have a similar BE to the slipped parallel structure [104]. The majority of the theoretical work on naphthalene has indicated similar findings. Some literature values for the optimum distance and binding energy are presented in Table 4.1. We can see that the DCP-DFT results are similar, except for the MP2/CBS data which demonstrates the pathological over-binding that occurs with this method.

In addition to the above commonly studied dimer structures, a displaced crossed structure has been identified as a competitive structure to graphite for the global minima structure [105, 106]. Previous calculations indicate that the binding energy of this structure is just slightly greater than that of the graphite-type structure. To search for this structure, the molecules were placed in an orientation visibly similar to that identified by Walsh et al. [105] and allowed to fully optimize. The resulting displaced crossed structure is shown in Fig. 4.2(f) and had an average dimer spacing [2] of 3.6Å, similar to the previously calculated configurations apart from T-shape, and binding energy of 5.76 kcal/mol. This results in an energy difference of only 0.09 kcal/mol greater than that of the graphite-type structure.

The calculations of the benzene and naphthalene dimer using DCP-DFT is very similar to previously reported results. The dimer structures of naphthalene and the intermolecular spacing of the structures will be found to be of interest in understanding experimental observations of vinylnaphthalene molecular lines in chapter 7.

[2]The optimized structure was close to but not fully in parallel planes and so an average distance is quoted.

4.6 Physisorption of Molecules on H-Si(100):2×1

While the dimer interactions between molecules is of great importance in understanding the behaviour of molecules with other molecules, in this dissertation we are particularly interested in the behaviour of molecules on silicon surfaces. The development of silicon DCP's by Johnson et al. [101] in addition to those of carbon [109] offered the opportunity to have a greater understanding of the physisorption interactions in such systems. We first look at the interaction of styrene with hydrogen terminated Si(100):2×1. We then look at how the change of a single atom on the molecule, to create 4-fluorostyrene, can modify the interactions. This then leads into a short survey into some possible interactions of heteroatomic molecules that are great interest due to their ability to act as electron donors and acceptors.

4.6.1 Physisorption of Styrene and Simple Styrene Derivatives on H-Si(100):2×1

Chapter 7 will be dedicated to the study of aspects of molecular line growth on hydrogen terminated Si(100). The initial starting point of such line growth is the ability of a molecule to interact with the surface such that it can diffuse along the surface to locate a reactive site (DB) with which to commence line growth. The surface structure of H-Si(100):2×1 offers the opportunity for molecules to have a variety of physisorption interactions, creating a complex potential energy surface (PES). The global minima on the PES is of particular importance as it dictates the possible extent of the interaction. In this first section, we determine the global minima structures of styrene on H-Si(100):2×1. We then observe how the substitution of hydrogen for fluorine or chlorine in the para-position can alter the interaction.

For calculations in this section, a 'slab' model of the H-Si surface consisting of the surface hydrogen atoms, the first contiguous layer of silicon and an addition row of silicon atoms under the gulley atoms. This model was taken from a larger model that was optimized using a periodic boundary DFT (PBE) calculation and was described by Anagaw et al. [82]. Hydrogen atoms were used to cap the dangling silicon bonds generated by cutting the slab out of the bulk. During the calculations, all atoms in the model of the surface where kept fixed with the exception for the surface hydrogen terminating atoms. All calculations were performed for a single styrene molecule on the surface. As such, molecule to molecule interactions are not considered and the theoretical results should only be compared to experimental studies where low dosing pressures are utilized. For all calculations, the B971 [110] functional was used with the 6-31+G(d,p) basis sets and DCPs on all carbon and

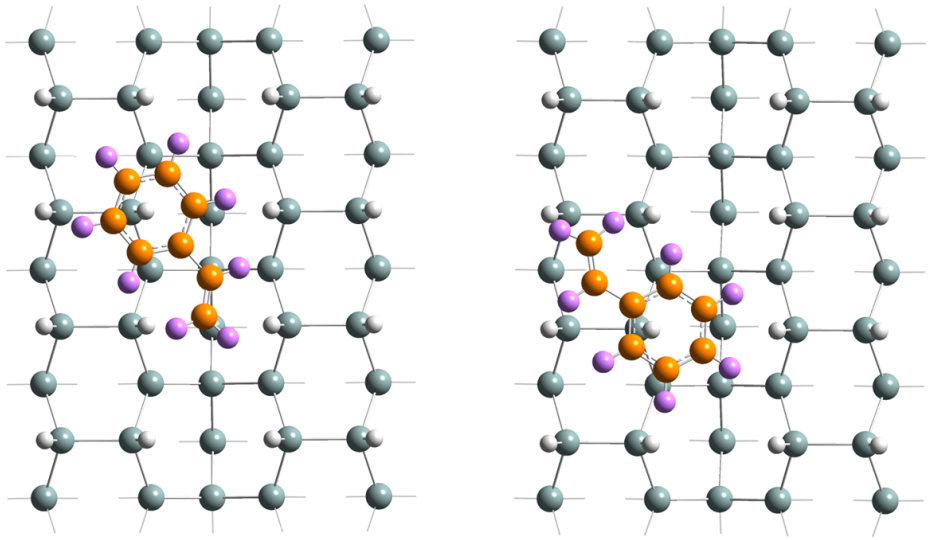

(a) (b)

Figure 4.3: Top-down view of the hydrogen terminated Si(100)-2 × 1 model used for the DCP-DFT calculations and the resulting two lowest-energy styrene physisorption configurations. The colors shown define the following atoms: orange, carbon; gray, silicon; purple, hydrogen on styrene; white, hydrogen atoms on the silicon surface. For ease of view, hydrogen atoms capping the interior silicon atoms are shown in stick format. Both optimized configurations have the aromatic ring centered upon a hydrogen-dimer atom, and the styrene molecule is located, on average, 3.9 above the silicon surface. Adapted with permission from [112]. Copyright (2010) American Chemical Society.

silicon atoms [99, 101, 102]. All calculations were performed using the Gaussian 03 package [111].

The local minima on the PES were determined on a surface model with two neighboring dimer rows of four dimers each for a total of 45 Si atoms (Fig 4.3). Optimizations were performed for 21 different starting orientations of the styrene molecule on the surface. These orientations were chosen to represent the variety of manners in which this asymmetric molecule may lie on the dimer rows of the surface. The starting orientations resulted in 17 different local minima - many of which were quite similar but not exactly the same. The two lowest energy minima had very similar binding energies [7.75 kcal/mol (0.34 eV) and 7.66 kcal/mol (0.33 eV)] and related orientations (Fig 4.3). Both have the aromatic group over a dimer row hydrogen atom. The ring is almost centered around the hydrogen atom - although in Fig 4.3 it does not appear this way due to a tilt in the molecule with respect

Table 4.2: Physisorption binding energies of styrene, 4-fluorostyrene and 4-chlorostyrene in structures minima styrene binding energy structures shown in figure 4.3.

	BE of 'a' structure (kcal/mol)	BE of 'b' structure (kcal/mol)
styrene	7.75	7.66
4-fluorostyrene	4.02	4.00
4-chlorostyrene	5.04	5.15

to the surface plane. This is similar to the global minima of benzene found on the same surface [101]. However, the minima here are differentiated by the location of the vinyl group. In one it is over the silicon dimer row while in the other it is over the gulley region. In addition, the vinyl group in both structures is slightly out of the plane of the ring (dihedral angle of 169 °).

To observe how the change of a single atom could alter the interactions with the surface, the hydrogen atom in the para-position of styrene was replaced with flourine and chlorine atoms to create 4-fluorostyrene and 4-chlorostyrene respectively. The geometry of these polar molecules were allowed to optimize starting from the two lowest energy optimized structures found for styrene. In each case, the aromatic ring of the molecule remained over a surface hydrogen. A slight shift in the exact position was found in some cases, but it remained very similar to the optimized styrene structures. However, in all cases, the vinyl group became slightly more in line with the ring and the halide-carbon bond length increased with respect to the optimized structure of the molecule when not interacting with the surface. In addition, the average distance of the molecule from the surface remained similar. However, the optimized binding energies changed dramatically. The results are summarized in Table 4.2. It can be seen that the physisorption binding energy decreased with the fluorinated molecule being the least bound. The hydrogen terminated silicon surface is hydrophobic in nature [113], so it is not surprising that polar molecules will have less interaction with the surface. However, the extent of the reduction in binding energy which is almost half in the case of 4-fluorostyrene, is somewhat surprising. It has been found that DCP-DFT calculations with fluoronated molecules do not always produce accurate results and indeed produced some of the greatest errors in the test dimer set used by DiLabio [102]. This has been largely associated to basis set incompleteness issues. It is suspected that some of the observed difference in binding energies may be due to this effect rather than a true reduction in interaction.

We can see that the change of a single atom in the molecule can significantly alter the interactions with the surface. In this case, the sample material modeled was pure silicon. In electronics, silicon is very rarely used in a pure form. As

highlighted in chapter 2, dopant atoms are introduced in the silicon in order to enhance conductivity. Although present in low densities, they can greatly modify the behaviour of the material. The primary dopant used in the experimental work of this thesis is arsenic - an n-type or electron donor type atom. Other common dopants include boron (p-type, electron acceptor) and phosphorus (n-type, electron donor). These dopant atoms may also modify the interaction of molecules with the surface. As a very basic test of possible interactions of an adsorbate molecule with a dopant in the bulk, styrene was studied on a silicon cluster containing a single dopant atom. A boron dopant was used for the case of a p-type (acceptor) dopant, while a phosphorus dopant was used for the case of an n-type (donor) dopant.

The model cluster had surface area containing three dimer rows of five dimers each and two adjacent gulley regions. Rather than cutting a slab from the surface, a trigonal pyramidal shape was cut to form a cluster, as depicted from the side view in Figure 4.4(a). For the case of a doped cluster, the dopant atom was placed at a fully coordinated position a couple layers from the surface as shown in 4.4(b). In addition to looking at the binding energy of the molecules with the clusters, the electronic populations were calculated for these structures using natural population analysis which makes use of Natural Bond Orbitals (NBOs). NBOs are essentially localized representations of MOs in an idealized Lewis type structure which aids in the removal of basis set dependencies on properties such as charges. NBO analysis calculates atomic charges by summing the occupancies of 'natural atomic orbitals'. The sum of the atomic charges in the adsorbate molecule can then provide a measure of the overall partial charge on the molecule.

It was found that both the binding energy and the molecule partial charge remained essentially constant for the undoped and doped clusters. The largest difference in binding energies was between the two doped clusters and was found to be only 0.02 kcal/mol (ie, less than 0.001 eV) with the binding to the boron doped cluster being very slightly greater than binding with the undoped cluster and binding with the phosphorus cluster being very slightly less than with the undoped cluster. Similarly the partial charge on the molecule was found to be approximately 0.004 electronic charge units in all cases. These results suggest that the presence of dopant atoms in the silicon, at the position studied, should not have a significant effect on the physisorption of styrene with the surface.

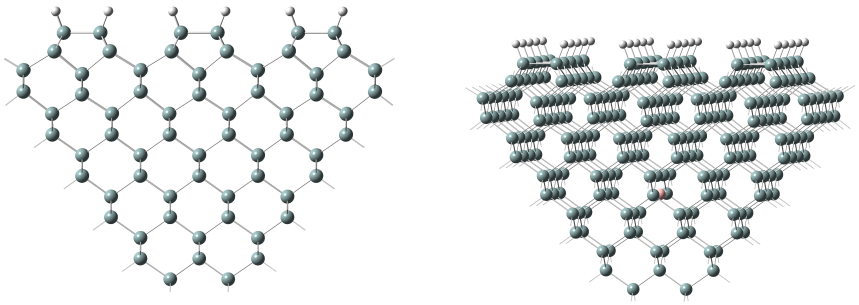

(a) (b)

Figure 4.4: (a) Side View of the all silicon cluster model of the H-Si(100):2×1 used for population analysis. (b) Slightly offset side view of the silicon cluster containing a single embedded boron dopant. This position was also used for phosphorus dopant calculations. The colors shown define the following atoms: light pink, boron; gray, silicon; white, hydrogen atoms on the silicon surface. For ease of view, hydrogen atoms capping the interior silicon atoms are shown in stick format.

4.6.2 Physisorption of Electronically Interesting Molecules on H-Si(100):2×1

While this dissertation is largely focused upon the behaviour of molecules of interest in molecular line growth experiments, there is an extremely vast array of chemistry that has become of interest in molecular or nano-electronics. In particular, a strong focus has been given to charge transfer complexes and individual entities that can behave as electron donors and acceptors. As mentioned in the introduction, the ability to interface with modern silicon technology will be of great benefit to any emerging technology. A natural question that then emerges is how might some of the aforementioned electron donors and acceptors interact with silicon surfaces? Moreover, how may dopants in the silicon crystal further influence this interaction?

The development of easy to use carbon and silicon DCPs provides us with the means of probing some of the interactions of electronically interesting molecules with the passivated silicon surface. Towards this end, five molecules (Fig 4.5) consisting of three well known acceptors [tetracyanoethylene (TCNE), tetracyanoquinodimethane (TCNQ), trinitrofluorenone (TNF)] and two well known donors [tetrathiafulvalene (TTF), dimethyl-1,4-phenelenediamine (DMPD)] were chosen for study. Geometry optimizations of each molecule in various positions on the H-Si(100):2×1 surface were performed in a similar matter to that of styrene in the previous section. However, in these calculations a slightly larger slab model consisting of three dimer rows with five dimers each and two gulley regions was used in order to accommodate the larger molecules. The number of starting orientations for each molecule was deter-

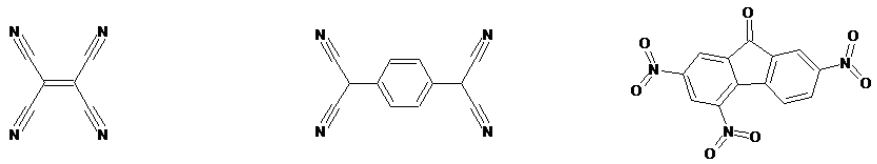

(a) TCNE (b) TCNQ (c) TNF

(d) TTF (e) DMPD

Figure 4.5: Structures of some (a-c) electron donor and some (d-e) electron acceptor molecules that were chosen for studies of their interaction with the hydrogen terminated silicon surface. (a) tetracyanoethylene (TCNE) (b) tetracyanoquinodimethane (TCNQ) (c)tetracyanoethylene (TNF) (d) tetrathiafulvalene (TTF) (e) dimethyl-1,4-phenelenediamine(DMPD)

mined based upon the symmetry and fit of the molecule on the surface. A top-down view of the optimized geometries are displayed in figure 4.6.

Each of the most stable optimized geometries were then placed on a larger cluster model of the the hydrogen terminated silicon(100):2×1 surface. The model used was the same as that presented in figure 4.4(a). In all cases, it was found that in going from the smaller slab model of the surface to the larger cluster model, the binding energy increased by 0.5%-0.6% per heavy atom in the molecule. As might be expected, all acceptor-type molecules had a very slight negative charge while donor-type molecules had a slight positive charge. The binding energies and charges are summarized in Table 4.3.

One of the major implications of a modification of the surface charge and therefore the dipole moment at the surface is a change in the surface work function. The change in the workfunction for a monolayer can be estimated by:

$$\Delta\phi = \frac{e}{\epsilon_0}(\frac{\Delta\mu}{A}) \tag{4.16}$$

where e is the elementary charge, ϵ_0 is the permittivity in vacuum, A is the area associated with one molecule and $\Delta\mu$ is the change in surface dipole associated with each molecule. The work function changes associated with the results of the population analysis are also shown in Table 4.3. These work function changes can

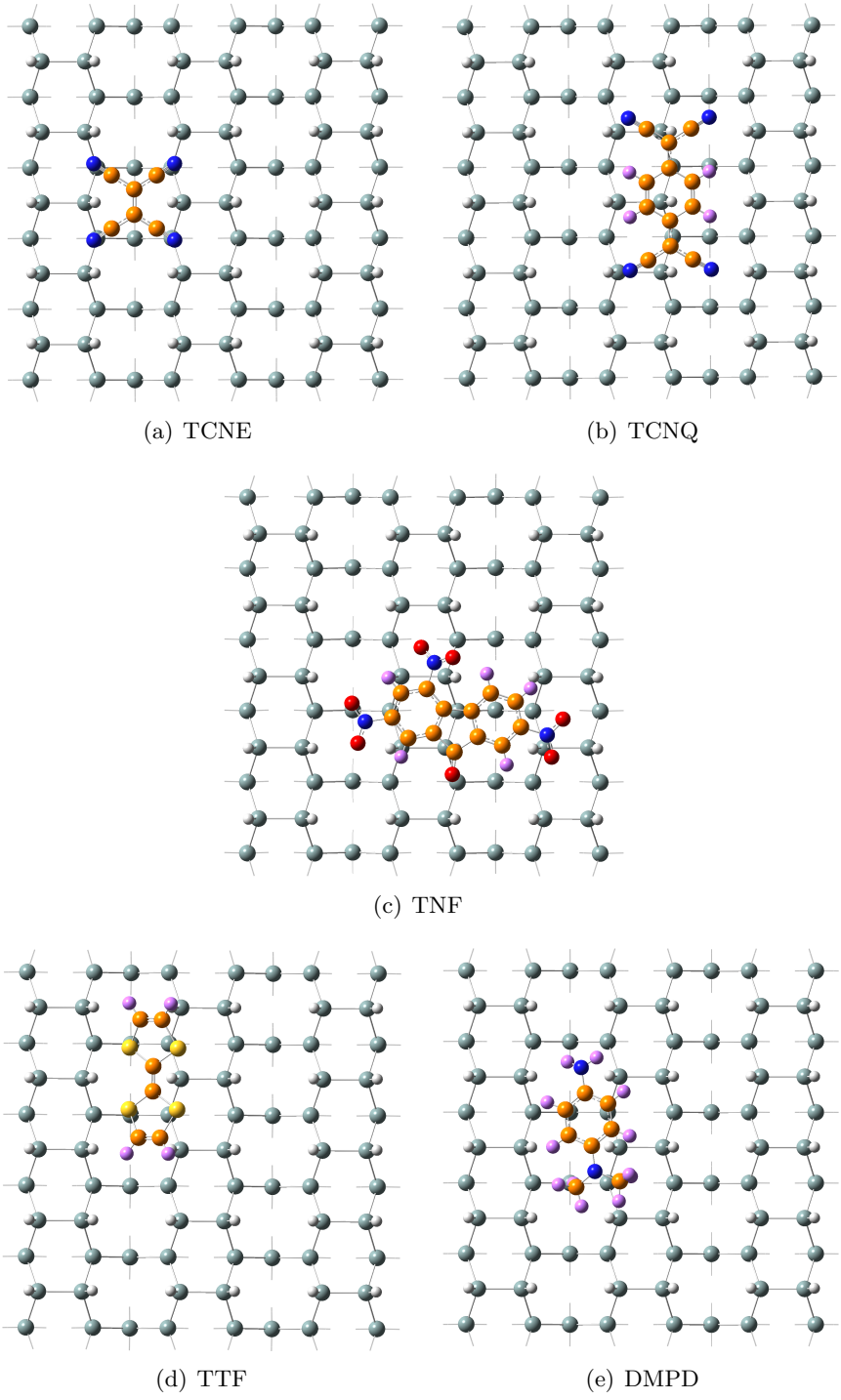

(a) TCNE (b) TCNQ

(c) TNF

(d) TTF (e) DMPD

Figure 4.6: Top-down view of Optimized Structures of some (a-c) electron donor and some (d-e) electron acceptor molecules on H-Si(100)2 × 1. The colors shown define the following atoms: orange, carbon; blue, nitrogen; red, oxygen; yellow, sulfur; gray, silicon; purple, hydrogen on styrene; white, hydrogen atoms on the silicon surface. For ease of view, hydrogen atoms capping the interior silicon atoms are shown in stick format.

Molecule	Molecule Type	BE (kcal/mol)	Molecule Charge	$\Delta\phi$ (eV)
TCNE	Acceptor	9.1	-0.011	-0.25
TCNQ	Acceptor	13.7	-0.021	-0.26
TNF	Acceptor	20.5	-0.010	-0.06
DMPD	Donor	10.8	0.024	0.29
TTF	Donor	12.8	0.031	0.36

Table 4.3: Results from interaction with all silicon cluster: binding energy, charge on the molecule as a result of NBO population analysis and associated expected change in the surface work functions.

greatly modify the electron transport properties to and from the surface.

As previously mentioned, the interaction of molecules with the surface of a doped silicon crystal is of great importance as the vast majority of real systems contain dopant atoms. To study this effect, a single dopant atom, phosphorus or boron, was again introduced into the silicon cluster used for population analysis 4.4(b). The results are presented in Table 4.4. It was found that when a donor molecule was paired with a donor dopant system or an acceptor molecule was paired with an acceptor dopant system very little change was seen in either the binding energy or the charge distribution. The more interesting interaction is of course the opposite pairing. Unfortunately, it has proven to be extremely difficult to achieve convergence in DFT analysis of such systems. The search for a method of achieving convergence has included bootstrapping the analysis to smaller basis sets and guessing a form of the wavefunction from the non-doped system or a charged version of the system. Convergence has only been achieved in one of the systems - that of TNF interacting with an n-type doped cluster. In this case the binding energy was found to increase by over 10kcal/mol or half the original binding energy. Moreover, the charge on the molecule was found to be greater than unity. A full charge transfer type interaction was not truly expected for molecules on hydrogen terminated silicon. The results for TNF suggest that there may be better methods of studying such systems, as charge transfer interactions are known to be difficult to study with DFT.

4.7 Chapter Summary

The basic theory behind density functional calculations has been presented. The need for corrections in standard DFT to include the effects of physisorption was highlighted along with the method of using dispersion correcting potentials to achieve such corrections with ease in standard computational packages. The use of DCP-DFT in the calculation of the benzene parallel dimer configuration PES was provided

	No dopant		B (p-type)		P (n-type)	
	BE (kcal/mol)	Molecule Charge	BE (kcal/mol)	Molecule Charge	BE (kcal/mol)	Molecule Charge
TCNE	9.1	-0.011	9.1	-0.010	???	
TCNQ	13.7	-0.021	13.7	-0.021	???	
TNF	20.5	-0.010	20.5	-0.009	31.3	-1.626
DMPD	10.8	0.024	???		10.8	0.024
TTF	12.8	0.031	???		12.8	0.031

Table 4.4: Physisorption Binding Energies and Molecular Partial Charges with Doped Silicon Clusters

as an example. Several cross-sections of the PES of the naphthalene dimer were explored. The results of benzene and naphthalene dimers agreed well with previous treatments of such systems. In particular, the displaced crossed configuration of the naphthalene dimer emerged as a probable lowest energy configuration of the dimer closely followed by the graphite-type configuration.

We then transitioned into the use of DCPs with molecules on hydrogen terminated silicon surfaces. The minimum energy binding structures for styrene on H-Si(100):2×1 were determined. Substituting a halide atom at the para-position of styrene significantly reduced this interaction. The effect of a dopant atom in the silicon was found to have a negligible effect on the physisorption of styrene on the surface. Electron donating and accepting molecules are are also of great interest in molecular electronics. Using DCP-DFT, the interaction of three acceptor molecules and two donor molecules with H-Si(100):2×1 was probed for a pure silicon cluster and doped silicon clusters. The later calculations were found to be difficult to implement, but the former demonstrated a slight partial charge of the expected type on the molecule. One of the major implications of such a charge is a corresponding change in the work function of the surface.

Chapter 5

Styrene Diffusion

5.1 Chapter Introduction

During the process of molecular line self-assembly discussed in section 7.1.1, the ability of the molecule to diffuse along the surface will be found to be critical in order for the molecule to be capable of 'finding' a dangling bond defect site with which to react. Surface diffusion is of great importance in a variety of other phenomena as well [114]. Island and thin film growth, catalysis and adsorbate ordering on surfaces are but a few examples. It is thus of no surprise that studies of surface diffusion have been of interest for several decades. In this chapter, we focus on learning about some properties of the diffusion process of styrene and 4-fluorostyrene on the hydrogen terminated surface - which is of interest in molecular line growth experiments.

Knowledge in the field of surface diffusion has been gained through both theoretical techniques, such as molecular dynamic calculations [115, 116] and Monte Carlo simulations [115–119] as well as experimental studies using techniques such as FIM [120, 121] and STM [121–125]. FIM, which was introduced in chapter 2, was the first experimental technique to directly resolve atomic and molecular surface diffusion [121]. However, FIM samples are limited by the requirement for high field which implies a sharp metallic sample with a small surface facet. STM, on the other hand can be used on much larger surfaces and with a greater variety of substrate and adatom materials. STM does have its own set of limitations.

One of the major concerns in STM studies is the effect of the scanning tip on the motion of adatoms and adsorbate molecules. We have already encountered some of the difficulties in earlier chapters of this thesis. In chapter 3, we observed a strong tip shadowing effect when dosing styrene on clean Si(100):2×1. This indicated that the adsorbate had an extremely high sticking coefficient on the surface due to the high chemical reactivity. The effect of tip shadowing is reduced as the molecules ability

to diffuse along the surface is increased. For example, in chapter 7 we will observe the ability for molecular lines to grow on the H-terminated surface under the STM tip without any obvious tip shadowing effect. In fact, this freedom of motion makes the STM incapable of imaging the entities at room temperature. Even when the species of interest is slightly more stable on the surface, the imaging conditions can directly influence the diffusion process. These conditions do not have to be extreme to have an effect; Standard imaging conditions of -2V sample bias and 100pA can influence the motion and mask diffusion properties. For instance, small preferences for the direction of diffusion on an anisotropic surface - diffusion anisotropy - can be masked entirely by the tip [122]. In some systems, if two temperatures are identified - one at which the adsorbate is 'frozen' in place and another where the adsorbate is free to move - it can be possible to study the diffusion using an "image-anneal-image" technique [122] which minimizes tip influences. However, the STM system and the temperatures in question must be such that very little thermal drift takes place during the process such that the same location can be imaged before and after thermal annealing.

In order to overcome these STM tip limitations and study the surface diffusion process of styrene on the H-terminated surface at room temperature, we used the knowledge gained from previous chapters of this thesis to devise a novel STM experimental procedure to study diffusion processes at a single temperature and no tip effects (section 5.2). In particular, we used this process to experimentally study the very small anisotropic diffusion properties present in the diffusion process of styrene and 4-fluorostyrene on H-Si(100):2×1 (section 5.3). To validate the experimental results, theoretical calculations of the anisotropic diffusion were also carried out and are discussed in section 5.4. The theoretical treatment combined DFT analysis of the dispersion binding and barrier heights associated with diffusion with Monte Carlo (MC) simulations of the dynamic system. Much of the work on styrene diffusion from both the experimental and theoretical treatments has been published in Sinha et al. [112].

5.2 Experimental Method Development

The system of interest is styrene and styrene derivatives on H-Si(100):2×1. On this surface the physisorbed styrene species is extremely mobile and can not be directly imaged with the STM. However, these same styrene molecules chemically react readily with the clean-Si(100):2×1 forming a stable covalent bond that localizes the molecule and allows it to be imaged [32, 126, 127]. By exploiting this reactivity, we can gain information about the diffusion process on the hydride surface. A step-wise

difference in the diffusion ability is created by making 'windows' of clean Si(100) on the hydogen passivated surface. Styrene molecules that are then dosed onto the surface can diffuse readily on the hydride regions but become localized or trapped if they arrive at the clean surface region.

STM tip-induced hydrogen desorption from the hydrogen passivated silicon surface is a well known phenomenon that has been studied in detail [51,128] and utilized to create STM lithographic patterns [128,129]. Following Avouris et al., sample voltages in the range of +5V to +8V and currents of 0.1-4.0 nA were used to create clean silicon windows. The large range in voltages and currents was found to be necessary in order to have different tips perform in a similar manner. In Figure 5.1(a), an STM image of one of the first attempts at creating such windows is shown. The darker - outer region of the image is the hydride surface while the lighter region on the inside is the clean surface. The reader is now reminded that STM 'topographic' images are in fact images of the electron density. As such, the hydride surface, despite having an extra hydrogen atom at the surface, appears lower in height due to the more localized electron density compared to the clean surface. It can be seen that the edge of the window is quite rough with a high density of single dangling bonds near the edge of the clean silicon dimers. This roughness was reduced through the use of voltages on the lower edge of the spectrum and currents in the higher end. For the first iteration of the study, styrene was dosed into the chamber at varied pressures and the rate of arrival at the clean surface - more precisely the rate of window coverage - was monitored. The pressures studied were kept low in order to ensure that several STM scans of the diffusion process could be taken. Figure 5.1 provides example images taken for one of these experiments. The area of the clean silicon region remaining at the end of each scan was measured by either fitting to a square or oval shape and taking ten measurements along each relavent dimension. This area was plotted as a function of the time (taken at the end of the scan) to produce one of the lines shown in the graph of figure 5.2(a). There was often a 'lag' period at the beginning of styrene dose followed by a relatively linear change in the coverage. The negative of the slope of the linear region was taken as the rate of window coverage which is plotted as a function of styrene dosing pressure in figure5.2(b).

As seen in figure 5.2, a large deviation in the rate of window coverage for the same pressure was found. Moreover, the 'lag' period mentioned above could vary dramatically. We related this variance to the surface quality: the more dangling bonds present on the surface the greater the competition between line growth and normal diffusion. This competition can play a significant role in the number of

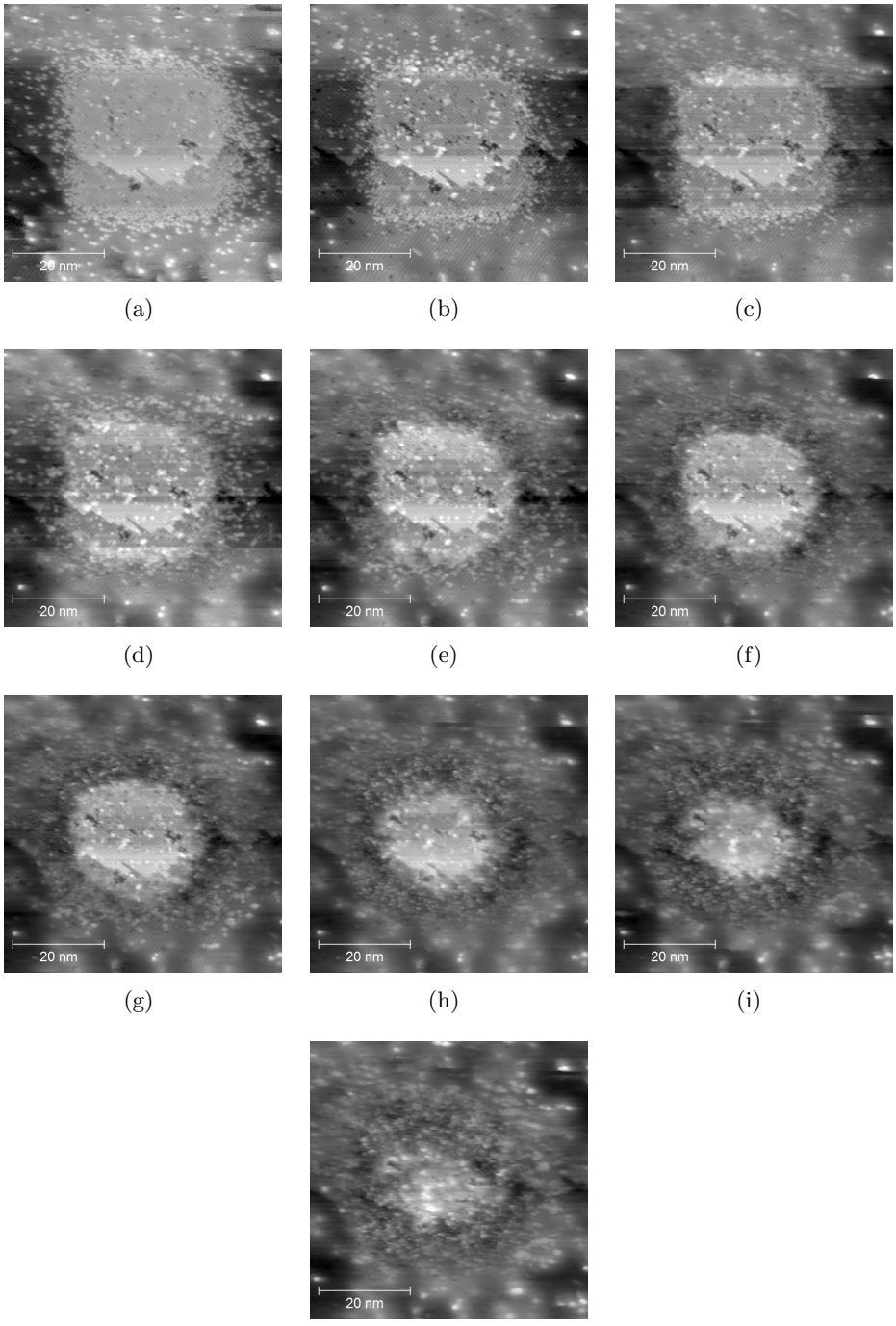

Figure 5.1: STM micrographs of styrene diffusion from hydrogen terminated Si(100):2×1 surface to clean Si(100):2 × 1. (a) Clean Window (b)-(j) successive images of window region during 8×10^{-9} Torr styrene dose. Imaging direction is from bottom to top with the dose starting at the botom of image (b). Imaging conditions: $V_S = -2$V, $I_T = 100$pA.

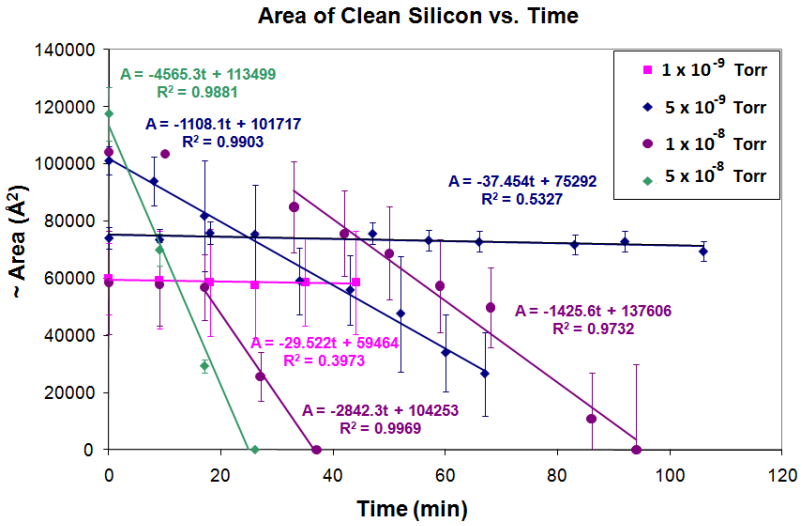

(a)

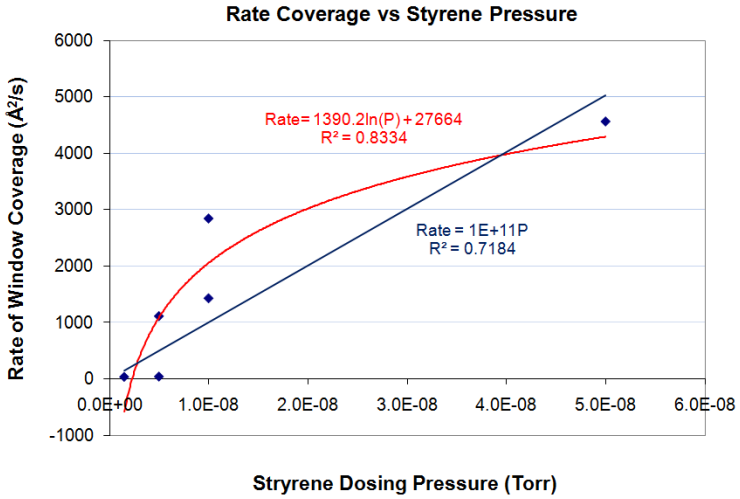

(b)

Figure 5.2: Styrene Diffusion: Imaging while Dosing. (a) Area of Clean Si(100):2 × 1 in window versus time. Error bars reflect result of one standard deviation of the dimension measurements for area measurements. (b) Rate of Coverage versus Styrene Dosing Pressure. The blue fit presents a linear fit to the data while the red fit presents a logarithmic fit.

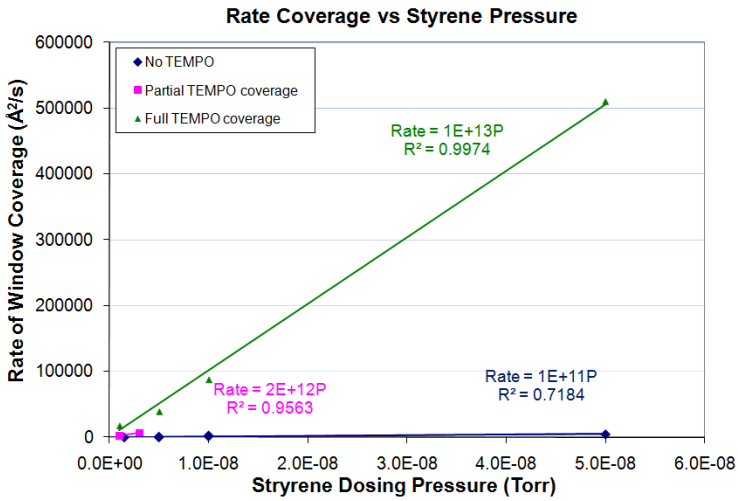

Figure 5.3: Styrene Diffusion: Imaging while Dosing on TEMPO Protected Surface. Blue: no TEMPO protection; Magenta: Partial TEMPO protection; Green: Full TEMPO Protection. Linear Fits to all data sets are presented.

molecules diffusing to the window. As the number of natural dangling bonds (DBs) on the surface can be very difficult to control, we chose to protect dangling bonds with a radical molecule. Pitters et al. has shown the remarkable efficacy of 2,2,6,6-tetramethyl-1-piperidinyloxy (TEMPO) in protecting dangling bond site on silicon [130, 131]. For a 2L TEMPO dose, extensive searching on other areas of the crystal after the full exposure to styrene provided no evidence of line growth - indicating extremely good DB capping. Generally low initial DB densities helped ensure that TEMPO sites did not greatly impact the adsorbate diffusion. As the window of clean silicon was created after the capping process, some stray DBs could still be found around the window of clean dimers.

The resulting rates of window coverage for the studies of diffusion on a TEMPO capped surface are provided in figure 5.3. The data from the TEMPO unprotected surface is reproduced here to highlight the large difference in the rate of coverage. As a point of interest, the graph also includes a few trials with partial TEMPO protection (some line growth was observed away from the windw). As expected, the rate of coverage is intermediate between the fully protected surface and the unprotected surface. It can be seen that by removing styrene line growth from the equation, the rate of coverage was increased over 10000 times. This provides some indication of the high number of styrene molecules that, once physisorbed to the surface, participate in line growth. In addition, with line growth removed,

we can see that a linear fit to the rate versus pressure data produces much better agreement with an R^2 value much closer to unity. A slightly better fit of the data in Fig. 5.2(b) is gained using a logarithmic fit. In general, on the unprotected surface, there is indication that as the dosing pressure increases, the rate of styrene coverage does not increase proportionally. This suggests that at higher pressures a greater percentage of molecules participate in line growth, which in turn suggests that molecule-molecule interactions aid in the line growth process.

The data presented for the TEMPO capped surface in figure 5.3 were produced with the same STM tip. Unfortunately, it was found that with different tips the rates of coverage could differ substantially. In fact, I was able to determine that tips used to determine slightly lower rates of window coverage also had increased tip shadowing of styrene on clean silicon. In section 3.5 it was mentioned that the shadow effect of different tips could vary from 400 nm up to 1.5μm. In this experiment, as the shadow region increases the molecules must diffuse longer distances over the H-terminated surface before reaching the clean silicon window.

In order to completely remove tip effects from the diffusion studies, it was necessary to retract the tip from the surface prior to exposing the surface to a specific dose of styrene. An 'image-dose-image' procedure was thus created. The final procedure followed in the remainder of this chapter was thus:

1. Terminate the clean surface with hydrogen
2. Image to ensure nice 2×1 termination and low DB density
3. Protect stray DBs with the TEMPO radical (and clean tip)
4. Create a window of clean silicon using tip-induced hydrogen desorption
5. Image the window
6. Retract piezo fully and retract tip by 3 course steps
7. Dose styrene at 1×10^{-8} Torr for 10s and allow chamber pressure to reach 5×10^{-10} Torr before approaching with tip
8. Repeat 5- 7 as able (in most cases, one repeat for a total of two doses was feasible)

5.3 STM Studies of Diffusion - Experimental

The method developed above was highly useful in its elimination of tip effects from the diffusion study. Unfortunately, with the retraction of the tip came the loss

of the ability to directly observe diffusion with time. However, unique aspects of the diffusion process could still be probed. Two such aspects of interest are the average diffusion length of a physisorbed species on the surface and the effect of the surface structure on the diffusion process. The Si(100)2 × 1 surface is composed of rows of dimers separated by gulley regions. The rate of diffusion along these rows could be different from the rate of diffusion across the rows. However, such diffusion anisotropies can be quite small and standard STM methods of study are known to have masked anisotropic effects [122]. Using the above prescribed method of removing STM tip influences, both the average diffusion length and anisotropy were studied. An interesting side question that arose was how the change of a single atom in the molecules may alter the diffusion process. As such, the study was also conducted experimentally for 4-fluorostyrene - a polar molecule also of interest in line growth studies.

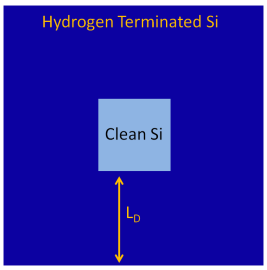

Figure 5.4: Description of Diffusion Length as the thickness of the frame around the clean silicon window.

The diffusion length, L_D, of an adsorbate on a surface provides a measure of the distance the adsorbate can travel before leaving the surface. Using the method above, an estimate of L_D can be made given three basic assumptions. (1) Clean silicon has a sticking coefficient of unity and can accomodate one styrene molecule per silicon dimer. This is reasonable based on the strong reactivity of the molecule with the surface and previous calculations of monolayer density (binding energy of 1.6 eV [132,133]). (2) The density of molecules landing on the hydrogen terminated silicon is the same as on the clean silicon. This assumption is essentially equivalent to assuming that there is no gradient in the vapor pressure of the molecule near the clean window and the surrounding hydrogen. For our system this assumption is very reasonable as the vapor pressure is quite low, the dosing line is over 20cm away from the sample allowing for ample dispersion and the combined area of the window and relevant hydride surface is quite small. (3) The final assumption is perhaps the most complex. Here, we assume that diffusion takes place from a frame shaped region surrounding the window, and all molecules in that area eventually diffuse to the window without leaving the surface. The frame shape region is taken to facilitate analysis with a square window. A circular window would be more appropriate for an average Ld analysis, however such shapes are much more difficult to create with STM lithography and would make the

anisotropic diffusion studies, which are conducted at the same time, more difficult. Assumption three also suggests that the number of molecules diffusing out of the frame is equal to the number diffusing into the frame which requires that there are no DB initiator sites, and thus no line growth, on the H-Si(100) surface. In reality some DBs are created near the edge of the clean window during the hydrogen desorption process. However, it is expected that the effect of these DBs is minimal.

With these assumptions in mind, L_D is defined as the thickness of the frame contributing adsorbates (Fig 5.4). To calculate L_D the density of molecules, (ρ_{ads}) that landed on the surface from the vapor was first determined by counting the number of styrene molecules that landed directly in the centre (still clean) region of the clean window divided by the area in question. The required area of hydride surface ($A_{hydride}$) contributing diffusing molecules (i.e. dark blue region in Fig 5.4) can be determined by:

$$A_{hydride} = \frac{1}{\rho_{ads}}[A_{adsorbatecoveredwindow} \times \frac{1molecule}{A_{Dimer}} - A_{adsorbatecoveredwindow} \times \rho_{ads}] \tag{5.1}$$

L_D is then:

$$L_D = \frac{1}{2}(A_{hydride} + A_{CleanWindow}) - (L_{window}) \tag{5.2}$$

where, L_{window} is the length of the window of clean silicon.

In order to study the anisotropic nature of the diffusion process, a comparison of the movement of molecules along the dimer row to the movement of molecules across the dimer row was required. While the general procedure for the experimental technique was outlined at the end of section 5.2, the following considerations were taken when the clean silicon window was created(i.e. step 4):

- The location of each experiment was carefully chosen such that the window of clean silicon as well as a surrounding region of H-terminated silicon could be created on a single silicon terrace.
- Attempts were made to have a buffer of at least 100nm of H-terminated silicon between the clean Si window and a silicon terrace step edge. However, due to irregularities in step shape this was not always possible.
- Window sizes varied from 70 nm × 70 nm to 100 nm × 100 nm depending upon the silicon terrace size.
- Alignment of the clean silicon windows with the dimer rows was ensured by aligning the tip scanning direction either parallel or perpendicular to the row

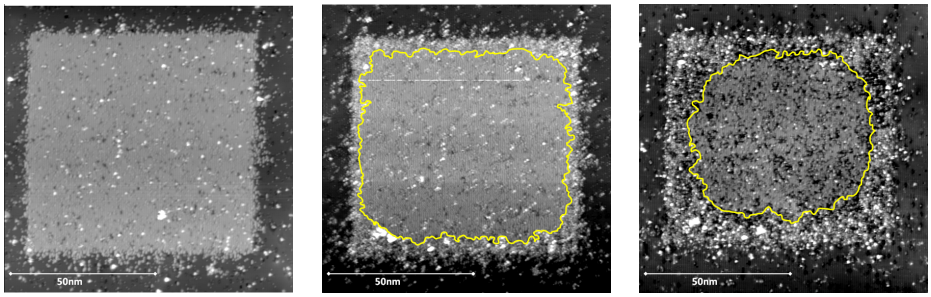

(a) (b) (c)

Figure 5.5: Styrene Diffusion: Imaging, Dose, Image. STM images of the clean Si(100) [light gray] window on hydrogen terminated Si(100)-2 × 1 [dark gray] at $V_S = -2$ V and $I_T = 100$pA. The dimers rows are oriented vertically in the images: (a) Before dosing styrene; (b) after one dose of styrene at 1×10^{-8} Torr (uncalibrated) for 10s; and (c) after a second dose of styrene at 1×10^{-8} Torr (uncalibrated) for 10 s. The yellow lines in (b) and (c) provide a guide to the edge of the styrene covered region of the clean surface. It is important to note that in the STM images bright areas on the hydrogen terminated surface near the window are not styrene; rather, they are DBs and other defects that are either naturally occurring or produced during the lithography process. The fast diffusion of styrene molecules makes it impossible to image them at room temperature on the hydrogen terminated Si(100) surface. Adapted with permission from [112]. Copyright (2010) American Chemical Society.

direction. This ensured that two edges of a window were aligned with the dimer rows on the terrace while the remaining edges were aligned perpendicular to the row.

Measurement of diffusion anisotropy was then taken from each of the STM images by comparing the average widths of the chemisorbed styrene at the outer edges of the clean silicon window. Ten width measurements were taken from the centre region of each edge so as to eliminate corner effects where molecules arrive from a wider range of directions and the flux of molecules is increased. The ratios of the widths resulting from diffusion along the dimer row to the diffusion along the dimer row provided a measure of the anisotropy. As such, each experiment provided four independent anisotropy measurements. For example, if the dimer row's were aligned from 'top' to 'bottom' of the window the four measurements ratios considered were: Top/Left, Top/Right, Bottom/Left, Bottom/Right. For alignment in the perpendicular direction the inverse ratios held.

Both the diffusion length and the anisotropy were studied in the same sets of experiments. In figure 5.5, representative initial (before dose), one dose, and two

dose results for an STM experiment of styrene diffusion are shown. For clarity, the border of the styrene on clean silicon has been outlined in yellow. In the images, the increase in molecular flux at the corners is noticeably discernible as a rounding of the corner edges of the window. Observation of the hydride surface surrounding the window after styrene exposure demonstrates that very few styrene molecules have reacted with stray DBs created by the desorption process. This helps to validate assumption (3) in the estimation of the diffusion length.

The average diffusion length for styrene was found to be 110 nm ± 30 nm while that for 4-fluorostyrene was found to be 77 nm ± 7 nm. These diffusion lengths were smaller than anticipated. Given the large tip shadow regions (400nm to 1.5μm) observed on the clean silicon surface and the ability to observe line growth (and other effects such as the window coverage experiments) while the tip is in tunneling contact with the surface, I had expected that the diffusion length would be on the order of the larger shadow regions. The determined diffusion lengths are, however, representative of an average diffusion length. Even if only a small number of molecules diffuse over greater distances, this may be enough to observe line growth and other phenomena under a tip with a large shadow region. The origin of the significantly larger distribution in diffusion lengths for the styrene experiments compared to the 4-fluorostyrene experiments is not well understood. However, the smaller diffusion length determined for 4-fluorostyrene is in agreement with the lower binding energy calculated in section 4.6.1. A lower binding energy implies that the molecule will have an easier time desorbing from the physisorbed state on the surface. As such, it will diffuse over a smaller distance over the surface. However, the calculatons predicted a binding energy difference of almost half where as the diffusion lengths, while smaller for 4-fluorostyrene, are not indicative of such great a difference - particularly when considering the standard deviations. In Chapter 4, it was suggested that the molecules with halides may suffer from basis set incompleteness issues in the calculations and this may be the differentiating factor between the experimental results and the calculations.

Qualitative observation of the images in figure 5.5, does not immediate make obvious any diffusion anisotropy in the system. Indeed, the quantitative measurements displayed an average diffusion anisotropy of only 1.1 ± 0.1. Moreover, experimental results for the anisotropy of the both styrene and 4-fluorostyrene were found to be both identical and within the margin of error, where the error is taken as one standard deviation. Such small anisotropic measurements could be interpreted in vastly different ways, including:

1. The experimental method is in fact quite sensitive and able to make out very

small diffusion anisotropies.

2. The experimental method is satisfactory, but considering the error there is no discernible diffusion anisotropy of the molecule on the surface.

3. The experimental method, which includes both energy and dynamic effects is not suitable for the study of diffusion anisotropy.

To understand which interpretation has greater validity, independent theoretical analysis of the diffusion of styrene was conducted.

5.4 Styrene Diffusion - Theoretical

5.4.1 Density Functional Theory

Understanding the nature of styrene diffusion on the hydrogen terminated Si(100):2$\times$ 1 surface, required two steps of theoretical treatment. Density Functional Theory (DFT) was first used to calculate the binding energies and the energy barriers to diffusion. Monte Carlo (MC) simulations, discussed in the next section, were then used to incorporate dynamic effects.

In section 4.6, density functional theory was used to determine the local minima of styrene on the H-Si(100):2 $\times$ 1 surface. The two lowest minima were very similar in structure and energy. In both, the carbon ring of the styrene molecule was centered upon a surface hydrogen atom - similar to the minima structure recently calculated for benzene on the same surface [101]. The position of the vinyl group served to differentiate the two minima: one had the vinyl group over the gulley region while the other had the vinyl over the dimer row itself. The later structure was used as the starting point of determining the potential energy surface (PES). However, the optimum structure of the molecule interacting with the surface has the vinyl group slightly out of the plane of the ring (dihedral angle of 169 °) and an average molecule distance of 3.9Å above the surface. To facilitate the calculations, the vinyl group was rotated into the plane of the ring and the molecule was placed parallel to the surface at the average distance. In addition, the surface terminating hydrogen atoms that were allowed to move in section 4.6 were placed in their original optimized positions. These simplifications decreased the binding energy by 0.01eV which is 4% of the binding energy.

The 'flattened' global minima structure was then used to acquire a description for the entire PES. From the PES, the minimum energy paths for diffusion were identified. DFT was again used to refine the calculated barrier heights. Using these barrier heights, the rate constants for diffusion across individual barriers were

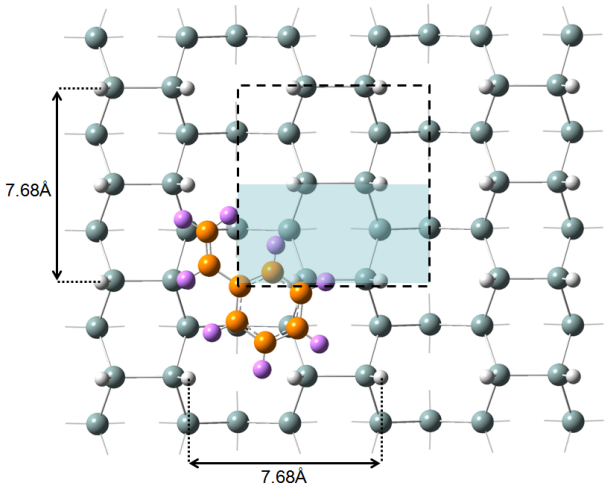

Figure 5.6: Top-down view of the hydrogen terminated Si(100)-2 × 1 model used for the single-point energy calculations of the translated styrene molecule. The colors shown define the following atoms: orange, carbon; gray, silicon; purple, hydrogen on styrene; white, hydrogen atoms on the silicon surface. For ease of view, hydrogen atoms capping the interior silicon atoms are shown in stick format. The inner square outlined by the dashed line represents a lattice site used in the MC calculations. The shaded region of this square represents the area used for the DFT potential energy surface calculations of the molecule using a grid of spacing of 0.33 Åby 0.33 Å. The position of the molecule depicted represents the starting coordinates for this grid. Adapted with permission from [112]. Copyright (2010) American Chemical Society.

calculated following the determination of the path diffusion rate constants. The calculations were accomplished using much of the same theory discussed in Chapter 4. The B971 [110] functional was used with the 6-31+G(d,p) basis sets and dispersion correcting potentials (DCPs) [99, 101, 102]. All calculations were again performed using the Gaussian 03 package [111].

The PES was determined on a surface model with a larger surface area than that described previously, but less depth into the surface. The slab model in this case consisted of three dimer rows of four dimers each and two gulley rows for a total of 64 Si atoms was used (Fig 5.6). In the figure, the shaded rectangle represents surface area over which the calculations were performed. The molecule was placed at the corner position as shown, and then translated along the xy-plane in a grid pattern of 0.33 Å spacing in both directions while the z-position was held fixed at 3.9 Å. At each point on the grid, a single-point energy calculation was performed. A linear interpolation between the energies was used to generate the final PES (Figure 5.7). The energies in this plot are shown with respect to the position of the ring carbon to which the vinyl group is bonded. For example, the starting grid point shown in

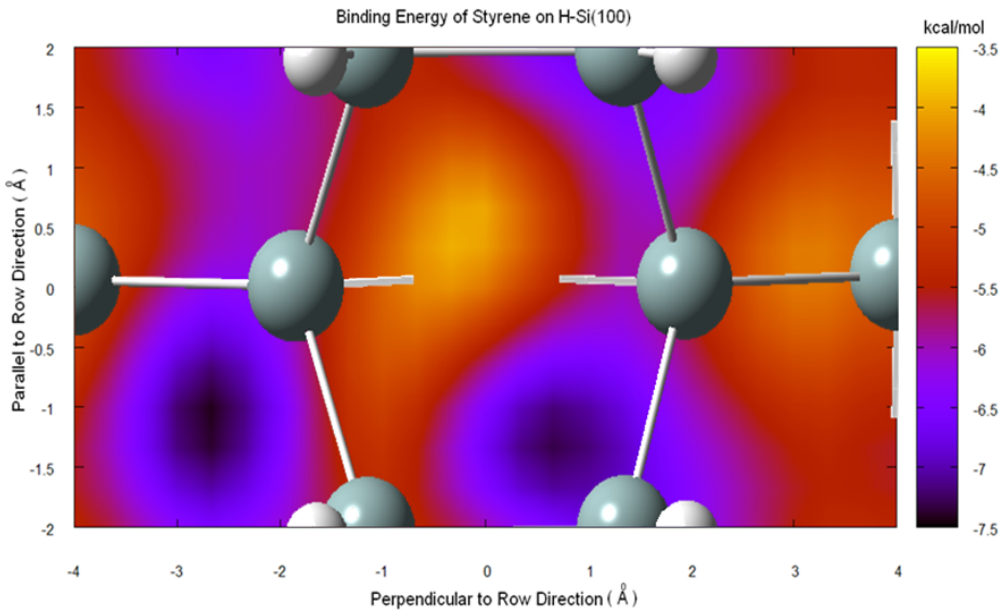

Figure 5.7: Topographical map of the potential energy surface of styrene on H-Si(100)-2 × 1 in kcal/mol. The energies are plotted with respect to the ring carbon attached to the vinyl group. For clarity, a corresponding section of the H-Si(100) model is superimposed. Adapted with permission from [112]. Copyright (2010) American Chemical Society.

figure 5.6, corresponds to (-4, -2) on the PES. The two lowest minima from the full optimizations are clearly visible as the dark purple and black regions of the map.

The identified possible energy barriers were then refined. The molecule was placed at the (x, y) coordinates that correlated with a diffusion energy barrier maximum. By exploring various styrene orientations above the structure to find possible lower energy structures. The energy of the lowest energy structure was then taken as the barrier height maximum.

Using the PES, the minimum energy paths for traversing from one minima to another were identified. As can be seen from the PES, diffusion in the perpendicular to row direction required that the stryrene traverse from one minima to a slightly energetically higher intermediate and then to a minimum that is equivalent to and 7.68Å away from the starting point. Diffusion in the reverse direction was also possible and the height of the barrier encountered during the diffusion depended on whether a gulley or row region is crossed first. Diffusion in the parallel to row direction is somewhat simpler. In this direction, all the minima positions are equivalent. However, by defining a diffusion event as the transition to the next nearest

Motion	Coordinate Change	From PES (kcal/mol)	Refined (kcal/mol)
Across	-2.66 : 0.66	2.1	1.4
	0.66 : -2.66	1.9	1.3
	0.66 : 5.33	1.9	0.9
	5.33 : 0.66	2.0	1.1
Along	-1.00:3.00	1.4	0.9

Table 5.1: Styrene diffusion barrier heights for motion across and along the dimer row direction. The 'coordinate change' is the change in the direction of motion and the coordinate system discussed with respect to the PES. The energy barriers calculated directly from the PES as well as the refined barrier heights are shown.

neighbour minima at a distance of 7.68Å away from the starting point make the parallel and perpendicular-to row diffusion events comparable.

The barrier heights for the diffusion process are listed in Table 5.1. It can be seen that the barriers to diffusion are only approximately 1.0 kcal/mol. This is significantly less than the approximately 7.7 kcal/mol physisorption binding energy so we would expect several diffusion events to take place before a physisorbed molecule leaves the surface. Each of the barriers listed has an associated rate constant for diffusion. This was modeled using an Arrhenius approximation, given by equation 5.3:

$$k = A\exp(-\frac{\Delta E_b}{k_b T}) \tag{5.3}$$

where ΔE_b is the energy barrier or activation energy; k_b is the Boltzmann constant; and T is the temperature. The pre-exponential factor, A, is related to the attempt frequency for the diffusion to take place and is assumed to be the same for all processes considered.

The rate constants for diffusion paths, ie parallel or perpendicular to the rows, are then determined according to a reaction with an intermediate state, given by eq 5.4:

$$k_{parallel} \quad \text{or} \quad k_{perpendicular} = \frac{k_I k_{II}}{k_{-I} + k_{II}} \tag{5.4}$$

where the rate constant subscripts I, -I, and II represent the diffusion from the initial position to the intermediate structure, the diffusion from the intermediate back to the initial position, and the diffusion from the intermediate to the final position, respectively. The assumption of the pre-exponential being the same in all cases, mentioned above, is utilized in equation 5.4.

Using the above equations and the calculated barriers, the room temperature rate constants were found to be $k_{parallel} = 0.11\text{s}^{-1}$ and $k_{perpendicular} = 0.06\text{s}^{-1}$. The

directional anisotropy $k_{parallel}/k_{perpendicular}$ was thus determined to be 1.8.

The DFT calculations determine anisotropy based upon purely energetic considerations. At almost 2-fold anisotropy, the difference is significant. Earlier in this chapter, experimental studies resulted in an anisotropy of only 1.1 ± 0.1. However, the experiments include both energy as well as dynamic effects. To make a fair comparison with theory, dynamic effects should be included in the theoretical treatment.

5.4.2 Monte Carlo Treatment

A common theoretical approach that combines energy considerations in conjunction with dynamic effects to more accurately simulate a system, is to utilize Monte Carlo (MC) type analysis. For this study, a simulation program was created in C++ using a Mersenne Twister random number generator [134, 135]. The simulation followed the general concepts of the random selection Monte Carlo method described in detail by Lukkien et al. [136]. The rate constants determined from the DFT energy analysis were used as input values into the simulation.

The base frame of the simulation consisted of a lattice representing the physisorption binding sites of styrene on H-Si(100):2×1 and the chemisorption binding sites of styrene on clean Si(100):2×1. The lattice gas model was adopted such that adsorbates could only occupy discrete lattice positions. Physically, each lattice site corresponded to two dimers on one row and the adjacent gulley region on the silicon surface - as shown by the square region in Fig 5.6 oulined by the dashed lines. The initial conditions of the simulation had styrene molecules randomly distributed across the surface with a coverage of 2.9% for one dose and 5.8% for two dose simulations. For simplicity, this coverage represented the total number of molecules that would arrive on the surface throughout the entire dosing period of the STM experiments. Therefore, the density on the surface at a particular time during the STM experiments was less than the density used in the simulations.

For each lattice position representing H-Si(100), only a single adsorbate molecule was allowed to occupy the space. A diffusion event on H-Si(100) was described as the movement of a styrene molecule on the lattice to one of four available nearest neighbor lattice sites. This in turn represents a molecules movement from one energy minima to an equivalent minima located at a distance of 7.68Å either along the row (two dimer units away) or perpendicular to the row (dimer in neighboring row). Such a diffusion event corresponds directly with the rate constants calculated above. The probabilities (P) for activating diffusion events in all four directions

were calculated according to:

$$P_{direction} = \frac{k_{direction}}{\sum k_{direction}} \tag{5.5}$$

where the diffusion rate constants, are the calculated results from equation 5.4. Random step directions were chosen according to these probabilities.

For each lattice position representing clean-Si(100), two styrene molecules could be accommodated. The higher occupancy on clean-Si(100) sites corresponds to the binding of one molecule to one silicon surface dimer. This is representative of the addition chemistry that occurs between this adsorbate and the clean surface [32,126, 127]. As the sticking coefficient associated with styrene on clean Si is assumed to be unity, once a styrene molecule encounters a free lattice site on the clean surface the position becomes fixed. For diffusing molecules that encounter lattice sites on the clean surface that are fully occupied by chemisorbed styrene, diffusion was allowed to occur isotropically. The isotropic diffusion rate was modeled as the average of the rates over the hydrogen terminated surface; however, due to the relatively low occurrence of this situation, the diffusion rate on styrene-covered clean silicon should have little or no impact on our calculated results. Only one physisorbed styrene was allowed on a lattice site that contained two chemisorbed styrene molecules.

Two different boundary conditions for the MC simulations, reflective wall and periodic, were explored. Both conditions produced similar results. The simulation was terminated when less than 0.5% of the adsorbates in the system remained on the hydrogen terminated silicon. The images of the lattice were analyzed using the same method used to analyze the STM images.

The simulation program was tested to ensure that the diffusion behaviour correctly reproduced the expected behaviour from the calculated energies. The method used to test the relative rates of diffusion was similar to an adsorbate tracking method in that the motion of each adsorbate is monitored as the simulation progresses. In each case analyzed, the ratio of the total jumps (for all the adsorbates on the H-Si surface) along the row over the total jumps across the row correctly reproduced the pure energy based anisotropy ratio of 1.8 obtained from the diffusion rate constants. MC simulations were run using a clean window size of 70nm x 70nm. This represents the lower end of the window size range used in STM experiments (70nm x 70nm to 100nm x 100nm). The simulation was run 10 times for both one and two doses using both periodic and reflective wall boundary conditions. Fig. 5.8 presents STM like images of the initial (random distribution of styrene), one-dose and two-dose results. To facilitate ease with comparison to STM results, the figure also includes results from STM experiments discussed in the experimental section.

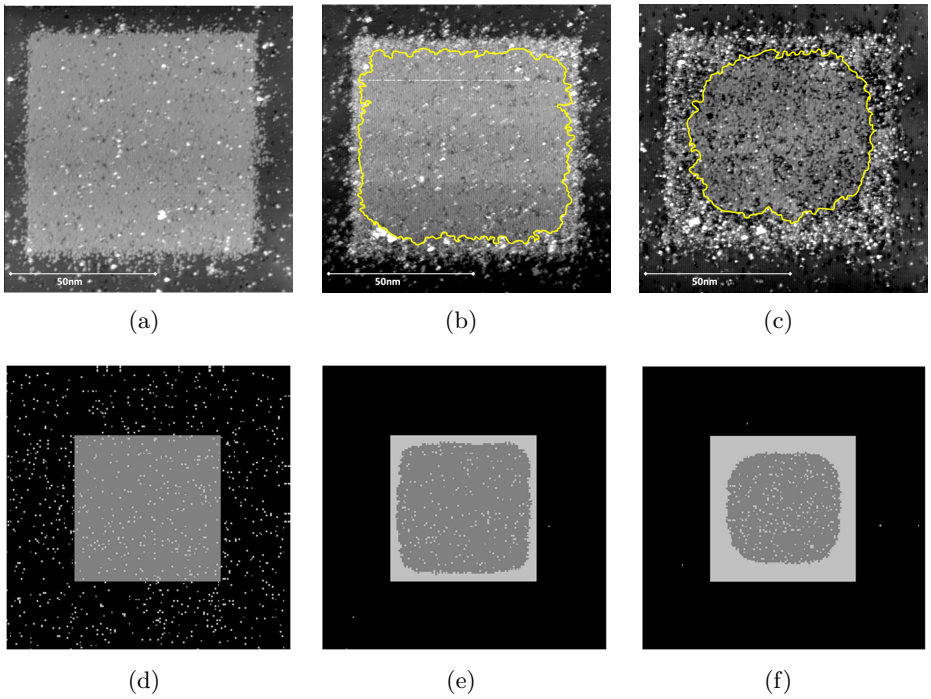

Figure 5.8: Styrene Diffusion: STM images of the clean Si(100) [light gray] window on hydrogen terminated Si(100)-2 × 1 [dark gray] at $V_S = -2$ V and $I_T = 100$pA. The dimers rows are oriented vertically in the images: (a) Before dosing styrene; (b) after one dose of styrene at 1×10^{-8} Torr (uncalibrated) for 10s; and (c) after a second dose of styrene at 1×10^{-8} Torr (uncalibrated) for 10 s. The yellow lines in (b) and (c) provide a guide to the edge of the styrene covered region of the clean surface. (d-f): Images from Monte Carlo simulations of the STM experiments. The dimer rows have the same orientation as in images a-c. For clarity only a small region of H-Si(100) [black] lattice around the clean Si(100) [dark gray] window is shown: (d) Initial setup showing the clean Si region surrounded by hydrogen terminated Si and a random distribution of styrene molecules [light gray] and (e) diffusion resulting from a one styrene dose simulation. (f) Diffusion resulting from a two-dose simulation. In these images, bright areas on the hydrogen terminated surface do represent styrene molecules. Reprinted with permission from [112]. Copyright (2010) American Chemical Society.

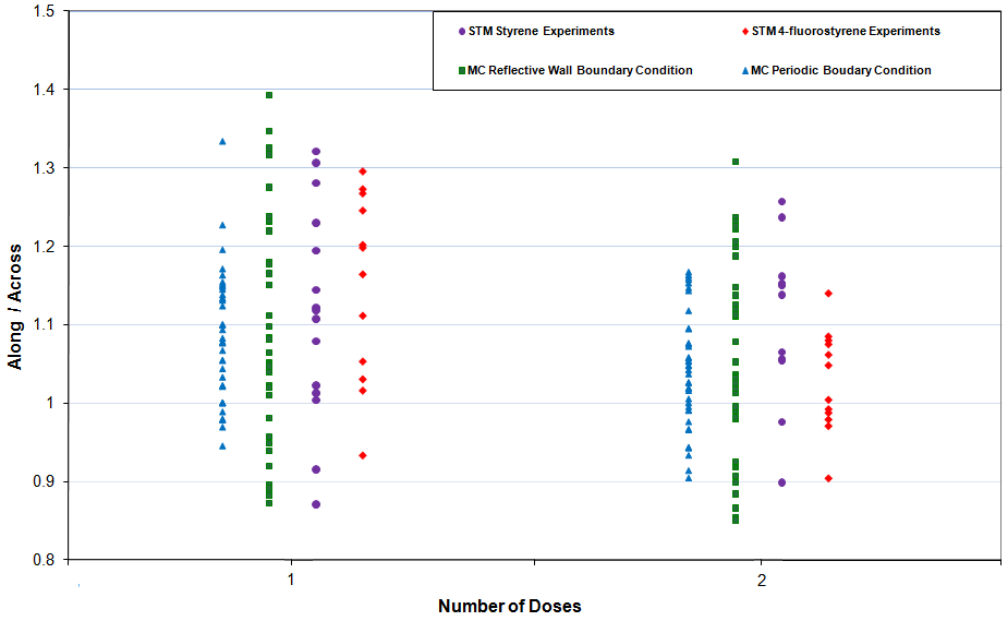

Figure 5.9: Directional anisotropy of styrene diffusion along and across dimer rows on the H-Si(100) versus the number of doses of styrene at 1×10^{-8} Torr (uncalibrated) for 10 s. Anisotropy is measured as the ratio of the average width of diffused molecules at the edge of the clean silicon window resulting from diffusion along the row over diffusion across the row. Results from STM styrene experiments (purple circle), STM 4-fluorostyrene experiments (red diamond), Monte Carlo with a reflective wall boundary condition (green square), and Monte Carlo with a periodic boundary condition (blue triangle) are shown. All results are for either one or two doses; however, results have been offset along the x-axis for clarity.

To mimic the STM images, only a portion of the centre of the full lattice is shown in the MC images. Lattice points representing hydrogen terminated styrene surface do in fact extend from each side.

The results of the quantitative analysis of anisotropy for both the MC as well as the experiments are provided in Fig. 5.9. The results for both boundary conditions agreed to within 0.1%. The overall average anisotropy was found to be 1.06 ± 0.04. This is in close agreement with the experimental results of 1.1 ± 0.1. In addition, both the experimental and MC simulations had a similar spread in the data. This spread is caused by the finite nature of the system.

To determine whether the range of window sizes used in the STM experiments, could have an effect on the outcome, MC simulations using the periodic boundary condition, were run using clean window sizes in the range of 50 nm x 50 nm to 200 nm x 200 nm. The average results and standard deviations for 10 runs for each

Figure 5.10: Average MC Anisotropy ratio over ten simulations (40 anisotropy) versus Length of clean Silicon Window

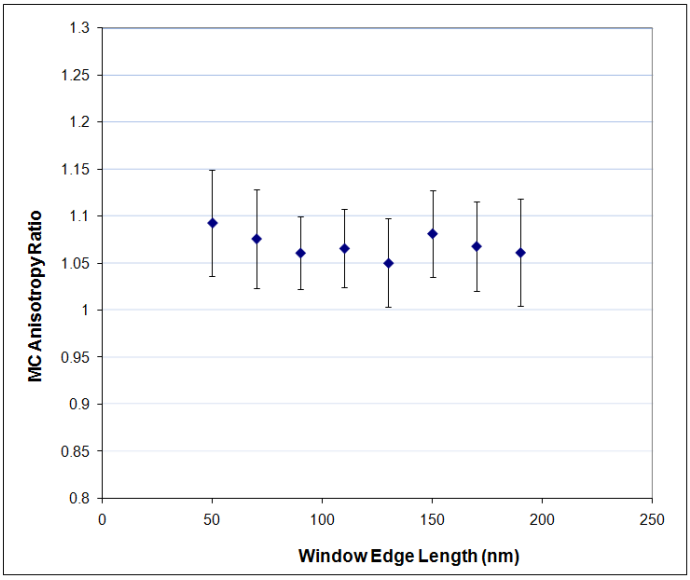

window size are provided in figure 5.10. It can be seen that the average is quite flat across the varied window sizes indicating that the analysis method appropriately accommodates for window size effects such as corner rounding.

The strong correlation between the MC and STM experimental measurements suggests that the experimental method is a useful approach to study diffusion parameters. However, to link the experimental results to pure energy related anisotropy ratios, dynamic effects must be accounted for. This suggests that a simple fitting of Monte Carlo measurements to experimental measurements could potentially be used to accurately estimate directional diffusion anisotropy ratios expected directly from diffusion rate constants.

To test this application, the MC simulation was run for a series of different energy anisotropy ratios. The average results and standard deviations for 10 runs for each ratio are plotted in figure 5.11. As expected, the anisotropy ratio included energetic and dynamic effects increases as the pure energy anisotropy ratio increases. Using Fig 5.11, a direct mapping of the experimental average anisotropy ratio of 1.1 ± 0.1 would map to an energy anisotropy ratio of 2 ± 1. While the value itself is close to the calculated energy anisotropy of 1.8, the large error range is concerning. However, the anisotropy ratios of some systems can be very large - they can indeed span a range of orders of magnitude [114, 124]. Moreover, theoretical calculation of diffusion rate constants of organic molecules on surfaces is an expensive computational task. The

Figure 5.11: Average MC Anisotropy ratio over ten simulations (40 anisotropy measurements) versus pure energy dependent Diffusion Rate Constant Ratios. The MC Anisotropy Ratio can be thought of as the expected STM Experimental Ratio for correlation with pure energy anisotropy expectations.

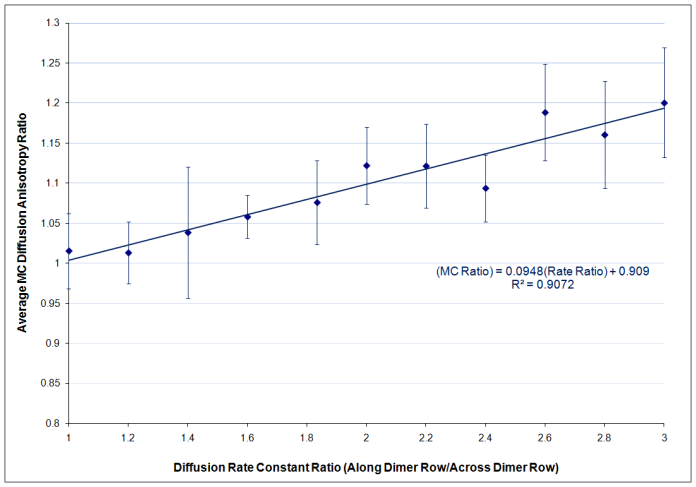

ease of the proposed correlation to theoretical relative energies may prove to be quite useful in identifying a good approximation of the pure energy related anisotropy ratio.

5.5 Chapter Summary

A novel method of studying aspects of surface diffusion which can be accomplished at a single sample temperature and is not prone to STM tip effects has been developed. In particular, the diffusion of styrene and 4-fluorostyrene on H-Si(100):2 $\times$ 1 has been conducted by taking advantage of the high reactivity of these molecules with the clean Si(100):2 $\times$ 1 surface. The molecules were found to have estimated diffusion lengths of 110 nm $\pm$ 30 nm for styrene and 77 nm $\pm$ 7 nm for 4-fluorostyrene. The smaller diffusion length of the fluorinated molecule is to be expected considering the greater hydrophilicity of the molecule and therefore the reduced interaction with the hydrophobic surface. Both molecules were found to have an experimental diffusion anisotropy 1.1$\pm$0.1. It is extraordinarily rare to be able to experimentally determine such small differences in the direction dependence of surface diffusion. To validate such small anisotropies, theoretical calculations of the anisotropy of styrene on H-Si(100):2 $\times$ 1 was conducted. The theoretical study involved DCP-DFT analysis of the potential energy surface and diffusion barrier heights followed by Monte Carlo

analysis which incorporated the DFT energies and dynamic effects of the motion along the surface near windows of clean silicon. The resulting theoretical anisotropy of 1.06 ± 0.04 is in good agreement with experimental findings. The use of combined experimental studies with MC simulations to estimate the energy barrier ratio was explored. It was found that such analysis could provide an order of magnitude expectation of the energy barrier ratio.

Chapter 6

STM Spectroscopy: Patterns

6.1 Chapter Introduction

In chapter 3 STM spectroscopic methods were employed to study the current transport from clean and chemically modified Si(100):2×1 surfaces. In chapter 7, similar techniques will be employed to try to study the current transport of nanostructured molecular lines on the silicon surface. While the former studies led to a model of the transport from such surfaces, the later studies will be found to be inconclusive. The inconclusive nature of the later studies brings into question the scalability of chemically tuning the transport properties to small features. In this chapter, methods developed in chapter 3 will be used to study the characteristics of mid-range features defined by STM lithography. In addition, the behaviour of silicon near electron beam lithographically defined patterns will be probed.

6.2 STM Lithographic Patterns

In the previous chapter, STM induced hydrogen desorption was used to fabricate patterns of clean silicon on an otherwise hydrogen terminated surface. Effectively, these patterns were then further utilized as masks for the fabrication of styrene and 4-fluorostyrene patterns. From our knowledge of the I_T/V_S characteristics of surfaces, we can anticipate that such patterned windows would indeed have unique I_T/V_S signatures.

The I_T/V_S characteristics of a similar window pattern has previously been studied by Dickie et al. [81]. The constructs previously reported consisted of windows of clean Si(100):2×1 on an otherwise benzene terminated surface. As mentioned in chapter 3, the benzene terminated surface had similar characteristics to styrene but with a slightly increased rectification of 30:1 at z=5Å. It was found that the windows displayed a hybrid character from that of the benzene terminated surface and the

clean surface. The change in the tunneling current with tip-sample separation was almost identical to the benzene surface suggesting that the workfunction was similar to the benzene coated surface outside the window rather than the clean surface making up the window. The forward to reverse rectification properties of the curves was slightly less but extremely similar to those of the surrounding surface as well. However, in the clean windows a curvature was introduced into the spectra that was reminiscent of the clean surface and the onset voltage was reduced with respect to the benzene terminated surface. The I_T/V_S characteristics remained the same for four windows varying in size from 20nm $\times$ 20nm up to 50nm $\times$ 50nm. It was surmised that lateral interactions allowed the low energy conduction band edge of the benzene surface to depopulate the π^* states in the clean surface. It was suspected that window sizes on the order of the minority carrier diffusion length would be required to regenerate some of the characteristics of the clean Si(100):2 $\times$ 1 surface.

Window patterns of clean silicon were prepared on hydrogen terminated n^+ Si(100):2 $\times$ 1, as described in chapter 5. Styrene and 4-fluorostyrene terminated window regions were created by exposure to the molecule of interest until the window was observed to be fully covered. Spectroscopy measurements were taken inside the window regions using the method of chapter 3. Data averaging was taken over 10-20 curves in each case. The standard deviations were similar to those of chapter 3. In all cases, measurements were also taken on the nearby hydride surface and demonstrated behaviour consistent with that of the fully hydrogen terminated surface. In one case, an odd curvature and lower than usual current magnitude were observed and were assumed to be a characteristic of the particular STM tip used. This will be discussed further later.

I_T/V_S information for a clean silicon window 30 nm by 30 nm in dimension is provided in figure 6.1. This case was found to be quite different from the case of a clean window on benzene. The change in current with tip-sample distance is exponential in nature, which is to be expected as both the clean and the hydride surface exhibit this behaviour. However, the small band gap at small tip-sample separation and the curvature of the spectra is generally similar to the clean surface rather than the surrounding hydride. Indeed, measurements of the forward to reverse rectification ratio were found to be stable near unity for all tip-sample separations, figure 6.2, as it was for the fully clean Si(100):2 $\times$ 1 surface. However, the spectra taken on the window is not identical to that of the clean surface. The primary difference lies in the conspicuous absence of an ohmic shoulder region in the spectra at low forward bias and small tip-sample separation as well as the lack of a zero bias current at small separation.

Figure 6.1: Averaged semi-logarithmic IV spectra for a clean 30 nm × 30 nm silicon window on H-Si(100):2 × 1. Spectra were taken at z = -3 Å(bottom curve) to +5 Å(top curve) towards the sample from the set-point of V_S = -2.0 V and I_T = 100 pA.

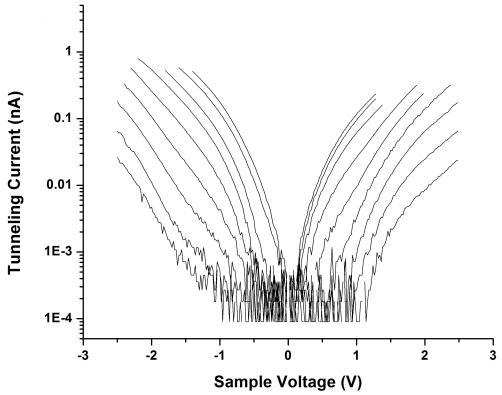

Figure 6.2: Forward to reverse current rectification ratios ($RR_{F/R}$) taken at ±1V versus z. As in previous measurements, z is indicative of angrstom steps away from the set-point with increasing z indicative of a smaller tip-sample separation. $RR_{F/R}$ for $z < 0$ are not shown as the currents in this region are very small (largely lie below the 1 pA current onset) and relatively noisy.

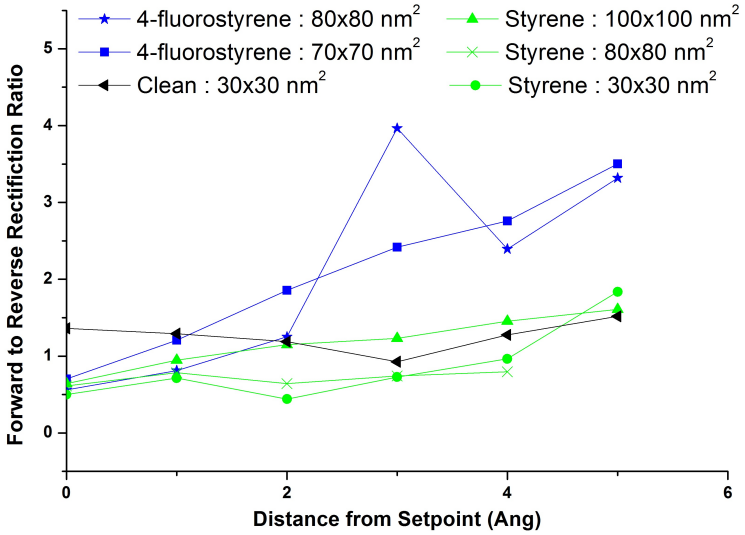

The I_T/V_S results suggest that band pinning by surface states is once again established in the clean window region and normal majority carrier transport is the dominant influence in either bias. However, the surface parallel conduction through π^* states that is present on the fully clean surface remains unavailable in the window region resulting in a loss of the ohmic shoulder. In the sample set-up, grounding and hence the counter electrode for I_T/V_S measurements, is at the edge of the bulk crystal. The hydride surface surrounding the window and separating it from the ground connection effectively blocks the surface channel. Moreover, the elimination of any effects in the shoulder region points towards the conclusion that the leakage current between the parallel conduction channel and the bulk is minimal. If the π and π^* surface states are truly reestablished within the window region, the surface conduction channel would still be available from one point of the window region to another point on the window. However, this would require that both the tunneling tip and the grounding of the sample take place in the window region. To accomplish this suggested test, a multiprobe STM instrument would be required. This will be discussed in detail later.

Three different window sizes were studied for patterns of styrene on the otherwise hydrogen terminated surface: 30nm $\times$ 30nm, 80nm $\times$ 80nm and 100nm $\times$ 100nm. These results are presented in figure 6.3. At first glance, the smallest window studied appears to be dissimilar to the larger windows: the current magnitudes are smaller, the band gap larger, the change in current with z is slightly less, and a slight curve is apparent in the spectra at higher biases. However, measurement of the hydride surface using this STM tip also produced similar differences in comparison to the general appearance of I_T/V_S spectra over hydrogen terminated Si(100):2 $\times$ 1. This suggests that these effects seen on this window are due to differences in tip density of states rather than window behaviour. The results were included here to once again highlight the importance of recognizing how particular tips may influence measurement results. Further discussion of the styrene terminated windows will thus concentrate on the larger windows, however it is noted that the same trends are still visible in the smaller window.

Comparison of the spectra for styrene covered windows with a fully styrene terminated surface indicate that the influence of the surrounding hydride is quite large. Largely exponential change of current with tip-sample distance is observed in both biases where as on the full styrene surface the reverse bias current had a sub-exponential change and current was suspected of being restricted to minority carriers. For all sizes of windows studied, the forward to reverse rectification ratio slightly favors the reverse bias near the set-point similar to the hydride surface,

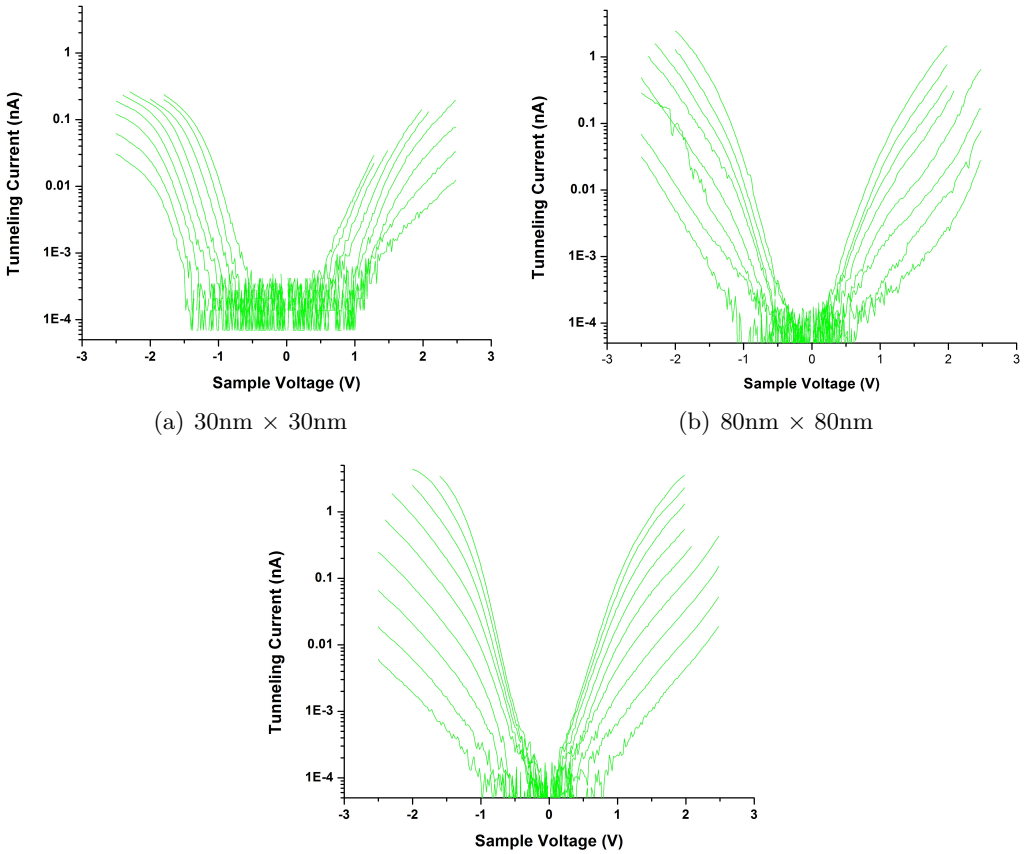

(a) 30nm × 30nm

(b) 80nm × 80nm

(c) 100nm × 100nm

Figure 6.3: Averaged semi-logarithmic IV spectra for styrene covered windows on H-Si(100):2 × 1. Spectra were taken at z = -3 Å(bottom curve) to +5 Å(top curve) towards the sample from the set-point of V_S = -2.0 V and I_T = 100 pA. Window dimensions were as indicated.

see figure 6.2. As the tip is moved closer to the surface ($z > 0$), the rectification behaviour does not follow that of the hydride. Rather, there is some indication that the ratio increases as the separation decreases indicative of behaviour similar to the styrene surface. However, the increase is very slight and considering the variability in the rectification of the clean surface - which we characterized as being near unity for all z - one could claim that the styrene windows also have rectification near unity. In either case, it is apparent that the rectification does not follow the trend of the surrounding hydride surface; the forward to reverse rectification ratio does not decrease with increasing steps towards the sample.

The observation of majority carrier transport in both bias directions suggests one of two possibilities. Either lateral interactions between the conduction bands of the hydrogen and styrene terminated surfaces allows for majority carrier transport into the surface or the opposite polarity of the nearby hydride surface causes a reduction of the barrier felt by conduction band electrons facing the styrene terminated surface. As the tip is brought closer to the sample, band bending will increase however lateral interactions between the conduction band should stay relatively similar. If the slight increase in the rectification as the tip is brought closer to the sample (following the full styrene surface trend) is to be believed, this would indicate that the barrier height effect may be the dominant factor. However, if the rectification is considered near unity, than this may indicate that lateral interactions may dominate.

I_T/V_S spectra were also taken for windows of 4-fluorostyrene on the otherwise hydrogen terminated n^+ Si(100):2×1 surface. Results for a 70nm $\times$ 70nm and a 80nm $\times$ 80nm window are presented in figure 6.4. It can be seen that the behaviour of the two windows is quite similar. However, for high forward biases a slight change in curvature is observed in the spectra on the 70nm $\times$ 70nm window. This is not understood but is suspected of occurring due to a difference in STM tip rather than a result of the slight increase in window size. It should be noted however, that such a difference was not apparent in the spectra over the hydride surface.

While a full 4-fluorostyrene terminated surface has not been studied, using the similarities in 4-fluorostyrene and styrene and the model described in chapter 3, some inferences can be made. The fluorine atom at the para position of the molecule will modify the dipole moment of the molecule while maintaining the bonding structure of the molecule on the surface. An indication of the molecular dipole can be gained by considering the dipole moment of the free molecule. It is understood that this will not be the same as the 'molecular' dipole once the molecule is covalently bonded to the surface, however, it can provide some indication of the expected results. The styrene molecule has an accepted dipole moment of 0.13D [137] and DFT

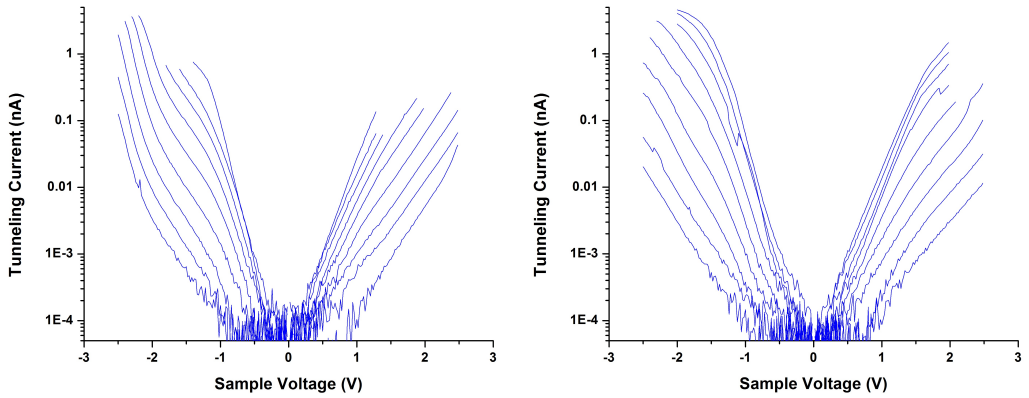

(a) 70nm × 70nm (b) 80nm × 80nm

Figure 6.4: Averaged semi-logarithmic IV spectra for 4-fluorostyrene covered windows on H-Si(100):2 × 1. Spectra were taken at z = -3 Å(bottom curve) to +5 Å(top curve) towards the sample from the set-point of V_S = -2.0 V and I_T = 100 pA. Window dimensions were as indicated.

optimizations performed in chapter 4 estimate a dipole moment of 0.20D. The dipole moment of 4-fluorostyrene has been reported through a combination of experimental and theoretical treatments to range from 1.31D to 1.57D [138]. DFT optimizations performed in chapter 4 estimate a dipole moment of 1.49 D, which falls nicely within this range. This increased dipole moment points roughly in the same direction to that of styrene. In the proposed model, the increased dipole moment at the surface would serve to further increase the barrier to majority carrier electrons in reverse bias. Thus, the behaviour of the 4-fluorostyrene terminated surface is expected to be similar to styrene but with greater forward to reverse bias rectification ratios.

The forward to reverse rectification ratio for the 4-fluorostyrene terminated windows are presented along with the rectification ratios for the other windows in figure 6.2. At the set-point, $RR_{F/R}$ is again less than unity. However, as the tip-sample distance decreases there is a marked increase in the rectification ratio. The rectification clearly follows the trend of the styrene surface with an average rectification crossing over unity and yielding 3.4:1 at a 5Å step towards the surface. This rectification is much less than the styrene terminated surface but significantly greater than the styrene terminated windows. These results support the hypothesis that the 4-fluorostyrene surface would produce I_T/V_S spectra similar to styrene but with increased rectification. Moreover, it supports the idea that the interaction of the window with the hydride surface outside the window lowers the rectification but still has the same trends as the fully terminated surface.

The results presented here point towards the concept that, in the window sizes

studied, the outer region of a window can greatly influence the I_T/V_S characteristics of the inside of the window. However, the general trends of the inside region will follow that of the surface making up the window. This is in contrast to the results previously reported for clean windows on a benzene terminated surface [81]. As mentioned in the beginning of this section, the results from such windows was reported to have a hybrid character with the general rectification trends following that of the outer surface. It may be suggested that if the outer molecule is a larger entity with less localized electron character than hydrogen, the I_T/V_S inside the window may be more inclined to interact with and take on the character of the outer region.

The above proposal is difficult to test with styrene as the medium due to difficulty in desorbing the molecule without damaging the tip. We can however, look back at results on I_T/V_S in tip shadowing regions presented in section 3.5. The shadow regions can be looked upon as very large windows with ill-defined borders. The centre of the 'window' is the location of the tip during the molecular dose and has the cleanest surface. The reader may recall that I_T/V_S characteristics of the centre region was shown to be very similar to the fully clean surface but lacking in the ohmic shoulder region. This is in fact very similar to the case of clean windows on the hydrogen terminated surface. As the tip was moved laterally away from the centre of the window towards the border, the styrene density slowly increased. At the same time the I_T/V_S characteristics took on a hybrid character looking more and more like the styrene surface as the distance increased. A very low molecular density was required to observe changes in the spectra. The spectra of the partially covered regions are very similar to those reported for the clean windows on a benzene surface. In that work, it was noted by the authors that 80%-90% of the benzene was removed from the window regions. The results of the windows studied here as well as the characteristics of the shadow regions, suggest that the hybrid character of those windows is a result of the remaining 10%-20% of benzene within the window rather than interaction of the clean window with the outer surface.

The above suggestion further highlights the conclusion found in section 3.5 that very few molecules are required to change the behaviour of the surface and that the STM tip need not be directly over a molecule to observe the effects. The result is in some ways in line with the transport model presented. If the dipole character of the molecule is of greater import than the direct orbital energies of the molecule, the observed effect would be less local - as observed. However, how the proximity of such dipole regions can modify the I_T/V_S of the pinned clean surface is an area requiring further investigation.

The I_T/V_S analysis of clean, styrene covered and 4-fluorostyrene covered windows on an otherwise hydrogen passivated surface revealed that in homogeneous windows the behaviour is highly influenced by the outer surface region can still follow many of the same trends as a full surface of the window region would follow. The clean window behaviour was very similar to that of a fully clean surface with pinned bands. However, the ohmic shoulder and zero bias current associated with surface conductance was missing. When the outer surface and the inner surfaces had opposite and similar magnitude rectification, the rectification of the inner window was found to be close to unity, however there was indication that the rectification changed from slightly favoring the reverse bias like the outer surface to favoring the forward bias like the styrene surface. This increase in forward bias current was more pronounced on 4-fluorostyrene windows which have a stronger dipole moment in the same direction as styrene.

6.3 Electron Beam Lithography Patterns

One of the particularly interesting aspects of the I_T/V_S results of the clean window regions in the previous section was the lack of any indication of surface conduction as a result of the π^* band in the clean window region. A natural interpretation is that the conduction channel still exists within the window but is blocked at the hydrogen terminated surface and thus inaccessible to the grounding contact which is located far away. This suggests that a unique surface channel can be created between points on the surface through the removal of a hydrogen resist between the points. Testing of the availability of such a channel can be accomplished by simultaneously probing two locations on a patterned region or at the edge of a patterned region directly with two independent STM tips or through metallic contact pads probed with tips. Such tests can be accomplished through the use of a multiprobe STM system.

The Multiprobe instrument designed by members of the Molecular Scale Devices group is an extremely powerful instrument consisting of three completely independent STM tips in addition to several other features previously listed in table 2.1. However, the optimization and use of the instrument was met with several challenges. Some of these are briefly outlined in the appendix. One of these challenges included the proper functioning of the attached commercial scanning electron microscope (SEM) column. The high resolution of the SEM allows for greater precision in the alignment of the three STM tips in relation to each other as well as features on the sample of interest. Without the SEM it can be extremely challenging to bring the tips close to each other without damaging the tips by hitting them together. Moreover, locating specific regions of interest on the surface using only the small

range of an STM piezo is impractical.

Temporarily circumventing the need for the SEM could be accomplished though the use of large metallic contact pads. A first step towards this is understanding how such contacts may themselves influence the surrounding silicon. Recently, Pitters et al. have studied how nanoscale $TiSi_2$ islands prepared by adsorbing and annealing titanium on silicon can affect the band bending of the nearby surfacein high doped n-type hydrogen terminated Si(100):2×1 [139]. They showed that the I_T/I_V spectra shift such that current injection from the tip (reverse bias, $V_S > 0$V), becomes increasingly difficult as the tip moves closer to the island. Such a shift in spectra is consistent with bands bending upwards in the silicon surface near the island. In addition, the authors demonstrated how the distance between the island and a surface dangling bond (DB) can be used to control the charge of the DB. Silicide islands grown using this method are very interesting due to their small size and ordered crystalline structure. However, the islands are randomly oriented on the surface and are generally not observable using the optical camera available on the system. Another method that can be used to make defined contact pads is electron beam lithography (EBL). The general process used to create such contacts will be discussed followed by a study of how such contacts affect the nearby silicon surface.

6.3.1 EBL Sample Preparation

EBL uses a focused electron beam to scan across a surface to expose a resist [140]. The EBL patterned resist is subsequently exposed to metal deposition followed by removal of the resist. For a positive resist, the final metal pattern is the same as the original resist pattern. Unlike optical lithography which is limited by the diffraction limit due to the wavelength of light, the ultimate resolution of EBL is determined by the quality of the electron beam and the interaction with the resist. EBL does not require a mask, however writing a large pattern can take a significant amount of time to write.

A process to manufacture and prepare EBL patterns on silicon in a manner compatible with UHV-STM studies has previously been developed by Drs. Dogel and Zikovsky [36]. The choice of metal and parameters for metal deposition were particularly difficult to optimize in order to maximize chances for the proper lift-off of the resist while maintaining good final contact of the metal with the surface. In addition, sample preparation inside the UHV chamber is required to remove the native oxide from the silicon and anneal the metal to create a metal silicide pattern while retaining the integrity of the original pattern.

The EBL patterns were prepared by Dr. Stanislav Dogel at the University of

Alberta Nanofabrication facility. The procedure followed has been described in detail in [36]. The basic steps include the following:

1. The silicon wafers were cut using a diamond dicing saw and cleaned using Piranha solution (H_2SO_4:H_2O_2, 3:1) for 30 min. They were rinsed with deionized water and dried.

2. A positive photoresist (PMMA 950 A2) was spun on the wafer at 4000 rpm for 30s for a thickness of roughly 90 nm. The resist was baked at 200 °C for 2 min, in air.

3. A Raith 150 EBL instrument was used to design and write the pattern using electron beam currents between 0.08 nA - 0.09 nA and writing speeds from 1.8 mm/s to 2.0 mm/s.

4. The resist was developed in a 1:3 solution of MIBK:IPA (Methyl isobutyl ketone:isopropyl alcohol) for 45s and then rinsed with IPA and deionized water.

5. Using the GATAN Precision Plasma Deposition and Cleaning instrument, the metal was sputter deposited to a thickness of 35 nm

6. Lift off was performed by dipping the samples in a 60 °C acetone ultrasonic bath for 20 min.

7. Samples were stored in standard wafer boxes until used and cleaned for 10min in a methanol unltrasonic bath at room temperature for 10 min directly before loading the into the UHV load lock.

8. The samples were flashed to 1100 °C several times. Hydrogen termination used the same procedure described in section 2.6.1 however with this lower flashing temperature.

The EBL pattern for this study consisted of two contacts separated from each other by a small gap and extended by long narrow regions that each ended in a large contact area that can be viewed optically to allow for the placement of STM tips, as shown schematically in figure 6.5. Generally three sets of contacts were written on each sample. Various different contact and gap sizes were tried. It was found that a contact size of at least 75 μm was required to observe the contacts with the optical camera available.

Small EBL titanium silicide patterns previously studied were found were found to be surrounded by a silicon trench [36]. Titanium silicide islands grown from a

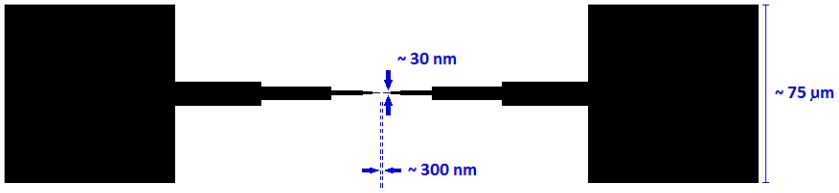

Figure 6.5: EBL Pattern Schematic. Not to Scale.

thin film, that were mentioned in the introduction, are also generally surrounded by a trench region. This has been associated with the movement of silicon towards the pattern during the formation of the silicide. The large EBL patters were also seen to be surrounded by a trench region. However, in addition to the trench, a hill of silicon was found to be present immediately after trench before leveling off at the base height of the silicon sample. The contact, trench, Si hill and base silicon can be observed in STM images of the contacts, Fig. 6.6(a), and more directly through derivative images, Fig. 6.6(b), which serve to highlight changes at the surface. The derivative image also highlights the roughness of the EBL defined silicide contacts. A profile of the topography image starting at the edge of the contact and moving outwards on the silicon surface, Fig. 6.6(c), indicates that the hill height is approximately 4 nm high. This may seem small, however it is of significance in comparison to standard height dimensions on a silicon wafer. Moreover, the height difference is associated with severe step bunching leading to poor quality surfaces for STM studies in the region. Several attempts at annealing at temperatures between 900 °C and 1100 °C for longer times (upto 15 minutes) were not successful in removing the hill region. Annealing over an even greater length of time and at higher temperatures was not attempted due to the limited ability to test the connectivity of the pattern without the SEM.

6.3.2 I_T/I_V Behaviour of Silicon near Patterns

In order to gain an understanding of how the titanium silicide contact may affect the behaviour of the nearby silicon, I_T/I_V measurements were taken as a function of the distance away from the contact. Example spectra taken at a set-point of $V_S = -2$V and $I_T = 80$pA is provided in figure 6.7. Spectra were also taken in increments of 1 Å starting from a distances of 2 Å away from the surface from the set-point to 3 Å towards the surface from the set-point. In order to simplify the analysis of many data sets, the 1pA onset voltage in both bias directions was plotted as a function of distance for low n-type Si(100):2×1, low n-type hydrogen terminated Si(100):2×1

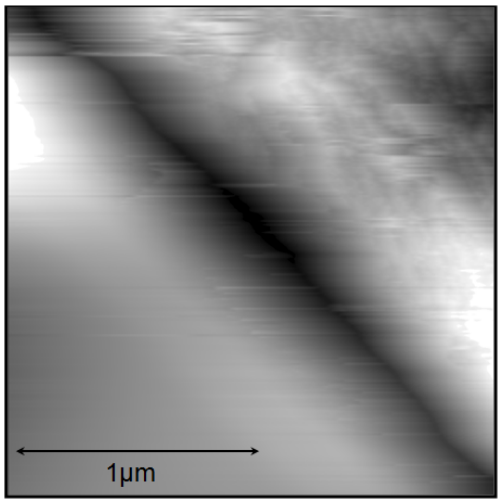

(a) STM

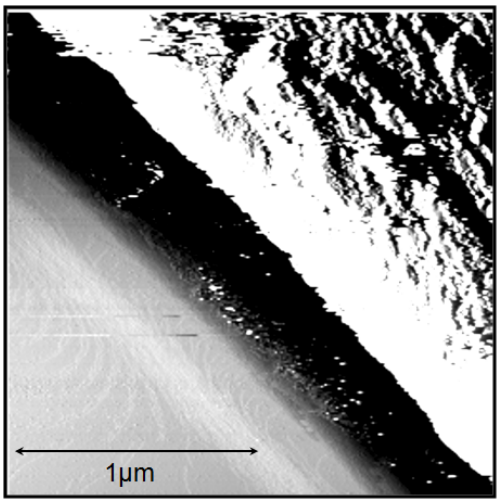

(b) Derivative STM

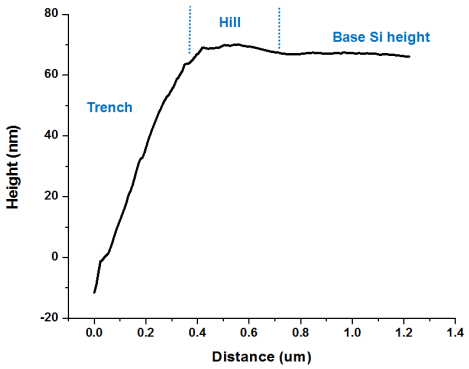

(c) Height Profile

Figure 6.6: (a) STM image of edge of silicide pattern $V_S = -2$V, $I_T = 100$pA. (b) Derivative of STM Image in (a) highlighting roughness of $TiSi_2$ pattern and steps in silicon (c) Profile starting at edge of the silicide. The trench and silicon hill surrounding the island are indicated.

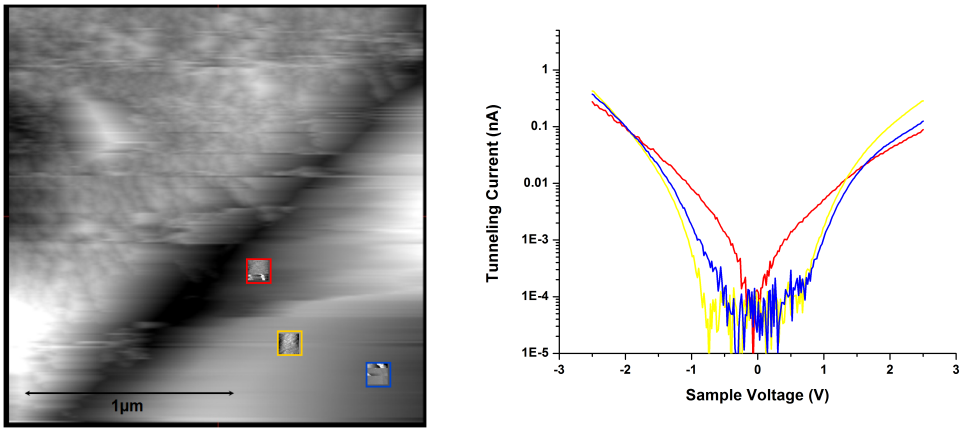

(a) STM (b) I_T/V_S

Figure 6.7: (a) STM image of edge of silicide pattern on low doped n-type Si(100):2 × 1 with 100nm ×100nm areas corresponding to spectroscopy outlined: $V_S = -2$V, $I_T = 100$pA (b) Example semi-logarithmic I_T/V_S results near Titanium Silicide patterns. Color of curve corresponds to locations in (a). Spectroscopy taken at set point $V_S = -2$V, $I_T = 80$pA.

and high n-type hydrogen terminated Si(100):2 × 1. Example results from each type of surface are presented in figure 6.8. Each graph presents data taken on the same sample with the same physical STM tip [1]. The set point used for the measurements was $V_S = -2$V, $I_T = 100$pA. Each point in the analysis represents the average onset of 40 spectra taken at a single location.

In studies of the low doped clean Si(100):2 × 1 surface, the set points were generally found to be quite stable at all distances from the contact. Occasionally particular areas in some data sets demonstrated a slight trend. For example, in the data shown, the data set pertaining to the furthest tip position (-2 Å) appears to decrease in onset voltage with increasing distance while the other tip positions remain fairly constant overall. However, such trends were not consistent leading us to believe the onset voltages are generally constant with respect to distance from the contact for all tip positions. A constant behaviour of the I_T/V_S spectra is consistent with band pinning by the π^* states. This would inhibit band bending due to a Schottky barrier contact between the metal silicide and the silicon.

The results for a low doped hydrogen terminated Si(100):2 × 1 surface are presented in Fig. 6.8(b). In this case we can see a relationship between the onset voltages and distance from the contact. As the distance from the contact decreases

[1] By physical tip, I mean the STM tip was never exchanged; however some slight changes in the apex of the tip may have occurred during the measurement process.

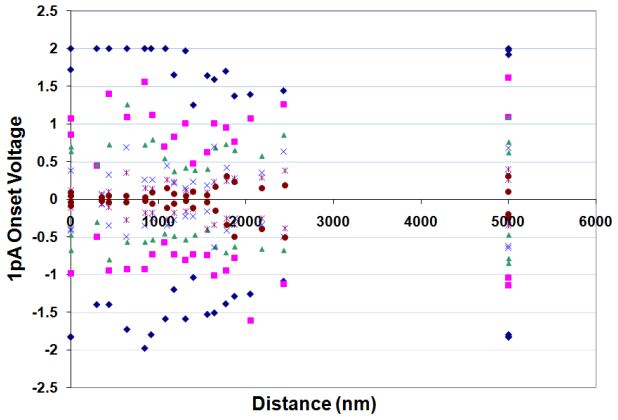

(a) Low Doped n-type Si(100):2 × 1

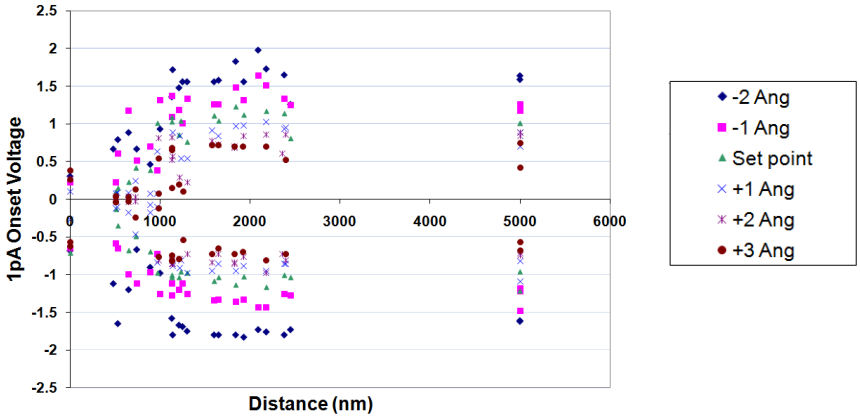

(b) Low Doped n-type H-Si(100):2 × 1

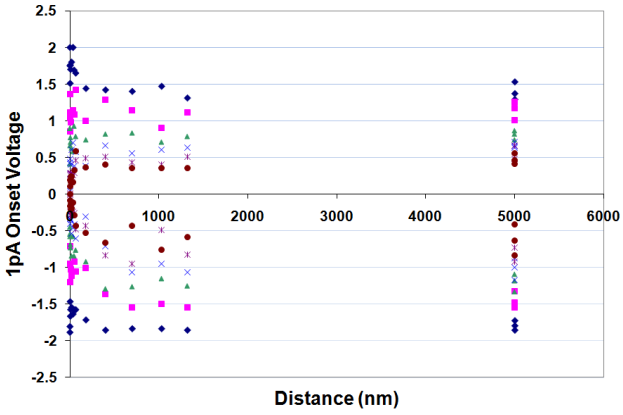

(c) High Doped n-type H-Si(100):2 × 1

Figure 6.8: 2pA Current onset Versus Distance from Contact for distances of 2 Åaway from the surface from the set point to 3 Åtowards the surface from the set point. Set point is $V_S = -2$V, $I_T = 100$pA. Each point represents the average from 40 I_T/V_S curves taken at one location. Data points presented for a distance of 5000 nm may in fact have been taken at a longer distance away from the contact.

the onset voltage decreases in both bias directions, indicating that the current transport is more facile in both biases. This relationship extends to slightly over 1 μm.

These I_T/V_S results for the hydrogen terminated low doped surface are inconsistent with a band bending model. Band bending would results in a shift of the spectra while retaining a similar band-gap. In this case, however, we see a decrease in the band gap closer to the large EBL patterned region. This band-gap decrease could potentially be a result of different factors or even a combination of factors. Some possibilities include:

- The incorporation of silicon in the creation of the metal silicide may cause a segregation of dopant atoms to the outside of the contact. The associated increase in donor concentration near the contact could result in more facile conduction.

- Titanium, as an impurity in silicon, has a donor level approximately 0.21 eV from the bottom of the conduction band. As such titanium near the contact that is not incorporated in the silicide may act as a donor impurity thereby causing an increase the conduction near the contact.

While the above possibilities exist, the lack of any clear distance dependencies on the clean surface suggest that something entirely different may be the root of the effects seen on the hydride surface.

On the high doped hydrogen terminated Si(100):2$\times$1 surface, the results demonstrated a consistent trend with a much narrower distance dependence in comparison to the low doped surface. In forward bias ($V_S < 0$V), as the tip moved closer to the contact from distances of approximate 400 nm, the current transport from the surface became more facile for all tip-sample separations. In reverse bias, the dependency varied with tip-sample separation. At large separations the current became more difficult to inject into the surface when close to the contact, and the apparent band-gap energy remained fairly constant. However, at small separations, the current was injected into the sample at smaller voltages leading to reduction in the apparent band gap.

The I_T/V_S behaviour at large tip-sample separations is consistent with band bending phenomena. The shift in the current onset voltages in both biases suggests upward band bending in the silicon close to the contact. The relatively small range of the observed effect can be attributed to a small minority carrier diffusion length in the high doped sample. This is very similar to the effects seen near the silicide islands studied by Pitters et al. [139]. At small tip-sample separations, a reduction in the onset voltage in reverse bias implies a reduction in band-gap. This is similar

to the observations on the low doped sample, however the effect is of smaller range on the higher doped sample. For the suggestion of dopant segregation, one would expect the effect to be stronger in the highly doped sample. On the other hand, residual titanium acting as dopant atoms would be expected to be similar in both samples.

The results and discussion presented here indicate that the relationship between STM I_T/V_S behaviour and distance from a large EBL pattern is identifiable but not yet clearly understood. For the clean surface, minimal change in onset voltage with distance from the contact appears to be consistent with band pinning resulting from π^* surface states. Similarly, band bending can explain a shift in the onset voltages apparent in high doped silicon at large tip-sample separations. However, a reduction in the apparent band-gap in the case of low doped silicon and high doped silicon with small tip-sample separation is, as of yet, not clear. While such effect are expected to be smaller on smaller contacts such as the small islands previously studied [139] as well as perhaps the thin area near the gap region of the proposed pattern, it is an area that must be further pursued and understood prior to initiating studies of the behaviour of structures between or even spanning such contacts.

6.4 Chapter Summary

In this chapter we studied the tunneling current-voltage behaviour of STM lithographically defined patterned regions of clean, styrene-covered and 4-fluorstyrene covered windows on hydrogen terminated silicon as well as silicon nearby electron beam lithography patterns of titanium silicide.

The clean window patterns behaved very similar to the fully clean surface, however the conduction channel attributed to π^* states was blocked. The current rectification on the styrene covered windows was found to be almost non-existent. This suggested that while the covered window did not respond in the same manner as the fully styrene terminated surface, neither did it behave as the hydrogen terminated surface surrounding the window. For 4-fluorostyrene covered windows the rectification was lower than we might expect for a fully covered surface, but the behaviour presented the same trend as expected. These results suggest that the I_T/V_S characteristics of small regions of modified surface termination are strongly affected by the surrounding surface but if the behaviour of the region is strong enough, the I_T/V_S spectra will follow the trends expected of the patterned region.

The observation of the controlled blockage of surface conduction by the hydride surface led us to the desire of confirming the continued existence of such a channel within a clean patterned region. Prior to preforming such studies the effects of

metal silicide contacts on the nearby silicon region must be understood. These effects were studied for $TiSi_2$ contacts defined by EBL on Si(100):2×1 samples. The clean low doped surface near contacts appeared to have fairly constant current onset voltages. The hydrogen terminated low doped surface had increasing facile conduction in both biases as the the distance decreased. The hydrogen terminated high doped surface had facile conduction close to the sample in forward bias and with small tip-sample separations in reverse bias. At large tip-sample separations the conduction in reverse bias became more difficult near the contact. This latter behaviour would be consisted with band bending effects in the silicon region near the contact. Overall, a satisfactory explanation for the I_T/V_S characteristics of the silicon region near these large contacts has yet to be found. Such an understanding would be beneficial prior to engaging in future studies using such contacts.

Chapter 7

Molecular Line Studies

7.1 Chapter Introduction

The self-assembly of ordered organic nanostructures on the monohydride Si(100) surface is a source of great future potential in hybrid silicon-organic molecular scale devices. A particularly interesting scheme for the formation of linear structures of organic molecules - referred to as 'molecular lines' - has recently produced much interest in the community. In this chapter we will take a brief look at the line growth process followed by some initial studies into particular aspects of molecular lines, such as spectroscopic behaviour and molecular ordering.

7.1.1 Molecular Line Growth Process

A simple method of describing the formation of molecular lines is accomplished by following the chemical reaction pathway that a participating molecule undergoes. The general pathway is a chain reaction of radical additions first proposed by Linford et al. for the creation of organic monolayers on silicon [141]. Styrene's interaction with the hydrogen terminated Si(100):2 $\times$ 1 surface, the prototype and most well understood system, will be used here as a general example.

As was discussed in section 2.6.1, the hydrogen terminated silicon surface generally has several natural defect sites caused by a missing hydrogen atoms on the surface. These missing hydrogen locations are often called dangling bonds (DBs) and can be thought of as surface radicals. DB sites can also be created on the surface in a controlled manner using an STM tip [128, 142, 143]. To create molecular lines the hydride surface containing DBs is exposed to a vapor of the candidate molecule, in this case styrene. A styrene molecule will first start interacting with the surface through physisorption. It may undergo several diffusion steps along the surface - a process that was discussed in detail in chapter 5 - before encountering a DB site.

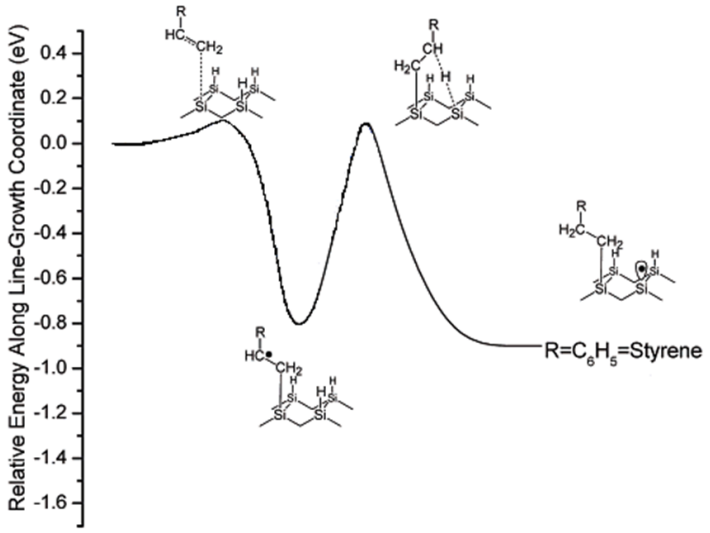

Figure 7.1: Reaction Coordinate for Styrene Line Growth. The molecule starts in a physisorbed state on the surface. It must be able to overcome a small energy barrier to interact with a DB in order to form a C-Si bond and a carbon centered radical. The C-Centered radical must overcome a large barrier for hydrogen abstraction which forms a stable covalently bound molecule with a neighboring DB site. Adapted with permission from [41]. Copyright (2004) American Chemical Society.

The DB and the C-C π-bond in the molecule interact to form one C-Si bond and a carbon centered radical on the molecule. For a molecular line to form, the radical must then be able to abstract a hydrogen atom from a neighboring surface site. This forms a stabilized chemisorbed species with a neighboring DB site which is then free to react with another molecule. The molecular line will thus grow in the direction most suitable for H-abstraction. On H-Si(100):2 $\times$ 1, non-equivalent abstraction sites include the next dimer in the same row, the neighboring site in the same dimer and the site across the gulley region. For styrene on H-Si(100):2 $\times$ 1 abstraction will preferentially take place in the dimer row direction. Occasionally, particularly if the line meets a defect site, the abstraction can occur from the neighboring dimer row and the line growth can either continue in the same direction or turn back on itself to create a 'double line'. The line growth process can terminate in several ways including annihilation of the DB with another DB or surface defect, spontaneous capping with a hydrogen atom, or simply a lack of molecules to continue the process.

The reaction pathway of a styrene molecule can be followed using Figure 7.1 [41]. For the case of styrene, the carbon centered radical is quite stable and the forward

reaction of hydrogen abstraction leading to line growth has a similar energy barrier to the reverse reaction of removal from the surface but results in the release of 0.1eV. At room temperature, styrene lines grow readily along the dimer row of H-Si(100):2×1 with as little as a 3L dose [33]. However, at slightly elevated temperatures, the reverse reaction is favored and lines can 'unzip' [37].

7.2 I_T/V_S behaviour of Styrene Lines

From chapter 3, we know that the conduction at a surface can be greatly tuned by surface molecules. This suggests that the conduction properties of molecular lines on H-Si(100) could find uses in information storage or transfer. In particular, Hofer et al. have theoretically shown that the delocalized π states of some of the molecules used in line growth lie at the valence band edge - making them potentially suitable for hole transport [144]. In addition, Piva et al, have experimentally demonstrated the ability of a point charge to regulate the conductivity in a molecular line [145]. Using STM, the authors observed a decrease in the apparent height of the molecule with increasing distance from a charged dangling bond. They also observed this effect as a decrease in the current onset in I_T/V_S with increasing sample distance. My wish was to reproduce these results and using the knowledge gained from chapter 3, further increase our knowledge of the I_T/V_S behaviour of the styrene lines. [1]

Both medium and high n-type hydrogen terminated Si(100):2×1 surfaces were prepared as in section 2.6.1 and then exposed to styrene doses in the range of 3L to 10L at room temperature. Molecular line growth was observed in all cases. Current-Voltage measurements were taken as in chapter 3. A reference point of -2V and 0.1nA was primarily used although several settings were tried. Z-steps of up to 4Å away from the set-point were also studied.

Unfortunately, the I_T/V_S analysis was inconclusive. In many cases, it was found that the tip had a severe influence on the basic structure of the molecular line. At its most severe, the I_T/V_S measurement process caused the local desorption of styrene molecules from within the molecular line - even when the lines remained intact during standard STM imaging using voltages at either extreme of the voltage ramp. Figure 7.2, provides an example series of STM images before and after I_T/V_S measurements, in which styrene molecules were removed during the process. In 7.2(c) and 7.2(e) the STM images taken during the measurement process are shown along

[1] It should be noted that scanning tunneling spectroscopy over styrene molecules in a molecular line is not expected to be the same as over styrene molecules passivating a clean Si(100):2×1 surface. In the former case, a single C-Si bond is formed and the molecule is expected to 'stand up' on the surface; in the later case, two C-Si bonds are formed and the molecule is oriented in a more parallel fashion with respect to the surface plane.

with the locations measured on the long line. The corresponding I_T/V_S curves are presented in 7.2(d) and 7.2(f). Observed spikes in the measured graphs may correspond to desorption events, however, this is difficult to quantify. The spectra also demonstrate some of the difficulty in attempting to analyze trends in the measurements.

For some tips, there appeared to be little tip effect in the form of desorption. However, even in these cases a clear trend in the I_T/V_S behaviour with respect to the distance from a dangling bond or a free end of a styrene line was not observable. Single I_T/V_S measurements along a single line, averages of I_T/V_S measurements along the same line, and averages over molecules of similar length were all analyzed but were unable to show any reproducible trend. Moreover, even the rectification of the spectra taken over the lines was inconsistent. In some cases it favored the forward bias (similar to styrene on clean silicon) while in other cases it favored the reverse bias (similar to the hydrogen terminated surface). It is likely that the tip was still influencing the stability of the system. Moreover, differences in tip structure may play a strong role in these observations. It is also unsure whether some of this deviation may be caused by sample drift. Since the molecular lines are small structures, it may be possible that with slower voltage ramps, the tip may have drifted off of the molecular line during the measurement process. This may help explain the rectification behaviour favoring that of the hydride surface. However, if this were the case one would also expect to see hysteresis in the I_T/V_S measurements indicative of the drift and this was not observed. In addition, the effects of the molecular line's proximity to surface defects such as missing dimers, step edges or even other lines is unknown.

Due to the observed tip induced instability as well as the inability to obtain reproducible observations, this avenue of study was not further pursued.

7.3 I_T/V_S behaviour of Silver-Styrene Lines

It was mentioned in the introduction that one of the major challenges in the development of hybrid silicon-organic molecular scale devices is the creation of connections between the components. One method that was presented was the self-assembly of silver islands at silicon dangling bonds. Such an interconnect is an attractive means of creating an initial connection to a molecular line which naturally terminate in dangling bonds. A second similar connection to the line could be created by using the STM tip to remove a hydrogen atom at the start of the line. How such a silver island may affect the overall behaviour of a molecular line is an intriguing question that may affect the usefulness of such an approach of interacting with molecular

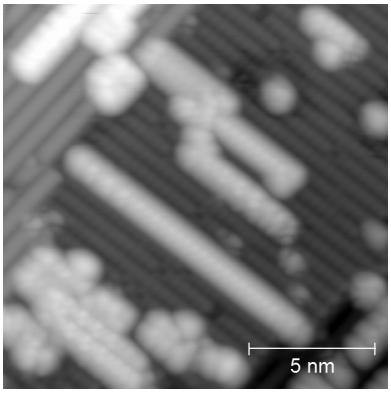

(a) Before I_T/V_S Measurements

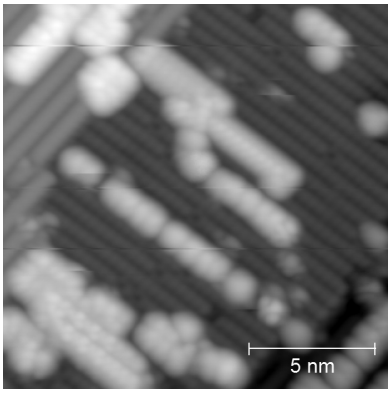

(b) After I_T/V_S Measurements

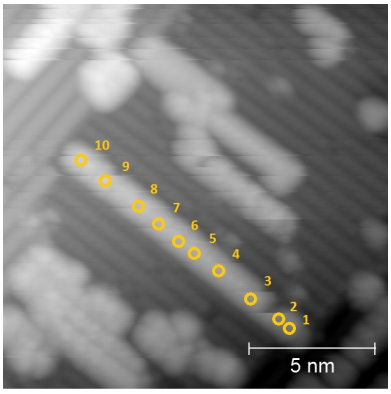

(c) During first set of I_T/V_S Measurements

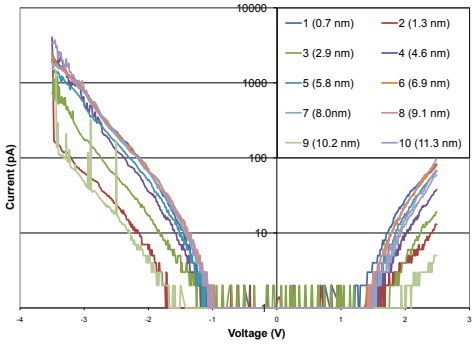

(d) First set of I_T/V_S Measurements

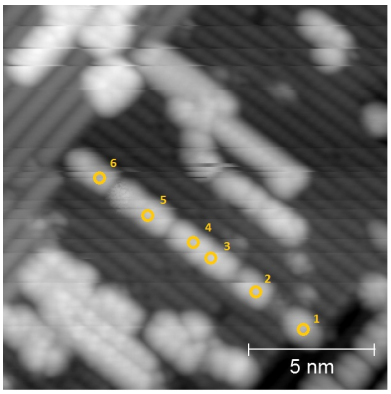

(e) During second set of I_T/V_S Measurements

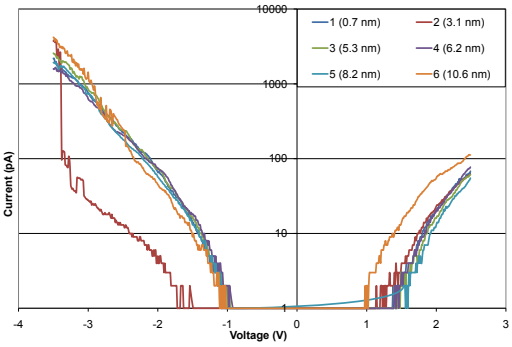

(f) Second set of I_T/V_S Measurements

Figure 7.2: STM micrographs of styrene desorption from molecular line during I_T/V_S measurements. All images were taken at $V_S = -2$V and $I_T = 0.1$nA. (a) Before Measurements (b) After Measurements (c, e) During Two sets of measurements in which I_T/V_S measurements were taken at points along the length of the long line in the center and the shorter one just above it. (d,f) The corresponding single I_T/V_S spectra taken at the locations given on the long line. Distances are estimated from the original bottom end of the long line.

Figure 7.3: STM Image of silver islands formed at the end of styrene molecular lines. $I_T = 100$pA, $I_V = -2$V

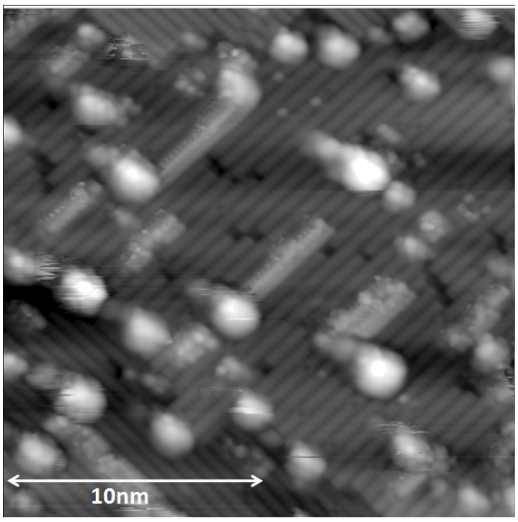

lines.

While the I_T/V_S characteristics of molecular lines has been previously shown to be difficult to study, the presence of a metal cluster at the end of the line may have had a significant influence on the molecules in the line - particularly those at the interface. For instance, the interface region in lines composed of sections of different molecular species has been shown to have significant conduction changes [35]. The presence of different molecules could locally modulate the conductance such that molecules appeared as greater protrusions or depressions near the interface.

To study the potential effect of silver islands on molecular lines, styrene lines were grown at room temperature on medium and highly doped n-type H-Si(100):2 $\times$ 1. Silver was deposited by metal evaporation. It was found that styrene lines on the surface did not impede the formation of silver islands at DBs. Several lines were found to terminate in silver islands. A large number of molecular lines also had silver islands close by but not directly at the end of the line. This is likely due to the ability for hydrogen atoms to easily interchange positions with a DB at room temperature as well as the length of time between the end of styrene exposure and the exposure to silver. An example image of the resulting surface is provided in Fig. 7.3. It can be seen that the silver islands had little effect on the manner in which styrene lines imaged with STM. Molecules along the whole length of the line ending in a silver cluster image similarly to each other and to molecules in lines not terminated with an island. These results were similar for imaging conditions ranging from -3V to +3V.

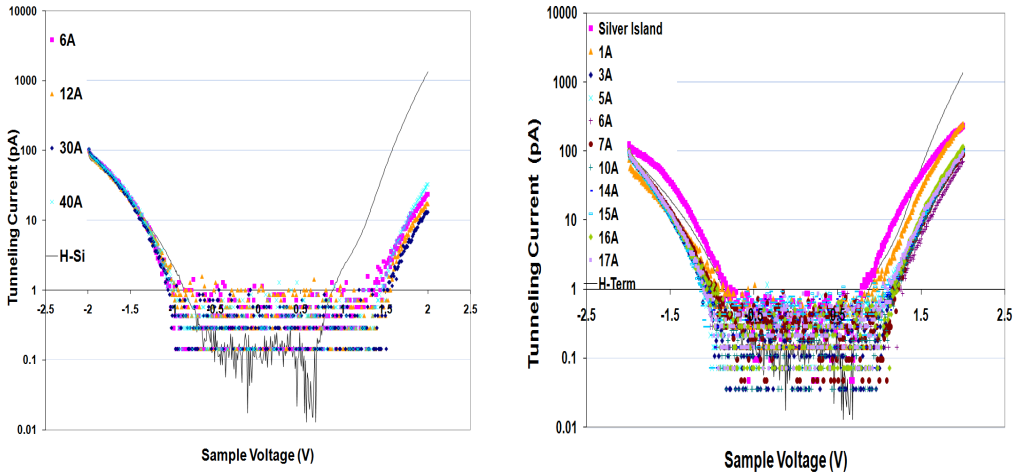

(a) DB-Styrene (b) Ag-Styrene

Figure 7.4: I_T/V_S at various distances from end of styrene lines terminating in either a dangling bond or a silver island. The I_T/V_S of the hydride surface region taken with the same tip is presented as a reference. This behaviour was found to be similar before and after styrene exposure and silver exposure. Distances are given in Angstrom. Set point: $I_T = 100$pA, $V_S = -2$V.

The STM images also provide a means of determining the size of the silver islands produced with the silver exposure. As can be seen in Fig.7.3, the island sizes were found to be similar locally; however, the size varied across the macroscopic length of the sample: the end of the sample closer to the silver source had larger islands while those at the further end were smaller. This is indicative of the expected high sticking coefficient of the metal atoms and the requirement for line of site exposure to the sample. The image presented was taken near the center of the sample. At this location, assuming a hemispherical shape and a density similar to bulk silver, the estimated number of atoms in a single average island was found to be roughly 130 atoms.

The I_T/V_S behaviour of lines terminating in silver islands was compared with those of styrene lines terminating in a DB. An example is provided in Fig. 7.4. The first notable observation is that measurements taken directly over the silver island did not indicate significant metallic character and the band gap region was found to be of similar size to the hydride surface, even for various different z-positions of the tip (not shown). This is likely a consequence of the barrier between the metal island and the underlying silicon sample. To test if the presence of the styrene line affected the silver island current/voltage behaviour, silver islands were also grown

on hydrogen terminated Si(100):2 × 1 that was not exposed to styrene. The I_T/V_S of such islands was very similar. In addition, no obvious differences were found for islands of different sizes.

I_T/V_S over molecules in lines terminating in a silver cluster, often demonstrated larger currents in reverse bias ($V_S > 0$) in comparison to the DB terminated lines. However, this was not always the case and the variability seen in the previous section for normal styrene molecular urges us to be cautious about our interpretations. It was also observed that the behaviour of lines did not appear to depend upon the distance from the silver end. This is similar to observations along lines terminating in a DB.

The results demonstrate the capacity to terminate a molecular line with silver islands in a very simple manner. For the case of silver at the end of styrene, the presence of the island did not greatly impact the imaging STM imaging characteristics of the styrene lines. The variance in the I_T/V_S behaviour of styrene lines makes it difficult to derive conclusions on the possible subtle effects of the islands on the current-voltage behaviour.

7.4 Exploring Line Growth with Cyclohexadienes

Until now, the exploration into molecular lines in this dissertation has focused on the prototypical example of styrene. The growth process of styrene lines has been studied in depth by both experimental and theoretical means and has served as a solid example of a line growth process. The process involved in the growth of molecular lines of many other compounds are not nearly as well understood. A particular example is 1,3-cyclohexadiene. On medium doped n-type Si(100):2 × 1, 1,3-cyclohexadiene has been found to grow short molecular lines composed of molecules along the dimer row but separated by one or even two dimers [36]. An example of this growth is shown in figure 7.5. This line growth structure is quite unusual and has yet to be satisfactorily explained. Based on the standard alkene reaction, the expected position of the carbon-centered radical on the cyclohexadiene intermediate is too short to abstract a hydrogen atom two dimers away. This suggests that another mechanism, possibly a ring opening reaction, is responsible.

In order to test the theory of ring opening, the reaction of 1,4-cyclohexadiene with the surface was conducted but revealed no line growth and was put aside. Re-examination of the images from this initial test showed that several protrusions which were large compared to both a standard DB and the expected size of the adsorbate, were visible on the surface after exposure to the molecule. The large size of the features and the associated expectation of a largely delocalized electron

Figure 7.5: STM Image of 1,3-cyclohexadiene molecular lines on medium n-type Si(100):2 × 1. 20 nm wide, $V_S = -2.7$V, $I_T = 50$pA.

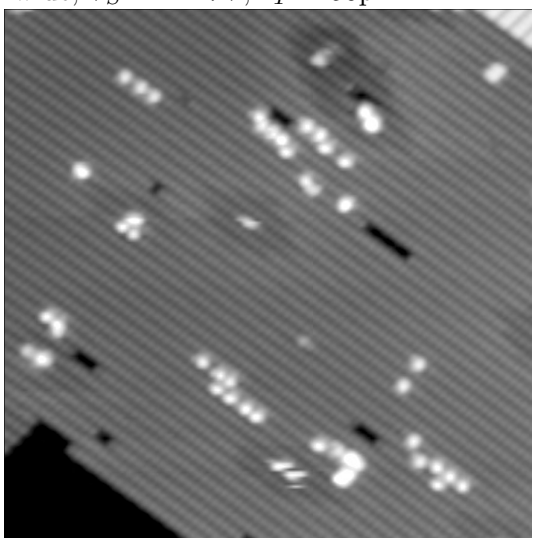

distribution, suggested the possibility that the molecule interacts with the DBs to form a structure that is not congruent with line growth but may in fact be a somewhat stable radical. However, these protrusions were of varying size and with the lack of before and after images of the same location on the sample, it was difficult to discern if the surface features were directly related to the molecule.

To gain a better understanding of the 1,4-cyclohexadiene system it was proposed that if a surface radical exists on the adsorbate, it may act at the initiator site for further line growth reactions. Experiments were thus conducted by exposing the H-Si(100):2 × 1 surface prepared as in section 2.6.1 to varying doses of 1,4-cyclohexadiene followed by exposure to styrene.

Exposure of 1,4-cyclohexadiene to n-type Si(100):2 × 1 was not found to reproduce the earlier observations. In fact, no evidence of the molecule was found on the surface even after being exposed to several hundred langmuirs of the molecule. Figure 7.6 provides example images of a surface exposed to several successive doses of the molecule. In all cases, protrusions on the surface appeared to maintain the features of a normal DB. The heights of the features were slightly above 2Å in all cases. The location of the tip during the exposure did not affect these results as no evidence of the molecule was found elsewhere on the surface in any trials.

Despite the lack of visibility of the molecule on the surface, several of the samples were exposed to styrene. It was found that larger doses of styrene were required to observe any line growth on the surface. Generally, only 4L - 10L styrene doses are required to observe significant line growth, however on the surfaces exposed to 1,4-

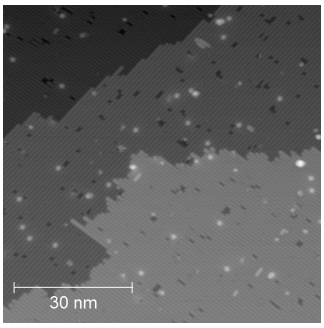

(a) H-terminated

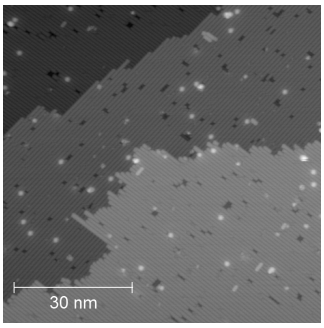

(b) 200L

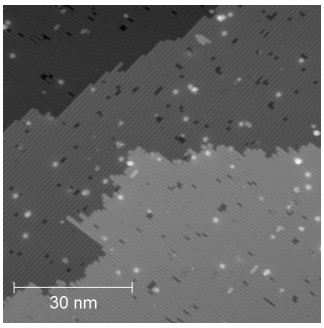

(c) 200L + 300L

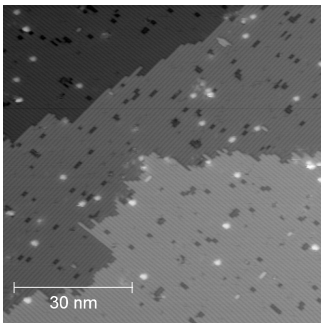

(d) 200L + 300L + 200 L (Tip withdrawn)

Figure 7.6: STM images of H-Si(100):2 $\times$ 1 exposed to doses of 1,4-cyclohexadiene. The first two doses of 200L and 300L were done while the tip was in contact with the surface 300nm away from the imaging location while the last dose of 200L occurred with the tip withdrawn 5nm from the surface and was again positioned 300nm away from the imaging location. $V_T = -2$V, $I_T = 100$pA.

cyclohexadiene doses closer to 40L were required. An example of a surface exposed to 100L of the 1,4-cyclohexadiene followed by exposure to 40L of styrene is given in figure 7.7. Despite the greater dose required, the styrene lines generally appeared quite normal. It was, however, observed that many of the double lines on the surface contained a high protrusion at the location of the original DB or very close to it. Several of these protrusions are highlighted with an arrow in figure 7.7. These protrusions had an average height of approximately 4.5Å from the silicon surface, which is almost double the normal DB height and roughly 2Å higher than the height of the styrene line imaged with the same conditions and tip. No difference was found between the original DB sites leading to the growth of such structures compared to other sites on the surface. One could potentially reconcile such observations by considering that the lines grew in a cyclic pattern such that the end of the line meets its original starting point leaving a DB defect that may be difficult for a molecule to approach. An increased height of the DB may also be caused by the steric effects of the molecules in the line. Observations of previous images of styrene lines on surfaces taken with similar imaging conditions does reveal that such protrusions within the line are occasionally seen. However, they are usually quite rare. The observation of several lines with such protrusions on samples exposed to 1,4-cyclohexadiene is interesting. Moreover, the greater density of such features was consistent for several trials involving different silicon crystal samples and different STM tips. The lack of differences observed prior to styrene dosing between samples exposed to the molecule and those not exposed inhibits the suggestion that the molecule is associated with both the protrusion and the initiator site for line growth. The greater density of such features on surfaces exposed to 1,4-cyclohexadiene is thus not well understood but still remains quite intriguing.

7.5 Preliminary studies of ordering phenomena

One of the unique aspects of the self-directed growth process is the creation of well ordered structures. The structure of the silicon dimer rows at the surface in addition to the structure of the molecule itself can impart order to the molecular line and indeed to the molecules within the line.

The energy barriers to hydrogen abstraction make up one of the most critical parameters for the order - and even creation - of linear molecular structures. The preference for abstraction along a particular direction of the surface dictates the ability for structures to grow linearly. The abstraction process can be quite complex and changes in the molecule can greatly impact the results. For instance, we have shown that 1,3-butadiene grows linear structures on the 2×1 surface, but that

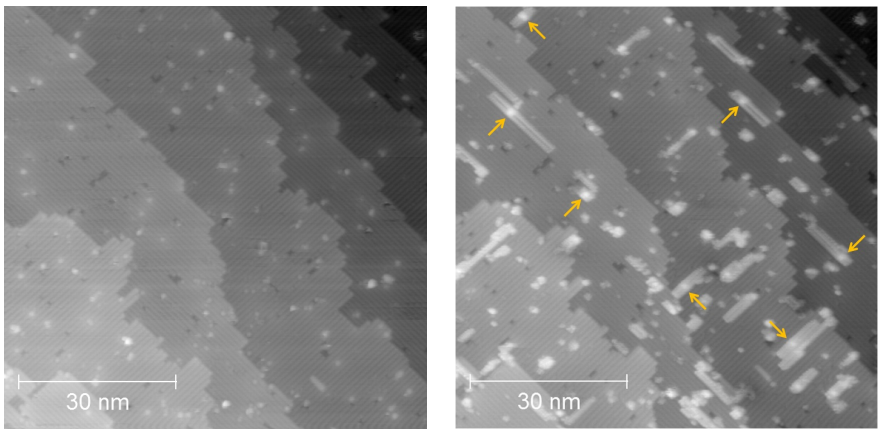

(a) (b)

Figure 7.7: (a) STM images of H-Si(100):2×1 exposed to 100L of 1,4-cyclohexadiene. (b) The surface in (a) after exposure to 40L styrene. The yellow arrows indicate locations where a protrusion of greater height is visible within the line. $V_T = -2$V, $I_T = 100$pA.

the structures often involve two dimer rows and appear much less ordered than styrene lines on the same surface [44]. The addition of two methyl groups to form 2,3-dimethyl-1,3-butadiene causes a steric hindrance to the rotation of the carbon centered radical group resulting in the formation of ordered nanostructures along one side of the dimer row [44].

In addition to the ordering of the structure as a whole to form linear lines, it is believed that the molecules within the structure can also preferentially orient themselves to create order within the line itself. In fact, STM imaging suggests that the molecules within the line are highly ordered. However, for even well studied systems, such as styrene molecular lines, the exact structure of the molecules is not yet understood in detail. Using theoretical techniques the search for stable configurations has resulted in various different lowest energy candidate structures depending upon the calculation method, basis sets and models [146]. Most predicted structures for styrene molecules in molecular lines suggest that the rings of the molecule are tilted or canted with respect to the orientation of the dimer bond. Some, in particular the PBE calculations on cluster models studied by Yang et al. [146], have also predicted a structure that has the surface dimer bond co-planar with the aromatic ring. Additionally molecules at the end of the line are found to be more flexible in orientation and have been predicted to take on fluxonal (T-shape) configurations.

For the case of canted styrene molecules, there are two energetically equivalent

directions (mirror images) that the molecule can face with respect to the dimer rows. However, this has been difficult to observe with STM and has not been noted in room temperature or low temperature studies. Another example of equivalent energy structures involves lines composed of vinylferrocene molecules. These molecules are known to arrange themselves in a zig-zag pattern along the dimer row in order to relieve steric crowding of the large ferrocene moieties [40]. One can imagine flipping all the molecules to form a mirror image structure of equivalent energy. However, in the case of vinylferrocene, STM triggered flipping may be inhibited by decomposition which is known to occur at imaging voltages greater than -4V. However, the search for a more stable molecule that grows ordered lines with two or more equivalent energy structures, or even an ordered phase and a disordered phase, is quite intriguing. If one could find a method of controlling the order (or disorder) a new paradigm for information storage or transmission could result.

Such a paradigm for information transfer is not unlike the molecular cascade approach proposed by Heinrich et al. [147]. In the molecular cascades demonstrated, individual carbon monoxide molecules are manipulated into precise locations on the surface using a low temperature STM - similar to setting up a series of dominoes. Once set, triggering the motion of one molecule at the beginning of the series triggers a ripple effect that proceeds throughout the length of the series. Using this approach the authors were able to build linear transport routes (wires) and two and three input logic gates [147]. However, like dominoes, it can only be used once. Once an operation is performed each individual molecules must again be manipulated into place using the STM tip in order to do a second calculation. In the envisioned case of utilizing molecular lines, the system could be likened to venetian blinds rather than dominoes; flipping the molecules from one orientation to the other and back should be relatively facile.

Initial molecular dynamics studies have been performed by Dr. DiLabio on a series of polyaromatic hydrocarbon molecules containing vinyl groups including styrene, vinylnaphthalene and vinylanthracene. All three of these molecules were observed to take on canted configurations that should have two equivalent energy structures on a defect free H-Si(100):2 $\times$ 1 surface. The molecules with a greater number of rings, such as vinylanthracene, were more constrained by sterics. As the barrier to flipping was predicted to be higher this suggests that the two equivalent configurations would be more easily observable in STM. Moreover, it would be of great interest if we were able to trigger the flipping. Fig. 7.8 is a model surface taken from a molecular dynamics simulation of fourteen 9-vinylanthracene molecules bonded to the surface in a molecular line. The molecules are oriented similar to a

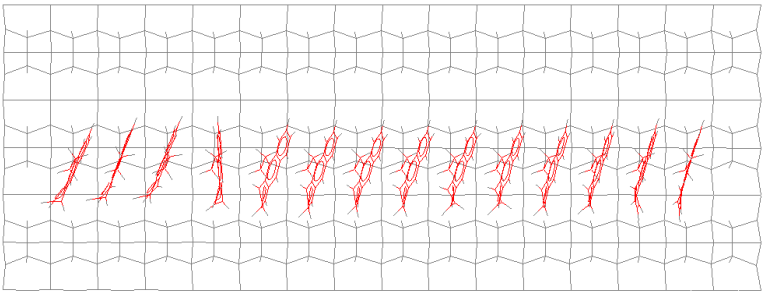

Figure 7.8: Example Still shot from a Molecular Dynamics calculation of 9-vinylanthracene on H-Si(100):2 × 1. Silicon and hydrogen atoms are shown in grey and carbon atoms are shown in red. 14 molecules have been attached to the surface as they would be in a molecular line. Thirteen of the molecules are oriented similar to a forward slash. An isoenergetic backward slash orientation is also available.

forward slash, except for the fourth molecule from the left which is oriented more parallel to the dimers at this moment of the simulation. Molecules, particularly those at the ends of the line, were observed to change orientation during the course of the simulation done at 300K. Due to the symmetry of the surface, one can see that an energetically similar orientation similar to a backwards slash is also available to the molecules.

Dr. Dilabio's calculations suggested that the conversion from one orientation to another may be possible. In a first approximation, it is expected that the sample temperature would have a significant effect on the ability of the chemisorbed molecules to overcome the barrier to switching between conformations. Sample temperature may also simply be used to define an ordered state (lower temperature) versus a disordered state (higher temperature). If such a transition point is found, at temperatures close to the transition temperature, we suspect that the STM tip may be effective in triggering a flipping event, for example with a voltage pulse. The coherence length of order within the structure as well its dependence on temperature, flip triggering method, length of line, line density and surrounding defects may then be interesting aspects to pursue. Figure 7.9 presents some of the molecules for which an initial survey on the possibility for studying controlled order was conducted. The last molecule in the figure, 4-(trifluoromethyl)styrene, was selected in the hopes of being able to manipulate order through electronic rather than steric interactions. The observations for each of these molecules will be briefly discussed below.

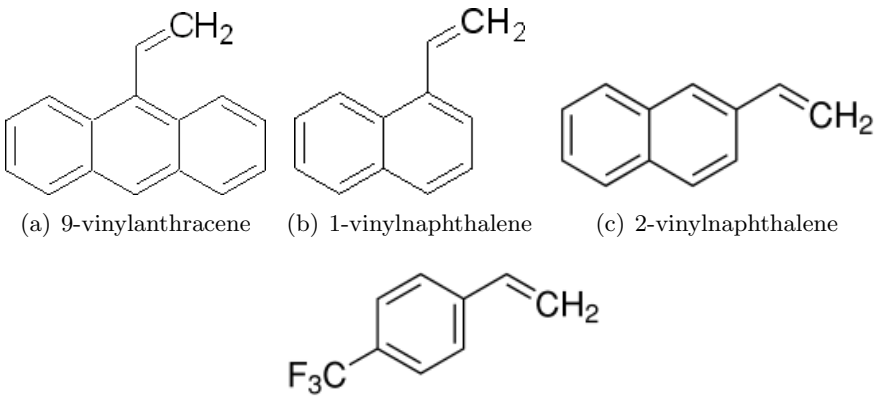

(a) 9-vinylanthracene (b) 1-vinylnaphthalene (c) 2-vinylnaphthalene

(d) 4-(trifluoromethyl)styrene

Figure 7.9: Molecules Explored for Ordering Effects in Molecular Lines

7.5.1 9-vinylanthracene

9-vinylanthracene consists of three fused benzene-like rings with a vinyl moiety on the centre ring. From molecular dynamics studies, this bulky molecule was expected to be the best candidate to demonstrate the existence of two stable orientations of the molecule with respect to the dimer rows. Several attempts were made to grow molecular lines from this molecule on low and medium doped silicon surfaces. 9-vinylanthracene is a solid at room temperature and has a melting point near 62 °C. As such, it was necessary to heat the molecule as well as the dosing line (approximately 90 °C) in order to achieve a high enough vapor pressure to dose the molecule into the chamber. The sample was also heated to approximately slightly in order to promote molecular diffusion at the surface. However, even with these measures, it was difficult to sustain a high or long enough vapor pressure to dose more than approximately 5L. In the VT-STM, at these conditions, no evidence of the molecules was ever seen on the surface.

Dr. Zikovsky, a former graduate student in the group, attempted to grow molecular lines of 9-vinylanthracene in the Multiprobe system using similar conditions [36]. In the Multiprobe, which has a dosing line with greater line of sight and shorter distance from the sample, he observed evidence of the molecule on the medium doped surface at 4L. Unfortunately, the STM images revealed mostly random 'clumps' rather than molecular lines. As these clumps were of variable dimensions in STM, there was also the question as to the possibility that the molecule underwent partial decomposition. However, despite this concern, evidence of a few, very short molecular lines within the clumps was observed. Unfortunately, with the limited cleanliness of the surface, it was difficult to maintain a good enough tip to obtain

high resolution images - which would be required for studies of molecular order. Moreover, we suspect that variable sample temperature, a feature unavailable in the Multirpobe, would be be required to study the ordering phenomenon.

7.5.2 Vinylnaphthalene

The steric interaction of vinylnaphthalene (two fused benzene-like rings with a vinyl group) also made it a strong candidate molecule in which to study ordering effects. Both 1-vinylnaphthalene and 2-vinylnaphthalene lines were successfully grown at room temperature on medium, low and high doped n-type H-Si(100):2 $\times$ 1 as well as high doped p-type H-Si(100):2 $\times$ 1 using various molecular doses; however, 2-vinylnaphthalene tended to have a greater line density for the same molecular dose. The highly doped surface was desirable to facilitate STM imaging at low temperature. However, for 1-vinylnaphthalene on high doped n-Si(100), it was found that doses as high as 40L produced few lines on the surface. It grew much more readily on the high doped p-Si(100):2 $\times$ 1. This difference has been observed for various molecules and is believed to relate to the difficulty of reacting with a negatively charged DB. The observations of structure in the molecular line, did not appear to change depending upon the substrate utilized.

1-vinylnaphthalene was the molecule of primary interest as the line growth mechanism would allow the rings of the molecule to lie somewhat parallel to the surface and slightly tilted in one of two directions with respect to the dimer row direction. 2-vinylnaphthalene was studied mostly as a comparison molecule as the expected upright structure of the molecules in the line should not easily lend itself to have two equivalently stable structures. Fig 7.10, demonstrates STM images of 1-vinylnaphthalene lines grown and imaged at room temperature. Resolution of structure in lines of 2-vinylnaphthalene was difficult to achieve. For both molecules, a high density of double and multiple lines was often observed on the surface. Fig 7.10(a) demonstrates that in 1-vinylnaphthalene, there is evidence for the existence of two stable structures with molecules in the line apparently tilted with respect to the dimer row direction. Many apparently single lines appeared to have a lighter and/or (depending upon the tip) thinner side region in which the structure appeared more parallel to the dimer row as in 7.10. Initially, this was thought to be a tip artifact, however it was seen rather consistently even when other features on the surface imaged very well. This region appeared to disappear in sections where the lines double over themselves. This suggested that the STM may be capturing a time averaged signal of the molecules flipping - a flip that may be hindered by the steric effect of the neighbor molecules in a double line. It may be possible that

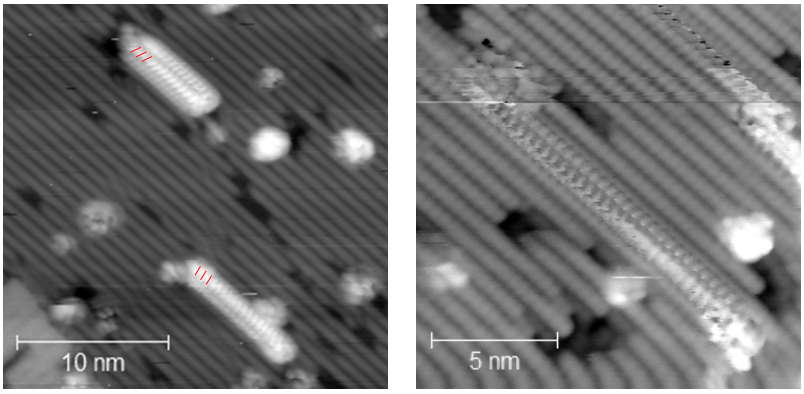

(a) (b)

Figure 7.10: STM images of 1-vinylnaphthalene at room temperature on high doped n-Si(100):2 × 1.(a) Image demonstrating opposite slanting of 1-vinylnaphthalene molecules in molecular lines. The red lines are superimposed to help guide the eye to molecular orientation. Imaging conditions: -2V, 80pA. (b) Closer view of structure in molecular line. Imaging conditions: -2V, 100pA.

the direction where it spends less time appears less tilted with respect to the dimer row than expected. Another possibility that has been suggested is that the lighter (lower) region may correspond to the vinyl group while the brighter (higher) region corresponds to the aromatic rings.

In an attempt to understand if the room temperature observations were indeed indicative of flipping actions, low temperature STM imaging was performed. The molecular lines were grown at room temperature and then the sample was cooled using a liquid helium flow cryostat [69]. It was found that even at 30K, the structure in the lines appeared very similar to room temperature; however, one side of the line or the whole line often appeared fuzzier than at the higher temperatures (Fig 7.11). It was difficult to determine whether the observations pointed towards fewer but still present flips in the molecule resulting in lower averages and less distinct features or if it was simply an artifact of a less stable tip which could be caused by a slight pressure gradient near the sample as a result of the temperature gradient. Attempts at increasing the gas flow in order to further reduce the temperature induced more vibrational noise into the system from the helium pump.

Attempts were also made at imaging the lines at an elevated temperature in the effort at finding a condition at which the disorder in the lines has increased such that no ordered structure was visible by STM. The sample was heated using Omicron's direct heating method of passing a current through the sample to exploit energy loss due to resistivity [69]. Unfortunately, even at the lowest current setting available

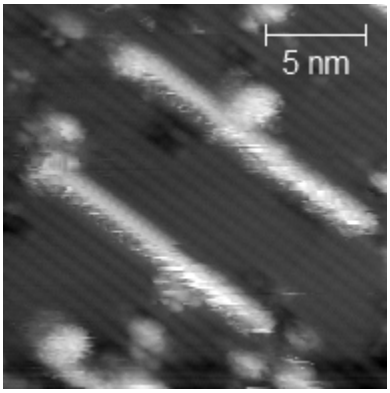

Figure 7.11: STM images of 1-vinylnaphthalene at 30K on high doped n-Si(100):2×1. Imaging conditions: -2.5V, 0.1nA

on the system's supply (0.001A), the tip induced effects destroyed the lines in the imaging region. For example, the centre region of Fig 7.12 was scanned with the STM tip at usual imaging conditions (-2V, 100pA) while the sample was elevated. In this region, the lines have been destroyed and the sample appears quite dirty. In the outer region, which was also heated but not scanned with the tip, the lines remained intact. It should be noted that the exact temperature of the sample at this current was unknown as the system did not have an appropriate window for a low temperature pyrometer. Modification of the system to include an appropriate window and/or connect to an external low current supply could be possible in the future.

The study of 1-vinylnaphthalene line structure did however reveal some interesting observations. Line growth with 1-vinylnaphthalene is expected to occur with hydrogen abstraction from adjacent dimer sites such that the molecules in the line are spaced apart with the same periodicity as the dimers in the row. This was most often the case. However, occasionally, molecular lines with double the periodicity of the styrene dimers were observed (Fig 7.13(a)). Such double periodic structures were never observed for lines composed of 2-vinylnaphthalene molecules. A change in the line structure as observed in the STM images could be attributed to two different scenarios. In the most direct case, the STM images truly reflect the topography of the molecules in the line and thus a direct structural difference between normal and double period lines. In the other case, the STM may be imaging a different molecular orbital-like structure of the line. The energy level of the molecular lines could potentially be shifted due to the local environment, including effects such as proximity to other lines, dopant centers close to the surface and other surface

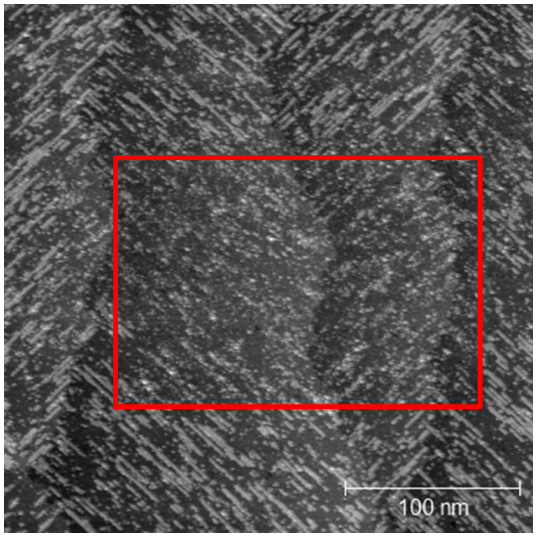

Figure 7.12: STM assisted desorption of 1-vinylnaphthalene at Elevated Temperatures from n-Si(100):2 × 1. The red box indicates the area where attemped STM imaging (V_S = -2V, I_T=100pA) at elevated temperatures (0.001A current for resistive heating) took place. In this region, the desorption of the molecules was assisted with the tip while the molecular lines remained intact elsewhere. Imaging conditions: V_S = -2V, I_T=100pA

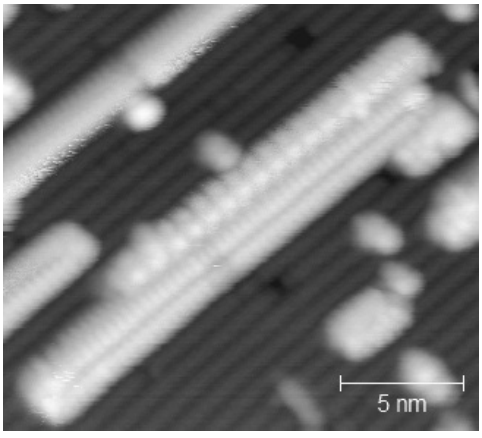

(a) Double Periodicity in Structure

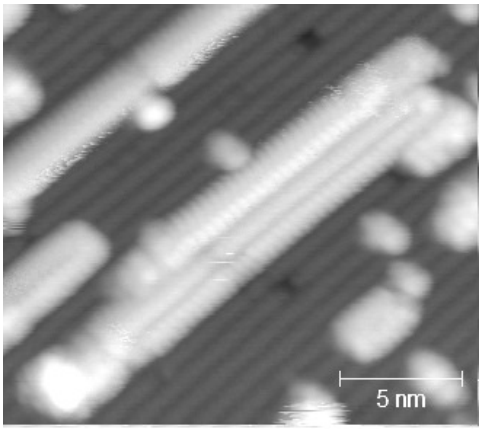

(b) Switch to Normal Periodicity

Figure 7.13: STM images of 1-vinylnaphthalene at room temperature on high doped n-Si(100):2 × 1. Imaging conditions: -2V, 80pA. (a) The top line in the image has double the periodicity of the normal lines and silicon dimer row structure. (b) The top line has switched structure and now appears with normal periodicity.

Figure 7.14: STM Image of a surface with a relatively high density of 1-vinylnaphthalene molecular lines. Lines circled had double periodic STM features at the beginning. Those circled in blue switched to the normal state within an hour or less of imaging. Those in yellow retained the double periodic structure. It was difficult to determine the state of the line circled in green after imaging for one hour. Imaging conditions: V_S = -2V, I_T=100pA

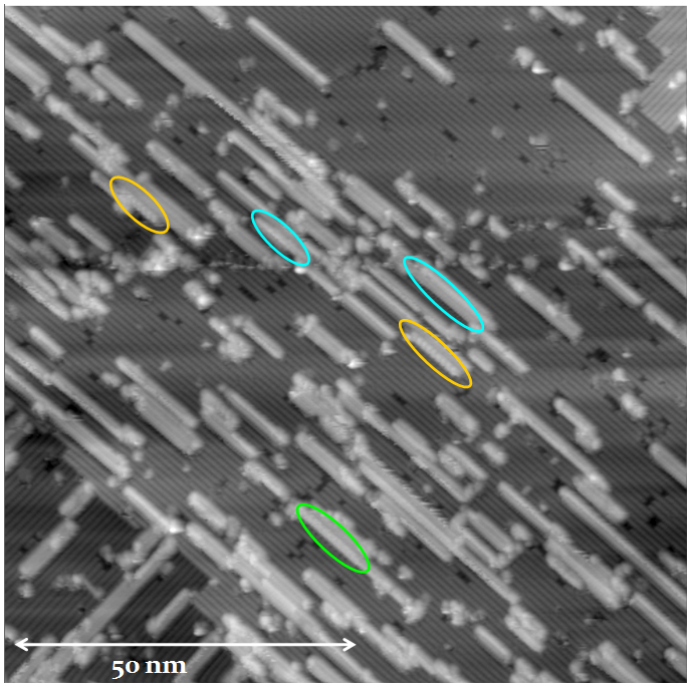

defects. While this can not be ruled out, my efforts in attempting to understand the double periodic structures focuses on the first case.

As shown in figure 7.13(b), many of these double periodic lines were observed to flip into a'normal' structure. Switching was seen to occur very quickly with some lines while other double period structures were stable for over an hour of continuous STM imaging and attempts at triggering conversion through pulsing or imaging at higher voltages (up to ±5V). Fig. 7.14 presents an example image of a surface with a relatively high density of 1-vinylnaphthalene lines after an hour of imaging the same location. All the lines circled had double periodic STM features at the beginning. Those circled in blue switched to the normal state within an hour or less of imaging at normal conditions of V_S = -2V, I_T=100pA. Those lines circled in yellow retained the double periodic structure. In this example it was also difficult to determine the structure of one of the lines which began as double periodic; it is circled in green.

Double periodic lines were also observed at temperatures of 30K with a qualita-

tively similar frequency to room temperature. Although an exhaustive search was not conducted, no double periodic lines were observed to switch into the normal structure at 30K. These observations are suggestive of a higher energy double period structure overcoming an energy barrier to fall into a more energetically stable single period structure. Although I could not determine any regularity of the switching based upon surrounding defects and lines, it is probable that the surrounding environment acts to stabilize the higher energy structure to varying degrees. In fact, the double periodic structures were most often seen in areas of greater line density. This unevenness in the spatial distribution of lines also made it difficult to determine an overall rate of occurrence.

With the hope of gaining a better understanding of the 1-vinylnaphthalene lines, the line growth process was monitored with STM. STM images were taken as the molecule was dosed into the chamber at a pressure of 7.5×10^{-8} Torr. One such series of images is presented in Figure 7.15. Unfortunately, no double-periodic structures were ever observed to grow. However, some interesting effects were observed and the series in Fig. 7.15 highlights both these features. The yellow circles in images (a) and (b) highlight an example of line growth occurring along the silicon dimer row resulting in the formation of a single line. This seemed to be the most prevalent growth mechanism. However, the label '1' presents a line where, through the correlation with the starting DB, it appears as though a double line segment has first formed and then growth continued in a single line. In most cases, the observed growth of lines was very quick and it was difficult to determine if a double line grew as a double line or if a single line doubled over itself, however through correlation with the starting point at several cases of probable direct double line growth have been identified. The double line growth is known to occur due to the relative energy barrier to abstraction along the row and across the row. Abstraction from across the row can have two different barriers depending on if the abstraction site is in the same row or across the gulley. If abstraction across the row is more facile than abstraction from a dimer in the same row from one position but not another, a square pattern of line growth can occur [36, 43]. In such cases, double lines grow directly rather than by formation of single line growth turning over itself. For 1-vinylnaphthalene, if square pattern growth is occurring in some instances it could suggest that the barriers are not that different from each other leading to a slight competition between growth mechanisms. However, it could also be caused by some local defect causing H-abstraction to be more difficult from certain specific locations than it may be on a pristine surface.

In the series presented in Figure 7.15, the effect of the dangling bond on neigh-

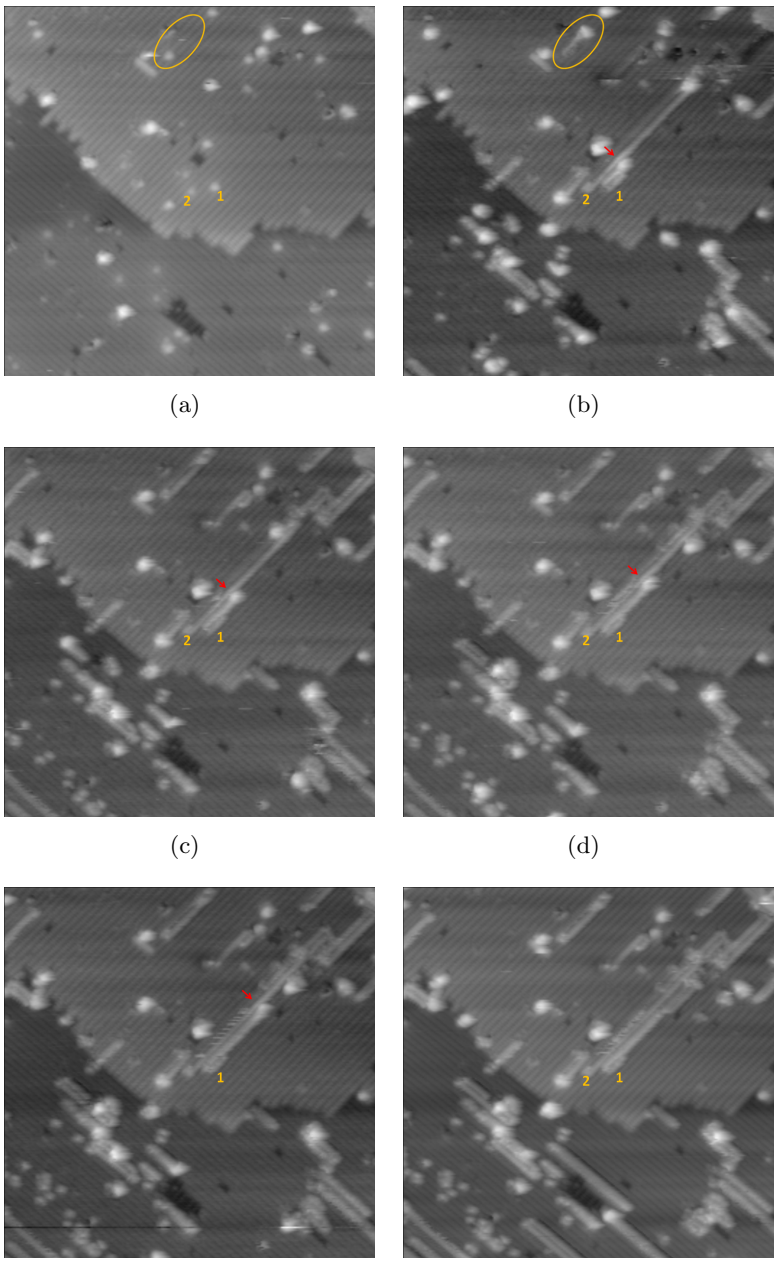

Figure 7.15: Consecutive STM images of the growth of 1-vinylnaphthalene lines on high doped n-Si(100):2 × 1 at room temperature. Imaging conditions: V_S=-2V, $I_T = 100pA$, 50nm ×50nm. The yellow circles in (a) and (b), highlight the growth of a single line along the dimer row. The growth of the line labeled '1' appears to begin in a square wave pattern and then continues as a single line. As '1' grows, the region in line '2' near the DB (marked by the red arrow) increases in brightness and decreases in width.

boring atoms is also quite interesting. As line '1' grows, the region of line '2' near the moving DB (indicated by the red arrows) decreases in width and increases in brightness. In STM, a slope effect in image brightness has also been shown as a result of the electrostatic field of a charged DB regulating the conductivity of nearby substrate-bound molecules [145]. However, as such a slope effect is not visible with these imaging conditions in line '1' , the effect in line '2' is likely related to topography rather than conductivity. It is rationalized that the less localized orbital of the DB restricts the motion of neighboring molecules. The increased brightness suggests that the molecules shift orientation slightly such that they appear taller with STM and then relax once the DB has moved on. A restriction in the thickness of lines was also observed around other surface defects, but did not usually appear to be accompanied with an increase in STM image brightness.

Returning to the question of the structure of the observed double periodic lines, we note that their ability to transition into a structure with the normal density of molecules suggests that the double periodicity may arise from a systematic pairing or dimerization of the molecules in the lines. From table 4.1 we can recall that many of the predicted stable dimer pair structures for free naphthalene molecules had optimal intermolecular distances ranging from 3.5Å-3.6Å. As the inter dimer spacing on Si(100):2 $\times$ 1 is known to be 3.86Å, if molecules within the line were to form dimers at the optimum distance, that leaves approximately 0.26Å between dimer pairs.

In order to search for a local energy minima that may correspond to a dimer-like structure within the lines, geometry optimization calculations were performed for sets of two vinylnaphthalene molecules chemically bonded to the H-Si(100):2 $\times$ 1 surface through the vinyl group as though they had undergone silicon line growth and the remaining DB had been capped with a hydrogen atom. The calculations were performed in a similar manner to those presented in previous chapters. The B971 [110] functional was used with the 6-31+G(d,p) basis sets and dispersion correcting potentials (DCPs) [99,101,102]. All calculations were again performed using the Gaussian 03 package [111]. The slab model used for the surface consisted of three dimer rows of four dimers each and two gulley rows for a total of 64 Si atoms. All silicon and capping hydrogens were held fixed for the optimizations. The molecules were placed in several different starting orientations that were visually similar to orientations of the low energy structures studied in section 4.5. An example starting orientation is presented in Fig. 7.16(a).

The optimized structures all resulted in canted naphthalene molecules with spacings between the naphthalene groups closer to the dimer row spacing rather than

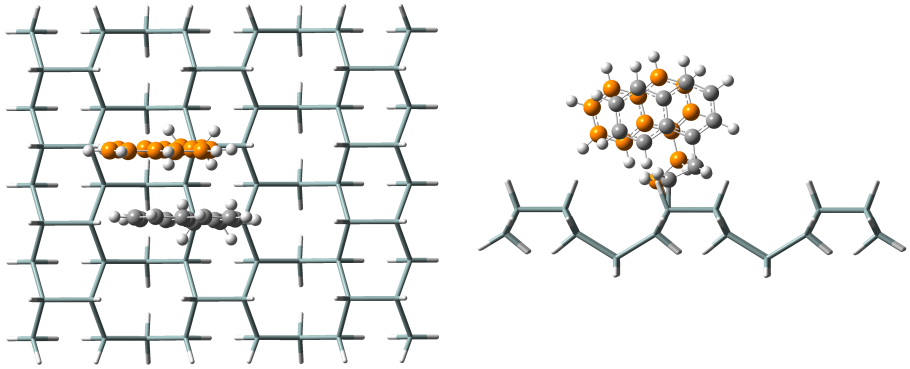

(a)

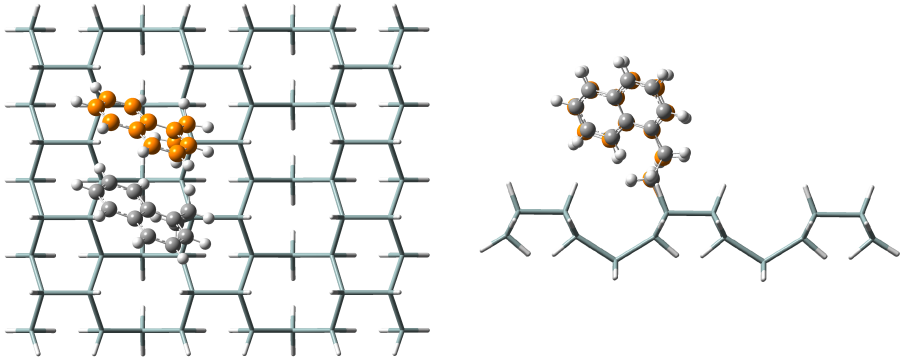

(b)

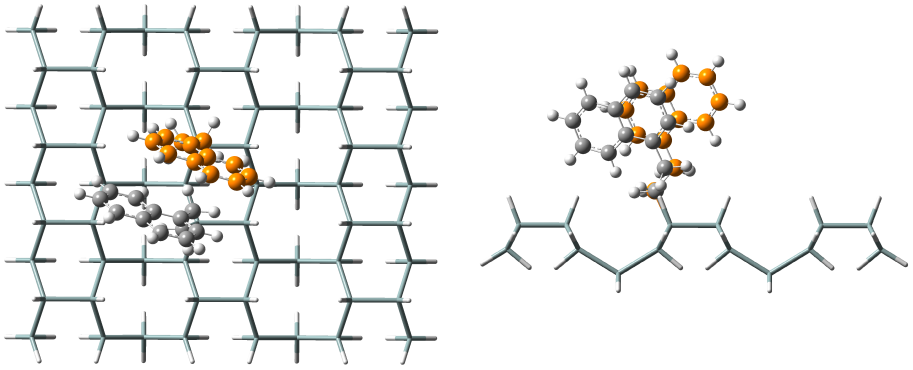

(c)

Figure 7.16: Top-down and Side Views of (a) an example trial 'dimerized' arrangement of the naphthalene groups and (b-c) stable optimized configurations found. Structure (b) was found to be approximately 2.7 kcal/mol more stable than structure (c). For ease of view, surface atoms are shown in tube format and carbon atoms in one molecule are colored orange while carbon atoms in the second molecules are colored gray.

the naphthalene dimer spacings. Two stable minima were determined. The lowest energy structure had both rings of both molecules over a gulley region, as shown in Fig. 7.16(b). The second configuration had one molecule with both rings over the gulley region while the other was more centered over the row, as shown in Fig. 7.16(c). The second structure was approximately 2.7 kcal/mol higher in energy than the first. Despite the slight increase in height of the molecules with one ring over the row, it is somewhat unlikely that the later structure would account for such a dramatic change in STM images of the lines.

Re-analysis of the STM images of the double periodic lines demonstrated that the vast majority of the lines with minority structure occurred in lines next to double lines. This suggests the possibility that the double line structure helps stabilize the double periodic structure. As density functional theory calculations of large structures is time intensive, the above possibility was explored using molecular dynamics using the HyperChem7 [148] computational package. Of the built in molecular mechanics force fields available in the package, the OPLS field was found to produce naphthalene-naphthalene dimer interactions most closely resembling those of the DCP-DFT calculations and was thus used in all calculations. Calculations were computed at 300 K with a ramp time of 30 ps to reach this temperature from 0 K. Surface hydrogen atoms and the bound naphthalene molecules were allowed to move while the base silicon atoms were held fixed. For simplicity, no dangling bond was left at the end of any of the models.

Molecular dynamics calculations on a double line of 1-vinylnaphthalene molecules indicated that the molecules in the double line structure were less prone to structural fluctuations than molecules in a single line, presumably due to steric interactions. Two different double line structures were explored. The first had all naphthalene molecular rings over the gulley regions while the second had one line of the double line set withs rings over the gulley and other line with one ring over the row. The increase in stability of the double line structures in comparison to single lines was observed for both structures and may help stabilize molecule structures in nearby lines.

A single line of 1-vinylnaphthalene molecules was added to the model spaced apart from the double line structure by one gulley region and one half of a dimer row. The starting structure of this line was varied to test for possible structures giving rise to the double periodicity observed in STM images. The starting orientations included structures similar to the uncanted dimer-like structures previously studied independent of the nearby double line with DCP-DFT. In all cases but one, the structure of the single line eventually optimized into the normal canted structure

of the molecules with the occasional exception of some of the molecules at the end of the line which have greater orientational freedom. This structure is shown in Fig. 7.17(a). However, in the remaining case, a structure was found that was stable for at least 300 ps at temperature. This structure, shown in Fig. 7.17(b) had a configuration reminiscent of a tilted T-shape dimer. For each pair of molecules in the single line, two T-like interaction occur with molecules in the double line and one with the molecules in the single line. For a line with fourteen molecules in a starting orientation in this structure run over 300 ps at 300 K compared to a line with fourteen molecules in the normal canted starting configuration run over 300 ps at 300 K, the T-like structure was, on average, 20 kcal/mol less stable than the normal configuration.

As indicated above the T-like structured line has merit as the possible double periodic structure due to the stability enabled by the interactions with the more stable double line and the overall slightly higher energy that may eventually relax into the normal configuration. However, a direct correlation between the T-like structured line and the STM images of double periodic lines is not immediately obvious. It is possible that the lower height of the canted molecules within the T-like structured line along with the T-like interactions centered around the molecules oriented with rings approximately perpendicular to the dimer bond may lead to a higher intensity STM signal at every second molecule thus leading to the observed double periodic structure.

The studies of vinylnaphthalene, particularly 1-vinylnaphthalene molecular lines proved to be quite intriguing. While the original goal of being able to manipulate the orientation of the expected canted molecules in the line was not attained with this particular molecule, the observation of a double periodic structure which can convert into the normal canted structure was quite surprising. The apparent need for the interactions between a stable double structured line and the T-shape structure is instructive to researchers as it highlights the complexities that may be involved in stabilizing the structures of molecules within lines. The more we learn about all the interactions that may be involved in ordering molecules in lines, the greater chance we will have of being able to manipulate such order in future studies.

7.5.3 4-(trifluoromethyl)styrene

The proposed order in molecular lines of 9-vinylanthracene and 1-vinylnaphthalene focused on the use of steric effects to control molecular orientation. In addition to steric effects, electronic effects have also been used to instill order in nano-structures. The repulsion between similar polar groups could potentially be used to restrict the

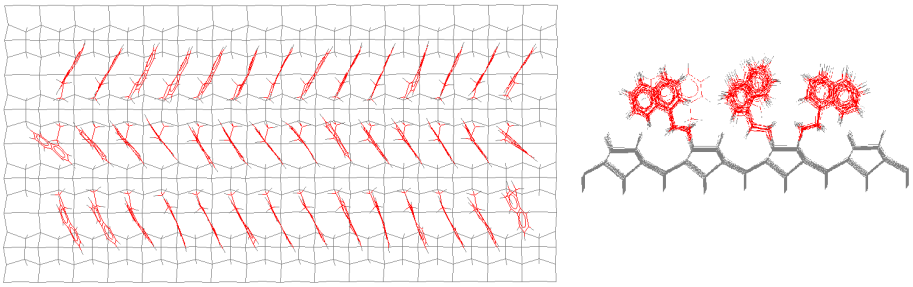

(a)

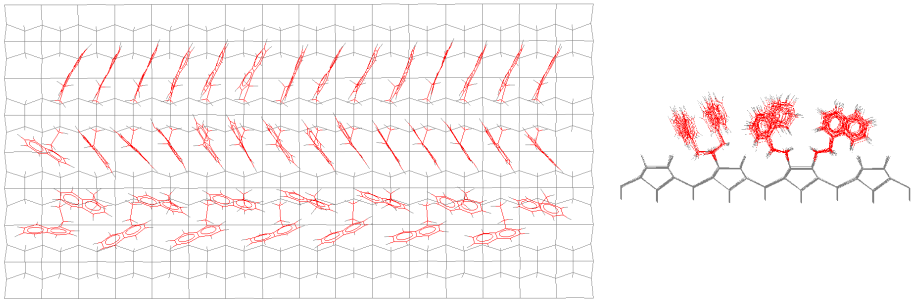

(b)

Figure 7.17: Top-down and Side Views from a Molecular Dynamics calculation of 1-vinylnaphthalene on H-Si(100):2 × 1 after running calculations for 300 ps at 300 K. Silicon and hydrogen atoms are shown in gray and carbon atoms are shown in red. In both cases, the double line had line containing molecules with both rings over the gulley while the other line - close to the single line - was oriented such that one ring was over the row. The single line was spaced apart by one gulley region and one half of a dimer row. In (a) the starting orientation for all molecules in the single line was the normal canted configuration while in (b) the starting configuration for all molecules was the T-like structure still observed in most of the molecules. It is less observable in the end molecules which have greater freedom of motion during the simulation.

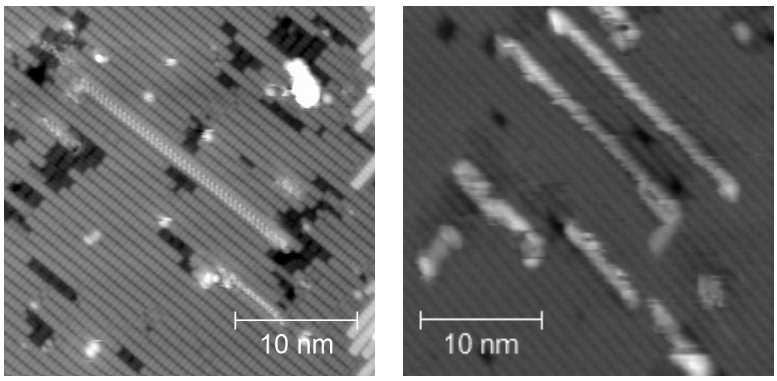

(a) Room Temperature (b) Low Temperature, 30K

Figure 7.18: STM images of 4-(trifluoromethyl)styrene at V_S=-3V, $I_T = 100pA$

movement of a molecule. As an initial venture into studying this prospect, lines of 4-(trifluoromethyl)styrene were studied. Molecular lines of the molecule were found to grow readily with a dose of 10L on medium dopes hydrogen terminated n-Si(100):2×1 at room temperature.

Fig. 7.18(a), shows an example of some single molecular lines. In the image, the longer line has a thicker width and a zig-zag pattern. If a line is drawn along the length of the line through the centre, the periodicity of the lobes on each side of the line is the same of that of the silicon dimer row. The thinner line consists of a single line of larger lobes with the same periodicity as the silicon dimer. Lines with the thicker width were seen to extend over the gully region, where as the thinner lines were generally located over the row. Some thin lines were observed over the gulley regions, however this most often correlated with one end of the line taking part in a double line. We suggest that when the molecule is bound such that it extends over the gulley it has the room to move into two conformations where as if it is bound over the row the movement is restricted. At low temperature (30K), it was again difficult to discern any structural information (Fig 7.18(b)). The observation of different structures depending upon the position of binding to the row is somewhat undesirable if one wished to take advantage of ordering phenomena, as such the exact nature of the structure has not yet been delved into in detail.

Another interesting observation of 4-(trifluoromethyl)styrene lines, was the interaction between lines. With certain rare STM tips, a large enhancement of the electron density could sometime be observed in areas where several lines were in close contact. Fig 7.19(a), presents such an image. Piva et al. [35] and Kirczenow et al. [149] have studied the effects of the modulation of electrical conduction through molecules on silicon by the electrostatic field of nearby polar molecules. The par-

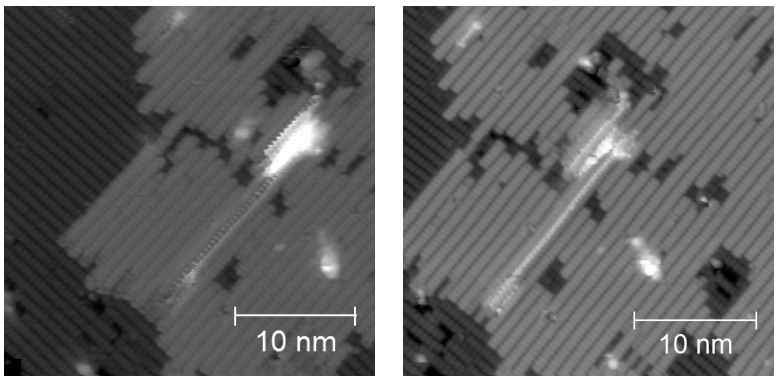

(a) (b)

Figure 7.19: STM images of 4-(trifluoromethyl)styrene demonstrating tunneling current enhancement betwen closely spaced lines. Imaging Conditions: V_S=-2.2V, $I_T = 100pA$ before (a) and after a tip (b) change

ticular case shown in Fig. 7.19 has yet to be studied in detail; however, the large enhancement of the conduction observed suggests that it would be of interest in future studies. Moreover, the same lines were imaged after a slight tip change and the effect, though still present, was significantly reduced, Fig 7.19(b). This suggests that the precise work function of the tip may play a crucial role in the study of such effect.

7.5.4 Future Outlook on Molecular Ordering

The preliminary outlook on ordering phenomenon within molecular lines demonstrates that while high order can be resolved within lines, much more research will be needed in order to gain a better understanding of the true structures. The observations of different stable molecular structures within lines (ex. double periodicity), different structures depending upon the bonding location over the silicon dimer row and enhanced tunneling current between closely spaced lines all raise new questions that could be followed. Whether or not such effects will prove to be manipulable and therefore potentially useful in molecular devices etc., is still debatable; nonetheless, the questions that have arisen from the work is highly intriguing from the view of basic science.

7.6 Chapter Summary

While the concept of molecular lines may seem deceptively simple, the variety of lines that can be grown and the variety of properties that can be observed, studied

and potentially made use of in future molecular scale devices is extremely vast. In this chapter we made an initial foray into the properties of conduction and ordering phenomena within molecular lines. The observations highlight the complexity involved in understanding molecular lines while at the same time demonstrating the future potential and the scientific knowledge that could be gained from the study of such structures.

Chapter 8

Summary and Future Directions

8.1 Directions for Future Investigation

The work presented in this dissertation suggests many possible avenues that may be pursued in future studies. Three primary areas of future studies arise. The first, and most interesting possibility, is the use of multiprobe techniques to study transport properties. An increased understanding of transport modification due to low density adsorbate coverage is also necessary. Finally, continued studies on the ordering properties of molecules in molecular lines would be necessary for tailoring molecular lines for use in molecular scale devices.

Zikovsky has recently demonstrated some of the powerful functions of the Mutliprobe STM system [36]. In particular, he demonstrated the use of a technique referred to as Scanning Tunneling Fractional Current Imaging (STFCI) to study surface conduction and even measure conduction changes associated with a single silicon step edge on the surface [36]. In STFCI, the two probe tips are brought into contact at a known position on the sample which is otherwise floating. The main STM tip is then scanned in the usual manner using the total current passing through the two probes as the feedback current. The fraction of the current going through each probe is also recorded and can be used to study changes in the conduction path from the position of the main tip and the probe. Using this technique, the surface conduction and differences in conduction due to different reconstructions and passivation techniques can be studied. Moreover, the I/V interaction between the two probes can provide further information about the conduction channels.

In this dissertation, it was observed that the I_T/V_S curves taken on a clean Si(100):2×1 window on the otherwise monohydride surface do not exhibit an ohmic shoulder region associated with π^* state conduction, that is visible on the fully clean surface. It was hypothesized that if the grounding point were located within the

window, the ohmic region would again be visible thus providing further evidence for surface state conduction. This can be directly probed with the multiprobe system either touching down with the probe on a window region or more realistically touching down on lithographically defined contact points and creating a window or strip between the contacts. STFCI micrographs of the window/strip region and the surrounding passivated region as well as probe to probe I/V measurements could provide evidence of any π^* state conduction as well as more qualitative measures of the surface conduction in the presence or absence of the π^* state. If surface conduction is indeed seen, potential quenching of the surface conduction through the chemi-adsorption of a molecule such as styrene on the window could also be studied. In addition to continuing studies of the Si(100):2×1 surface, the Si(111):7×7 may prove to be even more interesting as this surface reconstruction is expected to produce metallic surface-state conduction.

In conducting the above studies, the knowledge gained in understanding the behaviour of silicon surfaces near EBL defined patterns will be beneficial. Further studies on how this behaviour changes with the size of the EBL contact made will also be useful in determining the optimal size of the contact. The work done in this thesis towards optimizing the pressure and noise in the Multiprobe will be also be beneficial for future work done on this system. However, a functional system for probe placement is required. This necessitates further efforts in restoring the SEM and/or incorporating another high resolution observation method into the system.

Comparison of the window studies conducted in this thesis with those of Dickie et al. [81] as well as the change in I_T/V_S as a function of distance in tip-shadowing studies, suggest that a low density of adsorbates on the silicon surface can significantly alter the behaviour. When low adsorbate coverage was observed, the I_T/V_S curves took on a hybrid character of that of the clean and passivated surfaces, even when not directly on a molecule. In this dissertation, we suggest that these effects are consistent with longer range effects such as surface dipoles rather than local effects due to the alignment of molecular orbitals with the semiconductor energy bands. However, a detailed understanding of the mechanism leading to this hybrid character is not truly understood. Greater understanding could be achieved by studying the behaviour from molecules of varying surface dipoles at controlled densities at the surface. I_T/V_S measurements close to a single adsorbate and as a function of distance from an adsorbate on a very low covered surface may also help elucidate the mechanism leading to hybrid characteristics. The observation of hybrid character even when not directly on an adsorbate may have implications for molecular sensing applications. However, for such effects to be useful, similar effects

should be studied on surfaces that are less reactive in air.

Another area of future investigations that arises from this work is continuing efforts to acquire a detailed understanding of the structure of molecules within molecular lines. While the line growth mechanism and ordered appearance of lines in the STM appear simple, we have seen that the ordering of molecules in the line can be quite intricate. The combination of further experimental work along with calculations is still necessary to determine the key phenomena that lead to ordered molecules within lines. Manipulation of these phenomena by tailoring the structure of the molecule then remains a possibility.

8.2 Summary of Contributions

The objective of this dissertation was to advance our knowledge of the interactions, behaviour and properties of simple molecular entities and the Si(100):2×1 surface. Three areas were targeted: (1) the tunneling current behaviour of the surface from a monolayer, a patterned region, or a self-assembled nanostructure, (2) the ability of molecules to diffuse on the surface and (3) the structure of molecules within a molecular line.

STS methods were used to study the I_T/V_S behaviour of the clean Si(100):2×1 surface as well as the monohydride and the styrene passivated surfaces. The observations of these surfaces led to an energy band model that relies upon surface dipole characteristics and band bending to describe tunneling current transport. A particularly interesting proposition that arose from the model was that under certain conditions minority carrier transport may dominate the tunneling current. Additionally, the model suggests that tailoring the adsorbate molecule can significantly tune the current rectification properties of the surface. For example, the forward/reverse current rectification for the hydrogen passivated surface was found to be 1:10 at a tip distance of 5Åfrom the surface while that of the styrene passivated surface was found to be 10:1.

The transport behaviour from patterns of clean Si(100):2×1, styrene covered Si(100):2×1 and 4-fluorostyrene covered Si(100):2×1 on otherwise monohydride terminated Si(100):2×1 was also studied. Evidence of surface conduction through π^* states through an ohmic shoulder region which is present in the I_T/V_S of the fully clean surface, is missing on the clean patterns. In the case of styrene and 4-fluorostyrene, the observed current rectification from patterned regions is less than expected but still follows the expected trend with tip-sample separation.

The current transport behaviour from styrene molecular lines and styrene molecular lines terminated by a silver island were also studied. Unfortunately, in these

cases a clear trend could not be observed, possibly due to the influence of the STM tip on the individual molecules.

STM tip influences can also cause difficulties in other STM studies, including studies of surface diffusion. Diffusion of molecules on surfaces is intrinsic to various processes including the self-assembly of nanostructures on the surface. In STM diffusion studies, molecules that diffuse easily at the temperature of the study can not be investigated. Additionally, the tip can mask intrinsic diffusion effects such as small differences in the preference for motion. In this dissertation, a novel method for studying aspects of molecular diffusion that removes tip effects was developed and used to study the diffusion anisotropy of styrene and 4-fluorostyrene on monohydride Si(100):2×1. The diffusion lengths of the molecules were found to be 110 nm $\pm$ 30 nm for styrene and 77 nm $\pm$ 7 nm for 4-fluorostyrene. The smaller diffusion length of the fluorinated molecule is likely due to the greater hydrophilicity of the molecule and therefore the reduced interaction with the hydrophobic surface. Both molecules had diffusion anisotropies of 1.1 ± 0.1 favoring diffusion along the dimer rows of the surface as apposed to across the rows.

To help evaluate the effectiveness of the experimental method for studying diffusion, the diffusion of styrene was studied theoretically using density functional theory with dispersion correcting potentials to elucidate energy considerations and Monte Carlo methods in a C++ simulation to include dynamic effects. With energy considerations alone, the theoretical diffusion anisotropy, $k_{parallel}/k_{perpendicular}$, was determined to be 1.8. However, inclusion of dynamic effects resulted in a theoretical anisotropy of 1.06 ± 0.04, which is in good agreement with experimental findings. It was suggested that the use of the experimental technique along with the monte carlo simulations could provide an order of magnitude estimation of the expected energy-only anisotropy of molecules on surfaces. As the DFT (and other computation methods) studies of diffusion barriers can be quite time consuming, the order of magnitude expectation could potentially be quite useful.

Finally, self-assembled molecular lines were studied with respect to aspects not directly related to current transport measurements. The reaction of 1,4-cyclohexadiene with the surface was thought to potentially lead to a surface radical. Attempts were made to study this effect but the reaction of the molecule with the surface was still found to be debatable as there was no clear evidence of the molecule on the surface in STM micrographs. A preliminary study of possible ordering phenomena of molecules within molecular lines was also conducted. Of particular interest was molecular lines 1-vinylnaphthalene which demonstrated the ability to form lines which appear with double the periodicity of normal line and indeed the periodicity

expected from the dimer structure of the surface. Many of these unique lines transformed into 'normal' lines suggesting that they are in an energetically less stable configuration. Moreover, it was observed that many, if not all, of these double periodic lines were in proximity to double lines. This observation lead to the exploration of possible structures in single lines that may be stabilized by a nearby double line. Using molecular dynamics simulations, a stable T-like structure where for every two molecules in the single line, two T-like interactions between the double and single line and one T-like interaction within the single line was found. For molecular lines containing 14 molecules, this proposed structure was found to be 20 kcal/mol more energetic than the normal canted structure suggesting that conversion into the more stable structure may indeed be possible. Understanding how molecules in lines are ordered can be helpful to tailor molecules used in future line growth studies to order in a desired manner.

In summary, STM and theoretical techniques were used to increase our knowledge of simple molecular entities on the Si(100):2×1 surface. In doing so, an energy band model for current transport was devised, a novel technique to study surface diffusion properties with STM was created, the energy interaction of styrene with the surface were studied with DCP-DFT along with the creation of a Monte Carlo simulation to study the dynamics of diffusion and several of the intricacies involved in molecular line growth studies were elucidated. While much knowledge was gained with these studies, the door was also opened to further questions and avenues of study that can be pursued by researchers in the field.

Bibliography

[1] GE Moore. Electronics 1965. *38 (8)*, 114.

[2] G.E. Moore. Progress in Digital Integrated Electronics, Digest of the 1975 International Electron Devices Meeting, 1975.

[3] R.L. Carroll and C.B. Gorman. The genesis of molecular electronics. *Angewandte Chemie International Edition*, 41(23):4378–4400, 2002.

[4] G. D. Wilk, R. M. Wallace, and J. M. Anthony. High-kappa gate dielectrics: Current status and materials properties considerations. *Journal of Applied Physics*, 89(10):5243–5275, 2001.

[5] H. Choi and C. Mody. The Long History of Molecular Electronics. *Social Studies of Science*, 39(1):11, 2009.

[6] R. A. Wolkow. Toward hybrid devices. Chemical and Engineering News:Online.

[7] V. Beiu. Grand challenges of nanoelectronics and possible architectural solutions: what do Shannon, von Neumann, Kolmogorov, and Feynman have to do with Moore. In *Multiple-Valued Logic, 2007. ISMVL 2007. 37th International Symposium on*, pages a–a. IEEE.

[8] G. Binnig, H. Rohrer, Ch. Gerber, and E. Weibel. Surface studies by scanning tunneling microscopy. *Phys. Rev. Lett.*, 49(1):57–61, Jul 1982.

[9] B. Mann and H. Kuhn. Tunneling through fatty acid salt monolayers. *Journal of Applied Physics*, 42(11):4398–4405, 1971.

[10] EE Polymeropoulos and J. Sagiv. Electrical conduction through adsorbed monolayers. *The Journal of Chemical Physics*, 69:1836, 1978.

[11] R.M. Metzger. Unimolecular electrical rectifiers. *Chemical reviews*, 103(9):3803–3834, 2003.

[12] G.J. Ashwell, W.D. Tyrrell, and A.J. Whittam. Molecular rectification: Self-assembled monolayers in which donor-(π-bridge)-acceptor moieties are centrally located and symmetrically coupled to both gold electrodes. *Journal of the American Chemical Society*, 126(22):7102–7110, 2004.

[13] F. Favier, E.C. Walter, M.P. Zach, T. Benter, and R.M. Penner. Hydrogen sensors and switches from electrodeposited palladium mesowire arrays. *Science*, 293(5538):2227, 2001.

[14] J. Park, A.N. Pasupathy, J.I. Goldsmith, C. Chang, Y. Yaish, J.R. Petta, M. Rinkoski, J.P. Sethna, H.D. Abruña, P.L. McEuen, et al. Coulomb blockade and the Kondo effect in single-atom transistors. *Nature*, 417(6890):722–725, 2002.

[15] R.A. Wolkow. Controlled molecular adsorption on silicon: laying a foundation for molecular devices. *Annual review of physical chemistry*, 50(1):413–441, 1999.

[16] J. Leuthold, W. Freude, J.M. Brosi, R. Baets, P. Dumon, I. Biaggio, M.L. Scimeca, F. Diederich, B. Frank, and C. Koos. Silicon Organic Hybrid TechnologyA Platform for Practical Nonlinear Optics. *Proceedings of the IEEE*, 97(7):1304–1316, 2009.

[17] V. Sgobba and D.M. Guldi. Carbon nanotubeselectronic/electrochemical properties and application for nanoelectronics and photonics. *Chem. Soc. Rev.*, 38(1):165–184, 2008.

[18] V. Derycke, R. Martel, J. Appenzeller, and P. Avouris. Carbon nanotube inter-and intramolecular logic gates. *Nano Letters*, 1(9):453–456, 2001.

[19] RJ Hamers, RM Tromp, and JE Demuth. Scanning tunneling microscopy of Si (001). *Physical Review B*, 34(8):5343, 1986.

[20] R.A. Wolkow. Direct observation of an increase in buckled dimers on Si (001) at low temperature. *Physical review letters*, 68(17):2636–2639, 1992.

[21] A. Aviram and M.A. Ratner. Molecular rectifiers. *Chemical Physics Letters*, 29:277–283, 1974.

[22] NJ Geddes, JR Sambles, DJ Jarvis, WG Parker, and DJ Sandman. Fabrication and investigation of asymmetric current-voltage characteristics of a metal/Langmuir–Blodgett monolayer/metal structure. *Applied physics letters*, 56(19):1916–1918, 1990.

[23] A. Ulman. *An introduction to ultrathin organic films: from Langmuir-Blodgett to self-assembly*. Academic Press San Diego:, 1991.

[24] AS Martin, JR Sambles, and GJ Ashwell. Molecular rectifier. *Physical review letters*, 70(2):218–221, 1993.

[25] LA Bumm, JJ Arnold, TD Dunbar, DL Allara, and PS Weiss. Electron transfer through organic molecules. *The Journal of Physical Chemistry B*, 103(38):8122–8127, 1999.

[26] A.P. Labonte, S.L. Tripp, R. Reifenberger, and A. Wei. Scanning tunneling spectroscopy of insulating self-assembled monolayers on Au (111). *The Journal of Physical Chemistry B*, 106(34):8721–8725, 2002.

[27] R.M. Metzger. Monolayer rectifiers. *Journal of Solid State Chemistry*, 168(2):696–711, 2002.

[28] N. Armstrong, R.C. Hoft, A. McDonagh, M.B. Cortie, and M.J. Ford. Exploring the performance of molecular rectifiers: Limitations and factors affecting molecular rectification. *Nano letters*, 7(10):3018–3022, 2007.

[29] D. Vuillaume, S. Lenfant, D. Guerin, C. Delerue, C. Petit, and G. Salace. Electronic properties of organic monolayers and molecular devices. *Pramana*, 67(1):17–32, 2006.

[30] R.J. Hamers, S.K. Coulter, M.D. Ellison, J.S. Hovis, D.F. Padowitz, M.P. Schwartz, C.M. Greenlief, and J.N. Russell Jr. Cycloaddition chemistry of organic molecules with semiconductor surfaces. *Accounts of Chemical Research*, 33(9):617–624, 2000.

[31] GP Lopinski, TM Fortier, DJ Moffatt, and RA Wolkow. Multiple bonding geometries and binding state conversion of benzene/Si (100). *Journal of Vacuum Science & Technology A: Vacuum, Surfaces, and Films*, 16:1037, 1998.

[32] A. Calzolari, A. Ruini, E. Molinari, and M. J. Caldas. Surface nanopatterning through styrene adsorption on si(100). *Phys. Rev. B*, 73(12):125420, Mar 2006.

[33] GP Lopinski, DDM Wayner, and RA Wolkow. Self-directed growth of molecular nanostructures on silicon. *Nature*, 406(6791):48–51, 2000.

[34] G. Kirczenow, P.G. Piva, and R.A. Wolkow. Linear chains of styrene and methylstyrene molecules and their heterojunctions on silicon: Theory and experiment. *Physical Review B*, 72(24):245306, 2005.

[35] P.G. Piva, R.A. Wolkow, and G. Kirczenow. Nonlocal conductance modulation by molecules: scanning tunneling microscopy of substituted styrene heterostructures on H-terminated Si (100). *Physical review letters*, 101(10):106801, 2008.

[36] Zikovsky Janik. *Nanometer Scale Connections to Semiconductor Surfaces*. PhD thesis, University of Alberta, 2009.

[37] M.Z. Hossain, H.S. Kato, and M. Kawai. Competing Forward and Reversed Chain Reactions in One-Dimensional Molecular Line Growth on the Si (100)-(2× 1)- H Surface. *J. Am. Chem. Soc*, 129(11):3328–3332, 2007.

[38] X. Tong, GA DiLabio, and RA Wolkow. A self-directed growth process for creating covalently bonded molecular assemblies on the H-Si (100)-3x1 surface. *Nano Letters*, 4(5):979–984, 2004.

[39] X. Tong, G.A. DiLabio, O.J. Clarkin, and R.A. Wolkow. Ring-Opening Radical Clock Reactions for Hybrid Organic- Silicon Surface Nanostructures: A New Self-Directed Growth Mechanism and Kinetic Insights. *Nano Letters*, 4(2):357–360, 2004.

[40] P. Kruse, E.R. Johnson, G.A. DiLabio, and R.A. Wolkow. Patterning of Vinylferrocene on H- Si (100) via Self-Directed Growth of Molecular Lines and STM-Induced Decomposition. *Nano Letters*, 2(8):807–810, 2002.

[41] G.A. DiLabio, P.G. Piva, P. Kruse, and R.A. Wolkow. Dispersion interactions enable the self-directed growth of linear alkane nanostructures covalently bound to silicon. *J. Am. Chem. Soc*, 126(49):16048–16050, 2004.

[42] M.Z. Hossain, HS Kato, and M. Kawai. Controlled fabrication of 1D molecular lines across the dimer rows on the Si (100)-(2 x 1)-H surface through the radical chain reaction. *Journal of the American Chemical Society*, 127(43):15030, 2005.

[43] S.A. Dogel, G.A. DiLabio, J. Zikovsky, J.L. Pitters, and R.A. Wolkow. Experimental and theoretical studies of trimethylene sulfide-derived nanostructures on p and n-Type H-Silicon (100)-2 x 1. *Journal of physical chemistry. C*, 111(32):11965–11969, 2007.

[44] J. Zikovsky, S.A. Dogel, S. Sinha, G.A. DiLabio, and R.A. Wolkow. Scanning tunneling microscopy and computational study of the self-directed growth of 1, 3-butadiene and 2, 3-dimethyl-1, 3-butadiene on hydrogen-terminated silicon (1 0 0)-2× 1. *Chemical Physics Letters*, 458(1-3):117–121, 2008.

[45] LJ Chen. Metal silicides: An integral part of microelectronics. *JOM Journal of the Minerals, Metals and Materials Society*, 57(9):24–30, 2005.

[46] L. Borucki, R. Mann, G. Miles, J. Slinkman, and T. Sullivan. A model for titanium silicide film growth. In *Electron Devices Meeting, 1988. IEDM'88. Technical Digest., International*, pages 348–351. IEEE, 1988.

[47] G. Medeiros-Ribeiro, DAA Ohlberg, DR Bowler, RE Tanner, GAD Briggs, and R. Stanley Williams. Titanium disilicide nanostructures: two phases and their surfaces. *Surface science*, 431(1-3):116–127, 1999.

[48] GAD Briggs, DP Basile, G. Medeiros-Ribeiro, TI Kamins, DAA Ohlberg, and R. Stanley Williams. The incommensurate nature of epitaxial titanium disilicide islands on Si (001). *Surface Science*, 457(1-2):147–156, 2000.

[49] TI Kamins, R. Stanley Williams, and DAA Ohlberg. Annealing of chemically vapor deposited nanoscale Ti-Si islands on Si. *Applied Physics A: Materials Science & Processing*, 80(6):1279–1286, 2005.

[50] M. Sakurai, C. Thirstrup, and M. Aono. Nanoscale growth of silver on prepatterned hydrogen-terminated Si (001) surfaces. *Physical Review B*, 62(23):16167, 2000.

[51] T.C. Shen, C. Wang, GC Abeln, JR Tucker, JW Lyding, P. Avouris, and RE Walkup. Atomic-scale desorption through electronic and vibrational excitation mechanisms. *Science*, 268(5217):1590, 1995.

[52] S.M. Sze. *Physics of semiconductor devices*. John Wiley & Sons, Inc., New York, 2nd edition, 1981.

[53] Gerd Binnig and Heinrich Rohrer. Scanning tunneling microscopy—from birth to adolescence. *Rev. Mod. Phys.*, 59(3):615–625, Jul 1987.

[54] Russell Young, John Ward, and Fredric Scire. The topografiner: An instrument for measuring surface microtopography. *Review of Scientific Instruments*, 43(7):999 –1011, July 1972.

[55] M. Morgenstern, D. Haude, V. Gudmundsson, Chr. Wittneven, R. Dombrowski, Chr. Steinebach, and R. Wiesendanger. Low temperature scanning tunneling spectroscopy on InAs(110). *Journal of Electron Spectroscopy and Related Phenomena*, 109(1-2):127 – 145, 2000.

[56] John Bardeen. Tunnelling from a many-particle point of view. *Phys. Rev. Lett.*, 6(2):57–59, Jan 1961.

[57] J. Tersoff and D. R. Hamann. Theory and application for the scanning tunneling microscope. *Phys. Rev. Lett.*, 50(25):1998–2001, Jun 1983.

[58] Julien C. Chen. *Introduction to Scanning Tunneling Microscopy*. Oxford University Press, 2nd edition, 2008.

[59] Technical Manufacturing Corporation. Vibration isolation systems setup guide. Massachusetts, 2008.

[60] P.A. Redhead, J.P. Hobson, and E.V. Kornelsen. *The physical basis of ultra-high vacuum.* Amer Inst of Physics, 1968.

[61] GL Weissler and R.W. Carlson. *Vacuum physics and technology.* academic press, 1979.

[62] JE Demuth, U. Koehler, and RJ Hamers. The STM learning curve and where it may take us. *J. Microsc.*, 152(2):299–316, 1988.

[63] JA Panitz. Field-ion microscopy-A review of basic principles and selected applications. *Journal of Physics E: Scientific Instruments*, 15:1281, 1982.

[64] M. Rezeq, J. Pitters, and R. Wolkow. Tungsten nanotip fabrication by spatially controlled field-assisted reaction with nitrogen. *The Journal of chemical physics*, 124:204716, 2006.

[65] R. Wiesendager. *Scanning Probe Microscopy and Spectroscopy: Methods and Applications.* Cambridge University Press, 1994.

[66] TE Everhart and RFM Thornley. Wide-band detector for micro-microampere low-energy electron currents. *Journal of Scientific Instruments*, 37:246, 1960.

[67] HJ Leamy. Charge collection scanning electron microscopy. *Journal of Applied Physics*, 53(6):R51–R80, 1982.

[68] Omicron. The omicron uhv STM user's guide 1.2. Germany, 2000.

[69] Omicron. The omicron variable temperature STM user's guide 1.1. Germany, 1996.

[70] K. Byrappa and T. Ohachi. *Crystal growth technology.* William Andrews Inc., 2003.

[71] Unknown. Nc-afm. `http://www.jpo.go.jp/shiryou/s_sonota/hyoujun_gijutsu/spm/4_d_5_a.htm`, 2003.

[72] VA Ukraintsev and J.T. Yate. The role of nickel in Si (001) roughening. *Surface Science*, 346(1-3):31–39, 1996.

[73] R. Butz and H. Lüth. The surface morphology of Si (100) after carbon deposition. *Surface Science*, 411(1-2):61–69, 1998.

[74] Geert Luyckx and Jan Ceulemans. Deoxygenation, deaeration and degassing: A survey and evaluation of methods. *Bulletin des Socits Chimiques Belges*, 96(2):151–163, 1987.

[75] I. Mills, International Union of Pure, Applied Chemistry, International Union of Pure, Terminology Applied Chemistry. Commission on Physicochemical Symbols, and Units. *Quantities, units and symbols in physical chemistry.* Blackwell Oxford, 1988.

[76] S. Sinha, A.J. Dickie, and R.A. Wolkow. Tuning tunneling current rectification with chemical modification of silicon (1 0 0) surfaces. *Chemical Physics Letters*, 469(4-6):279–283, 2009.

[77] R.M. Feenstra, Joseph A. Stroscio, and A.P. Fein. Tunneling spectroscopy of the Si(111)2 1 surface. *Surface Science*, 181(1-2):295 – 306, 1987.

[78] RM Feenstra, JY Lee, MH Kang, G. Meyer, and KH Rieder. Band gap of the Ge (111) c (2× 8) surface by scanning tunneling spectroscopy. *Physical Review B*, 73(3):35310, 2006.

[79] ND Lang. Apparent barrier height in scanning tunneling microscopy. *Physical Review B*, 37(17):10395–10398, 1988.

[80] M. Weimer, J. Kramar, and J. D. Baldeschwieler. Band bending and the apparent barrier height in scanning tunneling microscopy. *Phys. Rev. B*, 39(8):5572–5575, Mar 1989.

[81] Adam J. Dickie and Robert A. Wolkow. Metal-organic-silicon nanoscale contacts. *Phys. Rev. B*, 77(11):115305, Mar 2008.

[82] A.Y. Anagaw, R.A. Wolkow, and G.A. DiLabio. Theoretical study of work function modification by organic molecule-derived linear nanostructure on H-silicon (100)-2 x 1. *Journal of Physical Chemistry C*, 112(10):3780–3784, 2008.

[83] P. Mårtensson, A. Cricenti, and G.V. Hansson. Photoemission study of the surface states that pin the Fermi level at Si (100) 2× 1 surfaces. *Physical Review B*, 33(12):8855–8858, 1986.

[84] Jason Pitters. Variation of surface doping with annealing temperature. Unpublished., 2010.

[85] R. Akiyama, T. Matsumoto, and T. Kawai. Capacitance of a molecular overlayer on the silicon surface measured by scanning tunneling microscopy. *Physical Review B*, 62(3):2034–2038, 2000.

[86] R.J. Hamers, J.S. Hovis, S.K. Coulter, M.D. Ellison, and D.F. Padowitz. Ultrathin organic layers on silicon surfaces. *Jpn. J. Appl. Phys*, 39:4366–4371, 2000.

[87] MA Green, FD King, and J. Shewchun. Minority carrier MIS tunnel diodes and their application to electron-and photo-voltaic energy conversion–I. Theory. *Solid-State Electronics*, 17(6):551–561, 1974.

[88] J. Shewchun, MA Green, and FD King. Minority carrier MIS tunnel diodes and their application to electron-and photo-voltaic energy conversion–II. Experiment. *Solid-State Electronics*, 17(6):563–572, 1974.

[89] O. Yaffe, L. Scheres, S.R. Puniredd, N. Stein, A. Biller, R.H. Lavan, H. Shpaisman, H. Zuilhof, H. Haick, D. Cahen, et al. Molecular Electronics at Metal/Semiconductor Junctions. Si Inversion by Sub-Nanometer Molecular Films. *Nano letters*, 9(6):2390–2394, 2009.

[90] GP Lopinski, DJ Moffatt, and RA Wolkow. Benzene/Si (100): metastable chemisorption and binding state conversion. *Chemical physics letters*, 282(3-4):305–312, 1998.

[91] RA Wolkow, GP Lopinski, and DJ Moffatt. Resolving organic molecule-silicon scanning tunneling microscopy features with molecular orbital methods. *Surface science*, 416(3):L1107–L1113, 1998.

[92] Axel D. Becke. *Modern Electronic Structure Theory*, chapter Exchange-Correlation Approximations in Density-Functional Theory.

[93] Vikram Gavini. Overview of electronic structure theories. Department of Mechanical Engineering, University of Michigan, Ann Arbor.

[94] E. Fermi. Un metodo statistice per la determinazione di alcune proprieta dell'atomo. *Rend. Acad. Lincei*, 6:602, 1927.

[95] P. Hohenberg, W. Kohn, et al. Inhomogeneous electron gas. *Phys. Rev*, 136(3B):B864–B871, 1964.

[96] W. Kohn and LJ Sham. Self-consistent equations including exchange and correlation effects. *Phys. Rev*, 140(4A):A1133–A1138, 1965.

[97] W. Kohn. Nobel lecture: Electronic structure of matter—wave functions and density functionals. *Rev. Mod. Phys.*, 71(5):1253–1266, Oct 1999.

[98] SA Wildman, GA DiLabio, and PA Christiansen. Accurate relativistic effective potentials for the sixth-row main group elements. *The Journal of chemical physics*, 107:9975, 1997.

[99] E.R. Johnson, I.D. Mackie, and G.A. DiLabio. Dispersion interactions in density-functional theory. *Journal of Physical Organic Chemistry*, 22(12):1127–1135, 2009.

[100] F. London. On Centers of van der Waals Attraction. *The Journal of Physical Chemistry*, 46(2):305–316, 1942.

[101] E.R. Johnson and G.A. DiLabio. Theoretical Study of Dispersion Binding of Hydrocarbon Molecules to Hydrogen-Terminated Silicon (100)-2$\times$ 1. *The Journal of Physical Chemistry C*, 113(14):5681–5689, 2009.

[102] G.A. DiLabio. Accurate treatment of van der Waals interactions using standard density functional theory methods with effective core-type potentials: Application to carbon-containing dimers. *Chemical Physics Letters*, 455(4-6):348–353, 2008.

[103] M. Pavone, N. Rega, and V. Barone. Implementation and validation of DFT-D for molecular vibrations and dynamics: The benzene dimer as a case study. *Chemical Physics Letters*, 452(4-6):333–339, 2008.

[104] R. Podeszwa and K. Szalewicz. Physical origins of interactions in dimers of polycyclic aromatic hydrocarbons. *Phys. Chem. Chem. Phys.*, 10(19):2735–2746, 2008.

[105] TR Walsh. An ab initio study of the low energy structures of the naphthalene dimer. *Chemical physics letters*, 363(1-2):45–51, 2002.

[106] C. Gonzalez and E.C. Lim. Evaluation of the Hartree-Fock dispersion (HFD) model as a practical tool for probing intermolecular potentials of small aromatic clusters: Comparison of the HFD and MP2 intermolecular potentials. *The Journal of Physical Chemistry A*, 107(47):10105–10110, 2003.

[107] S. Tsuzuki, K. Honda, T. Uchimaru, and M. Mikami. High-level ab initio computations of structures and interaction energies of naphthalene dimers: Origin of attraction and its directionality. *The Journal of chemical physics*, 120:647, 2004.

[108] T. Sato, T. Tsuneda, and K. Hirao. A density-functional study on π-aromatic interaction: Benzene dimer and naphthalene dimer. *The Journal of chemical physics*, 123:104307, 2005.

[109] I.D. Mackie and G.A. DiLabio. Interactions in large, polyaromatic hydrocarbon dimers: application of density functional theory with dispersion corrections. *The Journal of Physical Chemistry A*, 112(43):10968–10976, 2008.

[110] F.A. Hamprecht, A.J. Cohen, D.J. Tozer, and N.C. Handy. Development and assessment of new exchange-correlation functionals. *The Journal of Chemical Physics*, 109:6264–6271, 1998.

[111] M. J. Frisch, G. W. Trucks, H. B. Schlegel, G. E. Scuseria, M. A. Robb, J. R. Cheeseman, Jr. Montgomery, J. A., T. Vreven, K. N. Kudin, J. C. Burant, J. M. Millam, S. S. Iyengar, J. Tomasi, V. Barone, B. Mennucci, M. Cossi, G. Scalmani, N. Rega, G. A. Petersson, H. Nakatsuji, M. Hada, M. Ehara, K. Toyota, R. Fukuda, J. Hasegawa, M. Ishida, T. Nakajima, Y. Honda, O. Kitao, H. Nakai, M. Klene, X. Li, H. P. Knox, J. E. Hratchian, J. B. Cross, V. Bakken, C. Adamo, J. Jaramillo, R. Gomperts, R. E. Stratmann, O. Yazyev, A. J. Austin, R. Cammi, C. Pomelli, J. W. Ochterski, P. Y. Ayala, K. Morokuma, G. A. Voth, P. Salvador, J. J. Dannenberg, V. G. Zakrzewski, S. Dapprich, A. D. Daniels, M. C. Strain, O. Farkas, D. K. Malick, A. D. Rabuck, K. Raghavachari, J. B. Foresman, J. V. Ortiz, Q. Cui, A. G. Baboul, S. Clifford, J. Cioslowski, B. Stefanov, G. Liu, A. Liashenko, P. Piskorz, I. Komaromi, R. L. Martin, D. J. Fox, T. Keith, M. A. Al.Laham, C. Y. Peng, A. Nanayakkara, M. Challacombe, P. M. W. Gill, B. Johnson, W. Chen, M. W. Wong, C. Gonzalez, and J. A. Pople. Gaussian 03, revision D. 01. *As implemented in: Gaussian 03, Revision D.01, Gaussian Inc.: Wallingford, CT*, 2004.

[112] S. Sinha, GA DiLabio, and RA Wolkow. Experimental and Theoretical Exploration of the Anisotropy of Styrene Diffusion on Hydrogen Terminated Si (100)-2× 1. *The Journal of Physical Chemistry C*, 114(16):7364–7371, 2010.

[113] JK Bal, S. Kundu, and S. Hazra. Growth and stability of Langmuir-Blodgett films on OH-, H-, or Br-terminated Si (001). *Physical Review B*, 81(4):45404, 2010.

[114] G. Ehrlich and K. Stolt. Surface diffusion. *Annual Review of Physical Chemistry*, 31(1):603–637, 1980.

[115] J. Heinonen, I. Koponen, J. Merikoski, and T. Ala-Nissila. Island diffusion on metal fcc (100) surfaces. *Physical Review Letters*, 82(13):2733–2736, 1999.

[116] S. Somasi, B. Khomami, and R. Lovett. An Integrated Molecular Dynamics and Monte Carlo Approach to Study Epitaxial Deposition of Silicon. In *Materials Research Society Symposium Proceedings*, volume 672, pages 1–1. Warrendale, Pa.; Materials Research Society; 1999, 2001.

[117] P.L. Cao, M. Qiu, and L.Q. Lee. Chemical surface diffusion coefficient and ordered c (2×2) adsorbate layer. *Journal of Physics: Condensed Matter*, 8:1335, 1996.

[118] AP Van Bavel, MJP Hopstaken, D. Curulla, JW Niemantsverdriet, JJ Lukkien, and PAJ Hilbers. Quantification of lateral repulsion between coadsorbed CO and N on Rh (100) using temperature-programmed desorption, low-energy electron diffraction, and Monte Carlo simulations. *The Journal of Chemical Physics*, 119:524, 2003.

[119] MC Righi, CA Pignedoli, R. Di Felice, CM Bertoni, and A. Catellani. Kinetic Monte Carlo simulations of C diffusion on [beta]-SiC (111) based on ab initio calculations. *Computer Physics Communications*, 169(1-3):50–53, 2005.

[120] E.W. Müller and K. Bahadur. Field ionization of gases at a metal surface and the resolution of the field ion microscope. *Physical Review*, 102(3):624–631, 1956.

[121] T.T. Tsong. A historic perspective of FIM and STM studies of surface diffusion. *Materials Science and Engineering A*, 353(1-2):1–5, 2003.

[122] YW Mo. Direct determination of surface diffusion by displacement distribution measurement with scanning tunneling microscopy. *Physical review letters*, 71(18):2923–2926, 1993.

[123] BS Swartzentruber. Direct measurement of surface diffusion using atom-tracking scanning tunneling microscopy. *Physical review letters*, 76(3):459–462, 1996.

[124] R. Otero, F. Hümmelink, F. Sato, S.B. Legoas, P. Thostrup, E. Lægsgaard, I. Stensgaard, D.S. Galvão, and F. Besenbacher. Lock-and-key effect in the surface diffusion of large organic molecules probed by STM. *nature materials*, 3(11):779–782, 2004.

[125] F. Dulot, J. Eugčne, B. Kierren, and D. Malterre. STM-TIP induced surface diffusion of copper on copper (100). *Applied Surface Science*, 162:86–93, 2000.

[126] Q. Li and KT Leung. Thermal Chemistry of Styrene on Si (100) 2× 1 and Modified Surfaces: Electron-Mediated Condensation Oligomerization and Posthydrogenation Reactions. *J. Phys. Chem. B*, 109(4):1420–1429, 2005.

[127] Y. Wang, J. Ma, S. Inagaki, and Y. Pei. [2+ 2] Cycloaddition Reactions of Ethylene Derivatives with the Si (100)-2× 1 Surface: A Theoretical Study. *J. Phys. Chem. B*, 109(11):5199–5206, 2005.

[128] P. Avouris, RE Walkup, AR Rossi, HC Akpati, P. Nordlander, T.C. Shen, GC Abeln, and JW Lyding. Breaking individual chemical bonds via stm-induced excitations. *Surface Science*, 363(1-3):368 – 377, 1996.

[129] DP Adams, TM Mayer, and BS Swartzentruber. Nanometer-scale lithography on Si (001) using adsorbed H as an atomic layer resist. *Journal of Vacuum Science & Technology B: Microelectronics and Nanometer Structures*, 14(3):1642–1649, 1996.

[130] J.L. Pitters, P.G. Piva, X. Tong, and R.A. Wolkow. Reversible passivation of silicon dangling bonds with the stable radical TEMPO. *Nano Letters*, 3(10):1431–1435, 2003.

[131] J.L. Pitters and R.A. Wolkow. Protection- Deprotection Chemistry to Control Styrene Self-Directed Line Growth on Hydrogen-Terminated Si (100). *J. Am. Chem. Soc*, 127(1):48–49, 2005.

[132] M.P. Schwartz, M.D. Ellison, S.K. Coulter, J.S. Hovis, and R.J. Hamers. Interaction of π-Conjugated Organic Molecules with π-Bonded Semiconductor Surfaces: Structure, Selectivity, and Mechanistic Implications. *J. Am. Chem. Soc*, 122(35):8529–8538, 2000.

[133] Q. J. Zhang and Z. F. Liu. First principle study on the adsorption of styrene on Si(100)2×1. *The Journal of Physical Chemistry C*, 113(13):5263–5273, 2009.

[134] M. Matsumoto and T. Nishimura. Mersenne twister: a 623-dimensionally equidistributed uniform pseudo-random number generator. *ACM Transactions on Modeling and Computer Simulation (TOMACS)*, 8(1):3–30, 1998.

[135] A. Fog. Mersenne Twister Random Number Generator. *As implemented in: The GNU General Public License*, 2008.

[136] JJ Lukkien, JPL Segers, PAJ Hilbers, RJ Gelten, and APJ Jansen. Efficient Monte Carlo methods for the simulation of catalytic surface reactions. *Physical Review E*, 58(2):2598–2610, 1998.

[137] GW King and AAG Van Putten. Extended CNDO calculations upon styrene and aniline. *Journal of Molecular Spectroscopy*, 44(2):286–297, 1972.

[138] E. Bock and D. Iwacha. Electric dipole moments of ortho-, meta-, para-, and penta-fluorostyrene molecules. *Canadian Journal of Chemistry*, 46(18):2961–2962, 1968.

[139] J.L. Pitters, I.A. Dogel, and R.A. Wolkow. Charge Control of Surface Dangling Bonds Using Nanoscale Schottky Contacts. *ACS nano*, 5(3):1984–1989, 2011.

[140] P. Rai-Choudhury. *Handbook of microlithography, micromachining, and microfabrication*. Inspec/Iee, 1997.

[141] M.R. Linford, P. Fenter, P.M. Eisenberger, and C.E.D. Chidsey. Alkyl monolayers on silicon prepared from 1-alkenes and hydrogen-terminated silicon. *Journal of the American Chemical Society*, 117(11):3145–3155, 1995.

[142] M.B. Haider, J.L. Pitters, G.A. DiLabio, L. Livadaru, J.Y. Mutus, and R.A. Wolkow. Controlled Coupling and Occupation of Silicon Atomic Quantum Dots. *Arxiv preprint arXiv:0807.0609*, 2008.

[143] JN Randall, JB Ballard, JW Lyding, S. Schmucker, JR Von Ehr, R. Saini, H. Xu, and Y. Ding. Atomic precision patterning on Si: An opportunity for a digitized process. *Microelectronic Engineering*, 87(5-8):955–958, 2010.

[144] WA Hofer, AJ Fisher, GP Lopinski, and RA Wolkow. Electronic structure and STM images of self-assembled styrene lines on a Si (1 0 0) surface. *Chemical physics letters*, 365(1-2):129–134, 2002.

[145] P.G. Piva, G.A. DiLabio, J.L. Pitters, J. Zikovsky, M. Rezeq, S. Dogel, W.A. Hofer, and R.A. Wolkow. Field regulation of single-molecule conductivity by a charged surface atom. *Nature*, 435(7042):658–661, 2005.

[146] L. Yang and D.J. Doren. Structure of Styrene Molecular Lines on Si (100)-(2$\times$ 1): H. *The Journal of Physical Chemistry C*, 112(3):781–785, 2008.

[147] AJ Heinrich, CP Lutz, JA Gupta, and DM Eigler. Molecule cascades. *Science*, 298(5597):1381, 2002.

[148] HyperChem(TM). HyperChem 7 . Hypercube, Inc., Gainesville, Florida, USA, 2000.

[149] George Kirczenow, Paul G. Piva, and Robert A. Wolkow. Modulation of electrical conduction through individual molecules on silicon by the electrostatic fields of nearby polar molecules: Theory and experiment. *Phys. Rev. B*, 80(3):035309, Jul 2009.

Appendix A

Multiprobe Challenges

A.1 Multiprobe Challenges

The Multiprobe unit is a complex system. The remarkable capabilities of the system, including Multiprobe current/voltage analysis, have been demonstrated by Zikovsky [36]. However, it was found that several optimizations of the instrument were required prior to conducting further measurements with the system. In particular the vacuum pressure and system noise were optimized. In addition, the functionality of the SEM column and the probe control hardware were found to sources of great challenge.

A.1.1 Pressure

Achieving and maintaining UHV pressures is a non-trivial matter. While UHV technology is highly advanced the particularities of individual systems must be taken into account when optimizing system vacuum pressures. To achieve UHV pressures, the entire system must be heated, or 'baked', while running vacuum pumps in order to remove water and trace gases which adsorb on the internal surfaces of chamber. All of the systems used in this dissertation were baked to 150 °C under insulated bakeout tents with bakeout heater fans (Tectra GmbH). Some components such as small transfer arms were heated with standard electrical tapes and insulated with foil. The temperature was measured at various points on the machine with thermocouples. For the Multiprobe machine, the system was held at temperature for 3-4 days for optimum performance.

At the time of initiating studies on the Multiprobe, the base pressure in the STM chamber was in the low 10^{-9} Torr range. At this pressure, 1L would correspond to only 16 min of exposure to the chamber environment. As Multiprobe experiments using three probes can take several hours to set up, such base pressures were too

high to be confident about observations of the surface. Unfortunately, leaks of this small magnitude are extremely difficult to detect and require full bake-outs prior to testing. After several iterations of leak testing, which eventually required testing of each component, the replacement of a view port that was associated with a very small leak and replacement of the ion pump on the chamber, it was found that the SEM column contained an extremely small leak. The precise location of the leak has been difficult to determine. Although the column is rated to a 150 °C bake-out temperature, it is possible that the bake-out method used on standard JEOL components using heating tapes does not cause the entire column to reach the bake-out temperature. Baking the Multiprobe system under a tent may thus have caused internal seals to leak. It is suspected, but not yet known, that an O-Ring seal inside the column may be the culprit. Testing of the column has continued on a separate vacuum system.

The SEM column was replaced with a similar column, which had previously been mounted on a different system, and a base pressure in the mid 10^{-11} Torr range was achieved in the STM chamber. With the SEM filament and lenses on, the pressure increases to the low 10^{-10} Torr range. Thorough degassing of the lenses and the addition of an extra small ion-pump on the column did not alleviate this pressure increase. However, sample surfaces have been found to remain clean for an adequate period of time to conduct STM experiments.

A.1.2 Electrical and Vibrational Noise

For a stable tip and high image resolution it is imperative to minimize electrical and vibrational noise. At the time that I began work on the Multiprobe system, electrical noise was found to be the greater concern although some adjustments of vibrational isolation were also preformed. Optimization of the noise parameters was complicated as it often varied depending upon the day. The Multiprobe is housed in phase one of a new building, The Centennial Centre for Interdisciplinary Sciences, at the University of Alberta Campus. Construction of phase two of the building was ongoing during the time of optimizing the Multiprobe system. While all testing was done during quiet phases of construction, the transient connection of various equipment may have contributed to the observations.

Electrical noise is most often a manifestation of ground loops. An example of the effects of ground loops is presented in figure A.1. It can be seen that the effects of ground loops can lead to an increase in the noise at 60 Hz and associated harmonics by an order of magnitude or greater. Through careful testing, ground isolation and/or rerouting we were able to reduce the electrical noise (with all connections

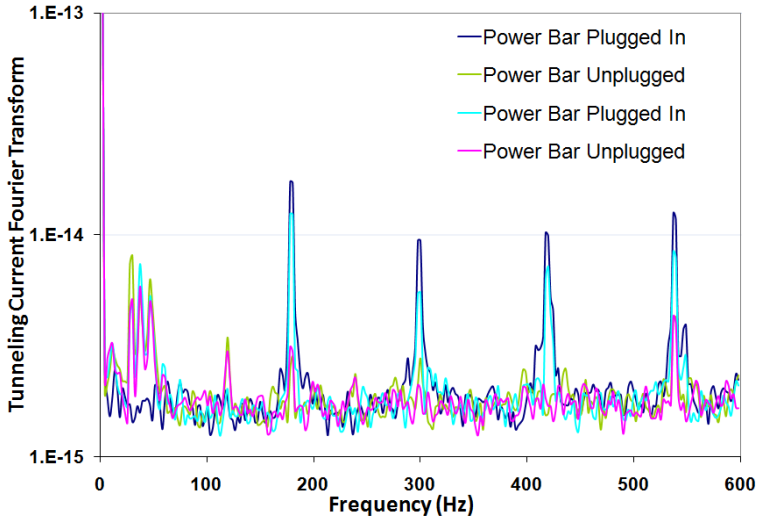

Figure A.1: Example of Ground Loop Noise. In this case, the noise was caused by plugging in an empty power bar to an electrical outlet in the room. All connections to the microscope had been removed except the main tip current collector. Taken with Nanonis Controller built in FFT Spectrum Analyzer. Average of 10 spectra.

to the system made) by almost two orders of magnitude. At present, the noise is comparable to a VT-STM [1] but is still greater than that of the STM-1 A.2.

The vibration isolation system on the Multiprobe includes suspension-springs with eddy-current damping of the whole scanning unit. In addition, the vacuum chamber itself was mounted on the STACIS Active Piezoelectric Vibration Cancellation System [59].

A.1.3 SEM Column

The SEM column has had many functional challenges apart from the effect on chamber pressure. In fact, both SEM columns available in the group have been undergoing rigorous testing. The vacuum pressure issue in one column (hereafter referred to as column 1) was previously mentioned. Several other issues have also arisen. Mose notably, the column with better pressure characteristics and which is currently mounted on the Multiprobe system (hereafter referred to as column 2), has had electron beam alignment difficulties. In fact, we have been unable to find a strong and stable primary electron beam, although a weak beam that

[1] This is not the same VT-STM system used in my dissertation but a similar instrument in the room next door which also uses the Nanonis controller and can easily acquire noise measurements in a manner similar to the Multiprobe.

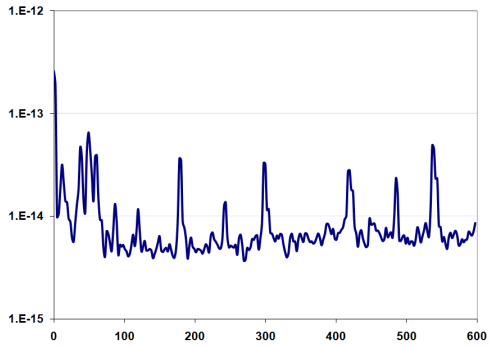

(a) Multiprobe

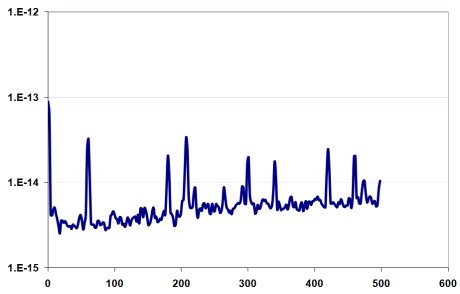

(b) VT-STM

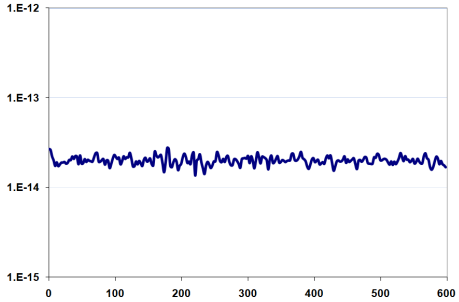

(c) STM-1

Figure A.2: Noise Comparison between Systems. Taken with Nanonis Controller built in FFT Spectrum Analyzer. Average of 10 spectra. Y-axis: Tunneling current Fast Fourier Transform; X-axis: Frequency in Hz.

disappears as the condenser lens voltage is increased has been located. Different filaments have been tested with the same result. A possibly related issue with column 2, is inaccurate readings of the suppressor voltage and changes in the readings of voltages and emission current when the controller is set to monitor (read) the values. However, the applied voltages and optical fibers used for reading appear to be functioning normally. Meanwhile, the gun of column 1 has had electrical connection issues (in addition to the pressure problem). In addition, the secondary electron detectors have both had problems with charging which manifests as spontaneous as well as gradual changes in the brightness and contrast levels of the images. Despite extensive comparing, contrasting and testing the SEM components from the two different columns as well as having a service visit from JEOL technicians, these difficulties have not yet been solved.

Current efforts are focused upon fixing the gun of column 1, for which we believe the connection issues can be remedied. Column 1 will then be used to verify that one full set of electronics is functional. These electronics may then be transferred to the less leaky column to determine if issues with the beam are related to the physical column or the electronics. The pressure issues in column 1 could simultaneously be tested. Unfortunately, this flow process has proven to be time consuming.

In the Multiprobe, fine alignment of the three tips as well as the sample under investigation is currently dependent upon the function of the SEM. While efforts at restoring the SEM columns continue, alternative means of alignment are also being explored.

A.1.4 Probe Control

The Multiprobe system currently has a different system for controlling each tip. As described in [36], the main STM is controlled using Nanonis electronics and software, the 'right' probe is controlled using new generation Createc (Createc Fischer & Co. GmbH) hardware and the homebuilt STM.net software and the 'left' probe is controlled with an older generation all digital Createc on a PC32 card again with the STM.net software. The later system has had several port and A/D as well as D/A converter failures which has required work-around changes in the STM.net code to continue functioning. Such changes can be difficult to implement without consultation with the original programmer. Moreover, it is becoming increasingly difficult to buy replacement PC32 cards. While Dr. Zikovsky has been extremely helpful in providing guidance in modifying the STM.net program, the future reliability of the system has come into question. In order to create greater integration between the probes while at the same time reducing the complexity and increasing the reliability

of the system for future users, a new Multiprobe Nanonis control system will be integrated to control all three tips.